JET PROPULSION

A publication of the

AMERICAN ROCKET SOCIETY

Research and Development

BIND

VOLUME 28 APRIL 1958 NUMBER 4

SCIENCE & TECHNOLOGY

SURVEY ARTICLE

Concepts for Future Nuclear Rocket Propulsion . . . . . *Robert W. Bussard* 223

CONTRIBUTED ARTICLES

Plasma Physics and Hypersonic Flight . . . . . *J. W. Bond Jr.* 228

A Practical Mathematical Approach to Grain Design . . . . *Max W. Stone* 236

Design, Fabrication and Testing of the Vanguard Satellite . *Robert C. Baumann* 244

A Recording Sodium-Line Reversal Pyrometer . . . . . *W. M. Broback, R. E. Clemensen and W. E. Voreck* 249

An Iterative Method of Determining Equilibrium Compositions of Reacting Gases . . . . . *S. T. Chu* 252

TECHNICAL NOTES

Ignition of Electrolytic Monopropellants by Submerged Electrical Discharge . . . . . *Marjorie W. Evans, Frank I. Given and G. M. Muller* 255

A Note on Sonic Sudden Enlargements . . . . . *R. H. Page* 256

Mach Reflections in Two-Dimensional Diffusers From Hydraulic Analogy Experiments . . . . . *E. V. Laitone and J. E. Stout* 257

Friction and Heat Transfer in a Rough Tube at Varying Prandtl Numbers . . . . . *R. C. Hastrup, R. H. Sabersky, D. R. Bartz and M. B. Noel* 259

Generalized Trajectories for Free-Falling Bodies of High Drag . *R. D. Turnacliff and J. P. Hartnett* 263

DEPARTMENTS

New Patents 268 Book Reviews 270 Technical Literature Digest 276

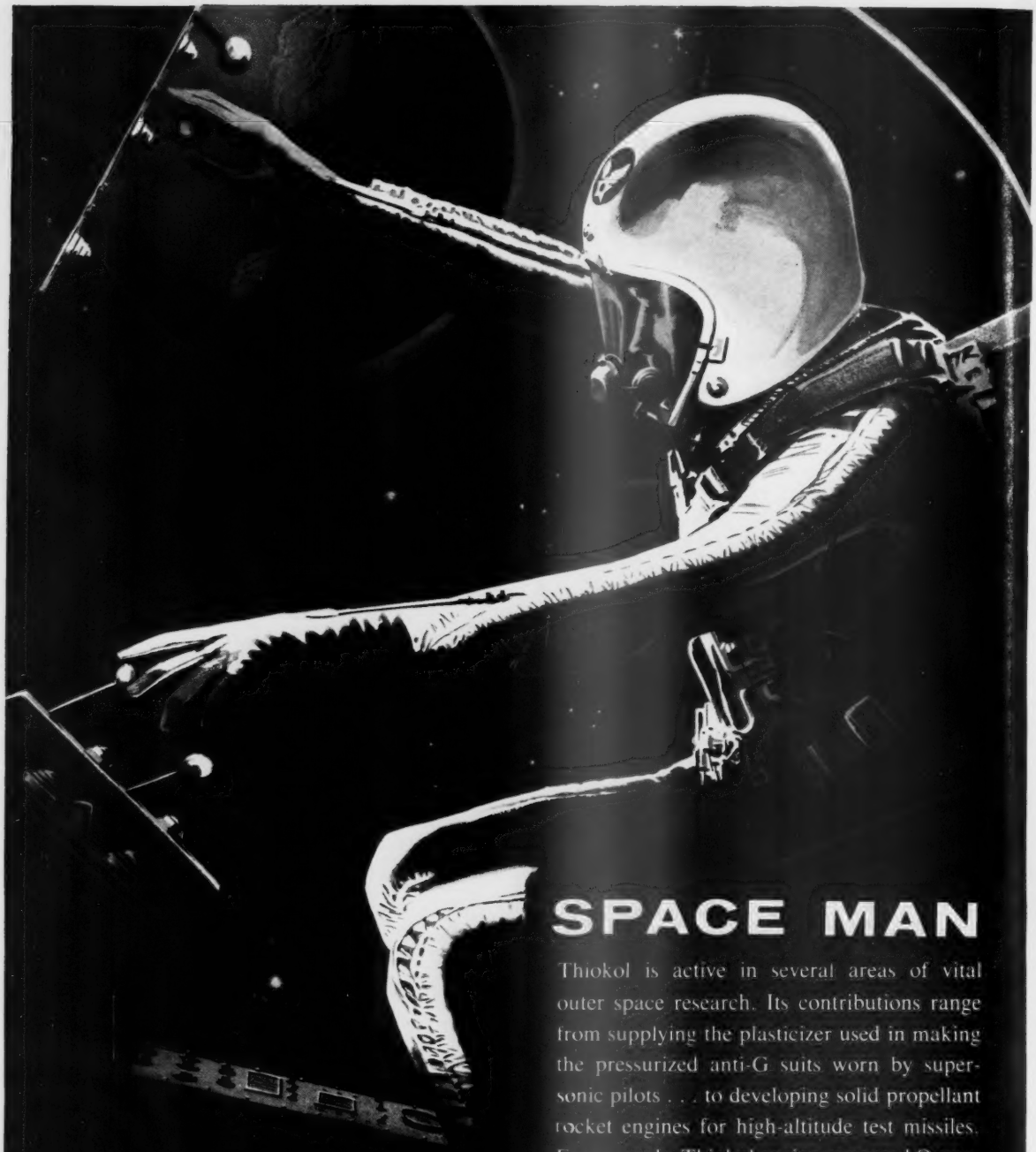

SPACE MAN

Thiokol is active in several areas of vital outer space research. Its contributions range from supplying the plasticizer used in making the pressurized anti-G suits worn by supersonic pilots . . . to developing solid propellant rocket engines for high-altitude test missiles. For example, Thiokol engines powered Operation Farside and X-17, providing essential data on atmospheric, cosmic and re-entry conditions.

Thiokol®

CHEMICAL CORPORATION

TRENTON, N. J. • ELKTON, MD.
HUNTSVILLE, ALA. • MARSHALL, TEXAS
MOSS POINT, MISS. • BRIGHAM CITY, UTAH

®Registered trademark of the Thiokol Chemical Corporation for its liquid polymers, rocket propellants, plasticizers and other chemical products

The RW-300 is the first digital computer for test control and data reduction

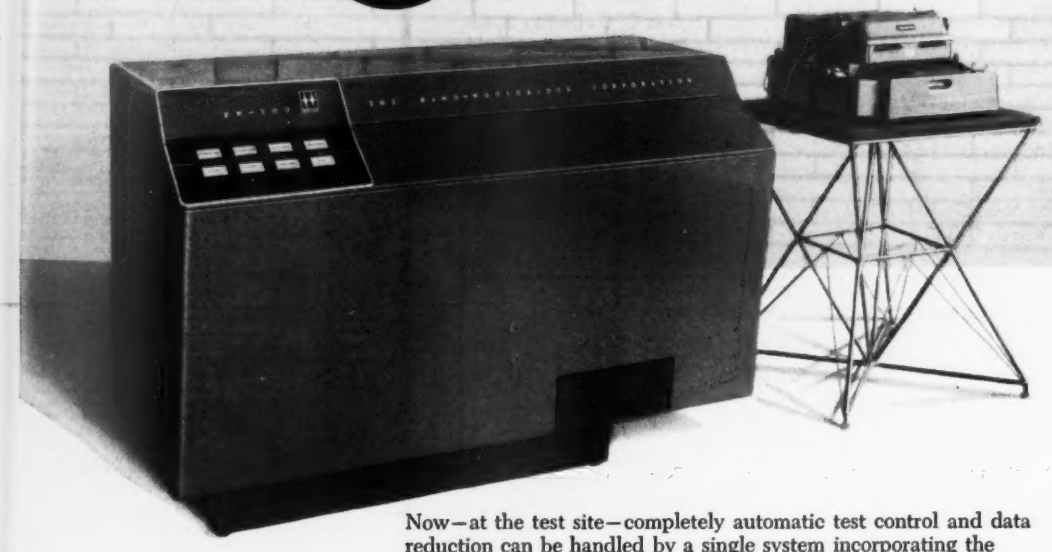

Now—at the test site—completely automatic test control and data reduction can be handled by a single system incorporating the Ramo-Wooldridge RW-300 Digital Control Computer. The new RW-300 can schedule and closely control test routines, and it can collect, analyze, and record test data.

The versatile RW-300 utilizes input data as feedback to modify control actions, thus substantially shortening many test routines. In addition, the RW-300 directly logs both instrument data and complex relationships among these data. Thus, test results are available immediately. The time-consuming task of processing raw data through a separate computer, often remote from the test facility, usually can be eliminated.

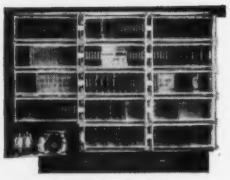

For technical information on automatic test control and data reduction with the RW-300 and with special digital systems which utilize solid-state components exclusively, write: Director of Marketing, The Thompson-Ramo-Wooldridge Products Company, P.O. Box 45607, Airport Station, Los Angeles 45, California, or call OSborne 5-4601.

THE THOMPSON-RAMO-WOOLDRIDGE PRODUCTS COMPANY

JET PROPULSION

A publication of the

AMERICAN ROCKET SOCIETY

Research and Development

Scope of JET PROPULSION

This Journal is a publication of the American Rocket Society devoted to the advancement of the field of jet propulsion through the dissemination of original papers disclosing new knowledge or new developments. As used herein, the term "jet propulsion" embraces all engines that develop thrust by rearward discharge of a jet through a nozzle or duct; and thus it includes air-consuming engines and underwater systems as well as rockets. JET PROPULSION is open to contributions dealing not only with propulsion but with other aspects of jet-propelled flight, such as flight mechanics, guidance, telemetering, and research instrumentation. Increasing emphasis will be given to the scientific problems of extraterrestrial flight.

Information for Authors

Manuscripts must be as brief as the proper presentation of the ideas will allow. Exclusion of dispensable material and conciseness of expression will influence the Editors' acceptance of a manuscript. In terms of standard-size double-spaced typed pages, a typical maximum length is 22 pages of text (including equations), 1 page of references, 1 page of abstract, and 12 illustrations. Fewer illustrations permit more text, and vice versa. Greater length will be acceptable only in exceptional cases.

Short manuscripts, not more than one quarter of the maximum length stated for full articles, may qualify for publication as Technical Notes or Technical Comments. They may be devoted to new developments requiring prompt disclosure or to comments on previously published papers. Such manuscripts are usually published within two months of the date of receipt.

Sponsored manuscripts are published occasionally as an ARS service to the industry. A manuscript that does not qualify for publication according to the above-stated requirements as to subject scope or length, but which nevertheless deserves widespread distribution among jet propulsion engineers, may be printed as an extra part of the Journal or as a special supplement, if the author or his sponsor will reimburse the Society for actual publication costs. Estimates are available on request. Acknowledgment of such financial sponsorship appears as a footnote on the first page of the article. Publication is prompt since such papers are not in the ordinary backlog.

Manuscripts must be double spaced on one side of paper only with wide margins to allow for instructions to printer. Include a 100 to 200 word abstract. State the authors' positions and affiliations in a footnote on the first page. Do not type equations; write them in ink. Identify unusual symbols or Greek letters for the printer. References are to be grouped at the end of the manuscript and are to be given as follows: for journal articles: authors first, then title, journal, volume, year, page numbers; for books: authors first, then title, publisher, city, edition, and page or chapter numbers. Line drawings must be clear and sharp to make clear engravings. Use black ink on white paper or tracing cloth. Lettering should be large enough to be legible after reduction. Photographs should be glossy prints, not matte or semi-matte. Each illustration must have a legend; legends should be listed in order on a separate sheet.

Manuscripts must be accomplished by written assurance as to security clearance in the event the subject matter lies in a classified area or if the paper originates under government sponsorship. Full responsibility rests with the author.

Submit manuscripts in duplicate (original plus first carbon, with two sets of illustrations) to the Editor, Martin Summerfield, Professor of Aeronautical Engineering, Princeton University, Princeton, N. J. Preprints of papers presented at ARS national meetings are automatically considered for publication.

JET PROPULSION is published monthly by the American Rocket Society, Inc., and the American Interplanetary Society at 20th & Northampton Sts., Easton, Pa., U. S. A. Editorial offices: 500 Fifth Ave., New York 36, N. Y. Price: $12.50 per year, $2.00 per single copy. Second-class mail privileges authorized at Easton, Pa. Notice of change of address should be sent to the Secretary, ARS, at least 30 days prior to publication. Opinions expressed herein are the authors' and do not necessarily reflect the views of the Editors or of the Society.

Concepts for Future Nuclear Rocket Propulsion

ROBERT W. BUSSARD

Robert W. Bussard is on the staff of the Division Office of the Nuclear Propulsion Division of the Los Alamos Scientific Laboratory. He received the B.S. and M.S. degrees in engineering from the University of California, Los Angeles. He entered rocket work in 1949, on the Falcon missile program at Hughes Aircraft Company. Following this he spent several years in high power density reactor development on the ANP Project at the Oak Ridge National Laboratory. Mr. Bussard has been active in the nuclear rocket program since its inception and is the author of numerous classified papers in this and allied fields. He is currently at Princeton University.

THE fundamentals, problems and potentialities of rocket propulsion systems powered by heat exchanger nuclear reactors have often been discussed in the technical literature (1a, b, c).[1] In such systems a reactor with solid fuel structure is used as an energy source to heat a working fluid which is then expelled through an exhaust nozzle, in the conventional fashion. Fission energy thus supplants chemical energy in the rocket motor combustion chamber. This straightforward approach is in the present tradition of reactor development—adapting the atom to the boiler, so to speak, rather than the other way around. Unfortunately this approach places an artificial upper limit on estimates of potential nuclear rocket performance, since all conventional heat engines, whether chemical- or nuclear-powered, are fundamentally limited by the energy of the molecular rather than the nuclear bond.

The energy available from fission of U^{235} is about 10^7 times that from chemical reaction of an equal mass of high explosive or other combustible mixture. In addition, fission energy appears principally as kinetic energy of the two fission fragments, each with an energy of 60 to 100 Mev, corresponding to a kinetic "temperature" of the order of 10^{12} R. The energy released as a result of other nuclear processes, such as fusion, beta decay and alpha emission, can also give rise to very energetic (several Mev) particles. It is clear that nuclear interaction processes offer a tremendous potential advantage over chemical reactions, which can never yield more than a few ev per particle.

Fusion

First in interest, and certainly most speculative, is the application of fusion energy to rocket propulsion. Fusion reactions in deuterium gas yield a variety of low mass particles (T, He^3, He^4, p and n) with energies of several Mev each. If it were possible to expel the products of these fusion reactions rearward from a rocket vehicle, the effective specific impulse of the "propellant" would be about 3×10^6 lb_f sec/lb_m,[2] some 10^4 larger than presently attainable from chemical rocket propellants. More likely, the products themselves could not practically be constrained to move unidirectionally; however large masses of nonfusioned gas could be heated to very high temperature by collisions with the energetic fusion products, resulting in high specific impulse performance even though only a small fraction of the fusionable fuel has been "burned." For example, a gas mixture in which only one D-D fusion reaction has taken place for each 10^4 D nuclei present will reach a bulk temperature of about 7×10^6 R (neglecting all losses) and will give a specific impulse of roughly 3×10^4 sec when expelled through a proper nozzle configuration. With this specific impulse a 100-ton rocket could take off from the earth, land on the moon and return, all under power, with the expenditure of only 5 tons of propellant.

Of course, gases at temperatures of the order of 10^6 R and higher cannot be contained by solid walls, at least at present, even with use of advanced methods of liquid cooling. However, since gases are highly ionized at these temperatures it is possible, in theory, to contain them within appropriately shaped magnetic fields. This approach is under investigation in the current thermonuclear power program (2), but no satisfactory solution to the containment problem has yet been announced.

It is evident that thermonuclear fusion reactions can yield propellant temperature and performance far beyond that available conventionally today if such reactions can be made to "go" in a controllable manner. It is equally evident that speculation on the possible forms (weight, size, performance, etc.) of thermonuclear-powered propulsion systems is fruitless until the controlled release of fusion energy is an accomplished fact.

Radioisotope Decay[3]

Many radioisotopes are found in nature (e.g., Ra, Rd, etc.). others result from the fission of uranium or plutonium nuclei (e.g., Sr^{90}, etc.) and still others can be manufactured by neutron irradiation of stable elements placed in nuclear reactors.

The prime difficulty in considering the use of fission product isotopes is that they do not appear singly, but are formed as part of a large group of "mixed" fission products. Chemical separation processes are necessary to isolate any one desired fission product from the mixture. On the other hand, radioisotope production by irradiation of a stable element results in the formation of the desired isotope mixed only with the parent target element. No chemical separation plants are required as for the extraction of single fission products; however, it is necessary to utilize reactors especially designed for irradiation usage. Some characteristics of potentially useful radioisotopes of both types are shown in Table 1.[3]

The decay of a radioactive isotope is generally accompanied by the release of fairly large amounts of energy carried by beta particles (electrons), gamma photons or alpha particles. Energetic photons are highly penetrating and must pass through large masses of material in order to lose their energy. Alpha particles and high energy electrons have mass and are charged, and lose their energy quickly by ionization processes in passage through matter. As a consequence gamma emitters are not as useful for radioisotope heat sources as are alpha and beta emitters. The decay energy for potentially

Received Feb. 7, 1958.

[1] Numbers in parentheses indicate References at end of paper.

[2] Subscripts f and m here denote "force" and "mass," respectively. For brevity hereafter the units of specific impulse are given simply as sec.

[3] Adapted by permission from material in "Nuclear Rocket Propulsion," by R. W. Bussard and R. D. DeLauer, McGraw-Hill, New York, 1958.

useful beta emitters averages about 1 Mev per disintegration, while alpha emitters yield about 4 Mev apiece. Each fission process yields two radioisotopes and about one excess neutron. Thus about 6 Mev of decay energy can be obtained per fission if the two fission product isotopes are beta emitters yielding 1 Mev each, and the excess neutron is used to produce a 4-Mev alpha emitter from some stable parent element, such as bismuth (yields alpha-active Po). Since the initial kinetic energy of the two fission fragments is about 160 Mev, only some 4 per cent of the total energy of the fission process can be converted for use as decay energy. Practical considerations reduce this to less than $\frac{1}{2}$ per cent for most cases (3).

The most obvious use of decaying radioisotopes is as heat sources, replacing fission reactors or chemical combustion used to heat a propellant gas to high temperature. One disadvantage of this application is that no control is possible over the rate of energy production; thus auxiliary cooling systems (heat dumps) are required to prevent melting or vaporization of the source while not in use. Another disadvantage is the present limited production capability (3) for radioisotope sources. This is a result of the low energy conversion ratio obtained when using the fission process to produce active isotopes. For an assumed conversion efficiency as high as 1 per cent an installed production reactor capacity of the order of 10^6 Mw would be required to provide the heat sources for one large rocket vehicle per month. This is about twenty times the present powerplant capacity of the United States. Still another disadvantage is that the specific power output of almost any of the useful radioisotopes is very low by rocket motor standards. It has been shown (1b) that a rocket reactor specific power of the order of 0.5 Mw/lb or higher is required for satisfactory missile propulsion by nuclear reactor heat-exchanger rocket motors. In contrast, the best isotope listed in Table 1, Tm^{170}, yields only 0.01 Mw/lb at initial use. The use of radioisotopes as heat sources for rocket propulsion thus does not appear very attractive.

The possibility remains of using directly the momentum of the energetic decay particles (4). Unfortunately these are emitted isotropically, and at least half of the total decay energy will be deposited within the vehicle if half is assumed to go rearward. This latter assumption implies a thin layer of radioisotope "painted" on the flat base of the vehicle to be propelled. For such a configuration it has been shown (5) that about 100 Mw must be dissipated by the vehicle for every pound of thrust produced by alpha emission. For beta emission the heat dissipation must be about 3500 Mw per pound of thrust. Clearly, such a scheme is impractical.

In general, it does not appear possible to make practical use of radioisotopes for rocket propulsion.

Table 1 Characteristics of some radioisotopes as heat sources[3]

Artificially Produced Radioisotopes

Parent element	Daughter isotope	Thermal power available at initial use[a] Kw/lb	Kw/10^3 Mw yr
Tm^{169}	Tm^{170}	10	1400
Cs^{133}	Cs^{134}	6.9	550
Tl^{203}	Tl^{204}	0.17	140

Production conditions:

[a] Material weights include both parent and daughter. Production by irradiation in large thermal reactors for two half-lives. Initial use assumed at end of irradiation period.

Chemically Separated Fission Products

Fission product	Production rate lb/10^3 Mw yr	Thermal power available at initial use[b] Kw/lb	Kw/10^3 Mw yr
Mixed	880	0.58	510
Sr^{90}/Y^{90}	25	0.32	8
Ru^{106}/Rh^{106}	40	4.2	19
Cs^{137}/Ba^{137}	93	0.15	14
Ce^{144}/Pr^{144}	84	2.4	200

Production conditions:

[b] Weights include weight of all chemically similar isotopes. Fission products produced in large thermal reactors with a fuel cycle time of 180 days (assumed). Initial use assumed at 90 days following removal from production reactors.

Fission Energy

Many possible applications of fission energy and reactor systems have been suggested for propulsion aside from the obvious direct-heat-exchanger approach mentioned previously (1a, b, c).

The possibility of using fission fragment momentum directly suffers from the objections given previously to use of radioisotope decay-product momentum. The ratio of kinetic energy to momentum is about the same for fission fragments as for energetic (several Mev) alpha particles, and the specific heat dissipation which must be achieved is about 80 Mw per pound of thrust produced.

Fission fragments lose their energy by ionization of the material through which they pass while slowing down. If fissions can be made to occur in a reactor in such a way that the fragment slowing down takes place in the propellant gas rather than in structure (i.e., solid fuel elements) it would be possible to heat the gas above the limiting temperatures of containing structural materials. In principle, this can be done if fissionable fuel can be applied in thin films to the outer surfaces of fuel elements in a reactor core. If the fuel film is thin enough ($<10^{-4}$ cm) very little self-absorption will take place, and half of the fission fragments will travel away from the fuel element to heat the surrounding gas directly, while half will lose their energy in the element structure, which thus requires internal cooling. In the limit, if the propellant gas is used both as the internal coolant and the external flowing gas (in series flow),[4] an increase in specific impulse of about 40 per cent appears possible over that attainable from the conventional high temperature heat exchanger system. Consideration of the practical reactor design problems associated with the exploitation of this phenomenon leads to the general conclusion that the potential propellant performance gain is outweighed by increased complexity, size and weight of the reactor system.

Another line of attack[3] is by making most of the fissions occur in the gas phase itself in a reflector-moderated "cavity" reactor (6). Here an intimate mixture of fissionable material and diluent (propellant) is fed into a large void space surrounded by a neutron moderating material such as D_2O. Fissions take place in the mixture within the void, principally by thermal neutrons returned from the reflector-moderator, and heat the mixture to a temperature limited only by pressure-temperature-stress limitations of the container. A convergent-divergent nozzle must be located at one end of the void core to allow the escape of hot gas. An annular nozzle is preferable in order to minimize neutron leakage or streaming from the core. Fig. 1 shows a schematic outline of such a device, similar to those proposed as early as 1949 (7).

In order to achieve superperformance, temperatures of interest in this system must be much higher than those reached in the combustion process in conventional rocket motors.

[4] Following a suggestion by W. C. Cooley. Private communication, 1955.

Since rocket motor combustion temperatures are within a few thousand degrees of the boiling points of most structural materials, it is clear that all superperformance reactors operating on the principal of interest here can be analyzed as gaseous reactors, whether the fissionable fuel and diluent are introduced in solid, liquid or gaseous form.

For a gaseous reactor operated at a temperature sufficiently high to assure that all core gases are monatomic, a simple, approximate relation can be found between various parameters describing the reactor and vehicle operating conditions. Neglecting ionization effects and assuming perfect gases this is

$$P_c = 0.045(I_{sp})(I_{tot})(S\rho_f/W_f) \quad [1]$$

Here P_c is core gas pressure in lb/in.^{2}, ρ_f is critical fuel density in lb/ft,^{3} I_{sp} is propellant specific impulse in seconds, and W_f is the weight in pounds of fissionable material expended during operation; I_{tot} is the system total impulse, and is simply the product of rocket motor thrust F in pounds and operating time t_b in seconds. It is certainly desirable to retain as many of the unfissioned atoms of fuel as possible to prevent their escape from the system with the outflowing diluent gas. The factor S in Equation [1] is a measure of this retention or weight separation ability, defined here as the ratio of fuel mass expelled during operation to that which would have been expelled if no separation had taken place.

The only nuclear requirement on Equation [1] is that the fuel density be sufficient to ensure reactor criticality. Fig. 2 shows the critical fuel density, taken from the work of Safonov (6), required for cavity reactors within reflector moderators of neutronically "infinite" thickness. In practice "infinite" means 5 to 10 neutron slowing down lengths, so that reflector thicknesses of several feet are of interest.

Consideration of two examples serves to illustrate the practical difficulties which confront useful gaseous reactor propulsion systems:

1 Assume no separation takes place, so that $S = 1$, and that criticality can be achieved with $\rho_f = 0.1$ lb/ft^3. Assume further that it is desired to fly a vehicle which requires 100,000 lb thrust for 200 sec with propellant of performance comparable to that from present chemical rockets; hence $I_{tot} = 2 \times 10^7$ lb sec and $I_{sp} = 300$ sec. For these conditions Equation [1] becomes

$$W_f P_c = 2.7 \times 10^7 \quad [1a]$$

Here a system pressure of 1000 lb/in.^{2} will result in the loss of 27,000 lb of fissionable fuel; this is clearly impractical. However, for an allowable fuel loss of 300 lb the system pressure must be 90,000 lb/in.^{2} which is equally impractical.

2 Approaching the problem from another viewpoint, assume an allowable fuel expense of 300 lb and a specific impulse of 3000 sec, some tenfold better than for present conventional rockets. With the vehicle impulse previously postulated, the system pressure is related to the separation ratio by

$$P_c = 9 \times 10^6 S \quad [1b]$$

For a system pressure of 1000 lb/in.^{2} the factor S must be 1.11×10^{-3}, implying retention of all but one fuel atom in 900 of those which would normally escape by being swept out with the diluent gas.

Steady-state gaseous reactors thus appear practical for rocket propulsion only if separation ratios of the order of 10^{-3} can be achieved. Although it is not clear at present how this can be done, the enormous potential value of a rocket propulsion system capable of producing both very high specific impulse and high thrust-to-weight ratio makes it imperative that serious consideration be given to the problem of gas-phase separation of atomic species.

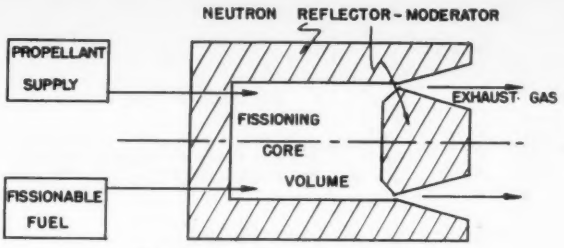

Fig. 1 Gaseous "cavity" reactor

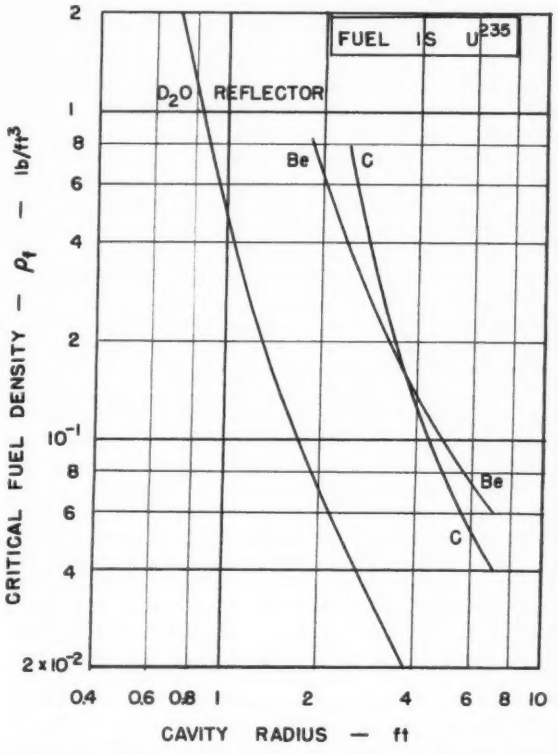

Fig. 2 Critical fuel density in "cavity" reactors (data from Reference 6)

Reactor Systems

Aside from the more or less exotic and novel schemes previously discussed, fission energy can play another role in the rocket propulsion systems of the future. For this, interest is in the application of conventional nuclear-powered heat engine equipment for the production of relatively small amounts of very hot gas, on a pulsed or steady-state basis.

Two general classes of such systems are the "thermomechanical" and "electrical" open cycles. The first of these typically makes use of a succession of nuclear-powered heat engines to heat a working fluid to successively higher and higher temperatures by use of conventional thermodynamic cycles. The resulting hot gas is expelled through a nozzle to produce the thrust output of the system. Of course, a great deal of waste heat must be dumped in the primary reactor circuit in order to produce a small amount of high temperature, high specific impulse exhaust gas from the secondary circuit. The cost of dumping this waste heat is reflected only in fixed equipment weight, not in increased propellant flow rate. Thus it appears possible to achieve high propellant performance at the expense of low over-all propulsion

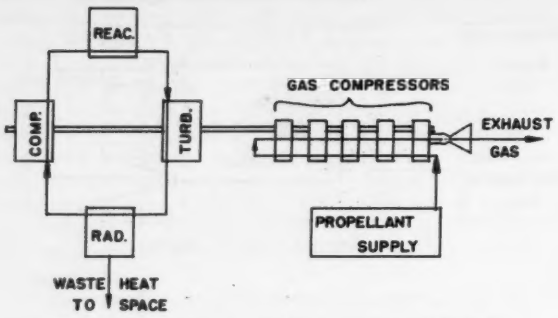

Fig. 3 Thermomechanical gas compression system

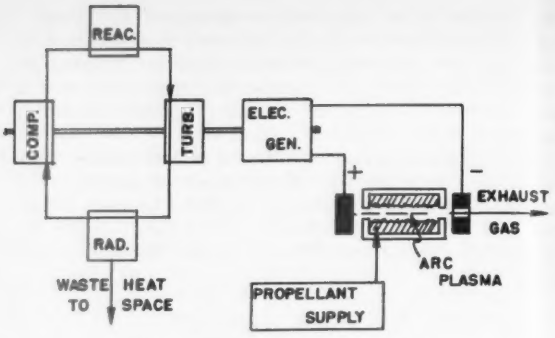

Fig. 4 Electric d-c arc system

system thrust-to-weight ratio. An illustrative example of a possible thermomechanical cycle is shown in Fig. 3. Here a conventional closed-cycle gas turbine system drives a series set of positive displacement gas compressors, each one fed from the preceding unit. The propellant is vaporized and heated by cooling the compressor bank and is then supplied to the first stage pumps. The high temperature outlet gas is exhausted to space to drive the vehicle. Waste heat in the turbine drive circuit is dumped to space by thermal radiation. Although not shown, an auxiliary circuit may be needed to dump exhaust circuit waste heat in excess of that which can be absorbed by the propellant within structural temperature limitations of the compressor bank.

Electrical open cycle systems follow a pattern similar to that just described for the thermomechanical cycles. Here, however, two basic methods of utilizing electrical energy are evident. First is that of heating gases in the bulk by passing a current through a flowing gas stream, causing dissociation and ionization, followed by recombination in the expansion process. This process is exemplified by the system shown in schematic outline in Fig. 4. Here a nuclear-electric generating system is used to drive a d-c arc maintained within a flowing, centrifugally stabilized cylinder of liquid propellant. Propellant vaporized from the liquid-walled cylinder feeds the arc plasma and is exhausted from the plasma core through a hole in the cathode. Russian experimental work (8) on such arcs has produced plasma temperatures as high as 90,000 R, capable of yielding exhaust gas specific impulse an order of magnitude higher than that attainable today from chemical rocket motors.

The second method of interest (first proposed by H. Oberth in 1929) is that of accelerating charged particles, using electrical energy to produce directed motion of the individual particles of propellant gas. This acceleration of ionized gases can be accomplished by use of static electric fields or by moving magnetic fields. Here, as for the arc system, a nuclear-electric generator set can be used to drive the electrostatic or electromagnetic accelerator. Waste heat in the reactor circuit must be dumped to space by radiation. In principle, the propellant exhaust velocity from such a device is limited only by the velocity of light.

However, power requirements are proportional to the square of the exhaust velocity while thrust is only linearly proportional; thus the specific power (per unit thrust) increases linearly with increasing exhaust velocity. Since the weights of power handling components such as turbines, compressors, radiators, electrical generators, pumps, and other heat engine or electrical plant equipment are generally rather directly related to their power capacities, it is clear that increasing exhaust velocity results in roughly linearly decreasing thrust-to-weight ratio for any of the reactor-powered systems discussed earlier. For these or similar systems yielding superperformance from the propellant gas, it is easy to show that an optimum exhaust velocity exists for each specified vehicle burnout velocity.

Consider a vehicle of gross weight W_0, composed of fixed weight (payload, guidance, etc.) W_d, propellant weight W_p, and propulsion system weight W_t. For a constant propellant weight flow rate the gross specific impulse of the complete vehicle is given by

$$I_g = \frac{Ft_b}{W_0} = \frac{I_{sp}W_p}{W_d + W_p + W_t} \quad [2]$$

A minimum weight system (arbitrarily chosen here as "optimum") results from operation at maximum I_g for any given value of W_d. This fixed load is related through the familiar mass-ratio equation to the gross weight and propellant weight by

$$W_d = \frac{W_p(W_d/W_0)e^{\xi}}{e^{\xi} - 1} = W_p(W_d/W_0)\Phi_{\xi} \quad [3]$$

The exponent ξ is the ratio of vehicle burnout velocity in free space to propellant exhaust velocity, $\xi = \Delta v/g_c I_{sp}$.

For no net energy losses in the equipment of the propellant exhaust circuit, the power required to produce the high temperature exhaust gas is given by

$$P_e = 2.18 \times 10^{-5} W_p I_{sp}^2/t_b\eta_e \quad [4]$$

where P_e is in Mw, and η_e is the exhaust gas expansion efficiency, generally greater than 0.75 for large nozzles operating at low ambient pressure.

By definition, the weight of the complete propulsion system is simply related to the propellant exhaust circuit power requirements by

$$W_t = \Phi_K P_e \quad [5]$$

where Φ_K is the propulsion system gross specific weight in lb/exhaust-circuit-Mw. The detailed functional form of Φ_K depends upon the choice of system type, since different components may be used to make up each different system.

Combining Equations [2 through 5] to eliminate direct weight terms, the vehicle gross specific impulse becomes

$$I_g = \left[\frac{2.18 \times 10^{-5} I_{sp}\Phi_K}{\eta_e t_b} + \frac{\lambda}{I_{sp}}\right]^{-1} \quad [6]$$

where $\lambda = 1 + (W_d/W_0)\ \Phi_{\xi}$. The maximum value of I_g occurs when

$$I_{sp} = 214\sqrt{\lambda\eta_e t_b/\Phi_K} \quad [7]$$

Note that the optimum propellant specific impulse or exhaust velocity thus depends principally upon the operating time and the propulsion system gross specific weight. For this condition Equation [6] reduces to

$$\left.\begin{aligned} I_g &= 107\sqrt{\eta_e t_b/\lambda\Phi_K} \\ \text{or} \\ I_g &= I_{sp}/2\lambda = 2.3 \times 10^4\ \eta_e t_b/I_{sp}\Phi_K \end{aligned}\right\} \quad [8]$$

Now, the vehicle thrust-to-weight ratio is found from Equations [2 and 8] to be

$$F/W_0 = 2.3 \times 10^4 \eta_e/I_{sp}\Phi_K \quad \ldots\ldots\ldots\ldots [9]$$

for the units given previously. Fig. 5 shows this relation graphically for several arbitrary values of Φ_K, for an expansion efficiency of $\eta_e = 0.8$. Note that one gravity acceleration (i.e., $F/W_0 = 1$) requires a propulsion system specific weight of 18.4 lb/exhaust-circuit-Mw for a propellant specific impulse of 1000 sec.

For the thermomechanical gas compression system previously discussed, the gross specific weight is made up of terms describing the turbine-compressor set, reactor, radiator, and the secondary (exhaust) circuit gas compressors. A "reasonable" estimate of a minimum value of Φ_K can be made for this system, assuming operation at a radiator temperature of 3000 R, reactor exit gas temperature of 4000 R, and the use of very lightweight rotating machinery. Similar estimates can be made for the d-c arc and ion accelerator electrical systems, using data on presently available lightweight electrical generators. Typical estimated minimum values for the principal components of each system are shown in Table 2, assuming operation at the conditions given above. In general it appears that the minimum system specific weight attainable with present-day equipment is the order of 1000 lb/exhaust-circuit-Mw. For this value Fig. 5 shows that the vehicle thrust-to-weight ratio will be less than 0.07 for propellant specific impulse greater than 250 sec. Such systems thus appear to be of potential use only in free-fall conditions where no artificial acceleration requirements (such as overcoming the earth's field) exist.

A reduction in system specific weight of about a factor of 100 seems necessary in order to permit operation with high specific impulse and high thrust-to-weight ratio. Unfortunately the outlook is not bright for order of magnitude reductions in the specific weight of heat engine rotating machinery. Great decreases in weight require corresponding increases in the strength of materials used in construction. These do not appear on the research horizon at present. Significant reduction in the weight of electrical generators may possibly be made if electrostatic fields can be used as the basis for generator design (9), rather than electromagnetic fields with their attendant massive magnetic flux guides. However, reduction of the generator weight in electrical cycle systems simply reasserts the problem of reducing the turbine-compressor-radiator weight in the reactor circuit. What is really needed here is a conceptually new, and lightweight, method of producing shaft power or electrical power from fission. The efficient production of electricity directly from nuclear processes (10) would at last provide the key to space travel and the practical exploration of our solar system.

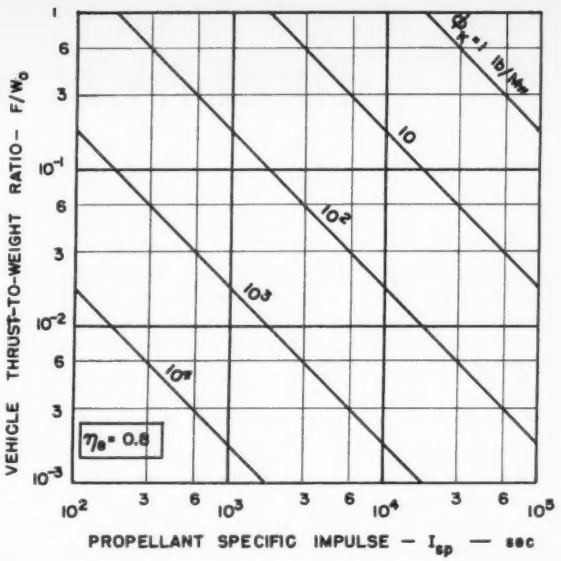

Fig. 5 Generalized performance of reactor system powered vehicles

Table 2 Estimated minimum specific weights for reactor system components

Thermomechanical Gas Compression System

Component	Estimated specific weight per unit power handled	Specific weight per unit power in exhaust circuit
Turbine-compressor	300 lb/Mw	= 300 lb/Mw
Radiator	50 lb/Mw, 20% reactor circuit efficiency	= 200 lb/Mw
Reactor	5 lb/Mw, 20% reactor circuit efficiency	= 25 lb/Mw
Gas compressors	100 lb/Mw, 5 compressors assumed in series	= 500 lb/Mw
TOTAL	Φ_K	= 1025 lb/Mw
Electric d-c Arc or Ion Acceleration System		
Reactor circuit	(see above)	= 525 lb/Mw
Electrical generator	1000 lb/Mw	= 1000 lb/Mw
Arc electrodes and container, or accelerator structure	25 lb/Mw	= 25 lb/Mw
TOTAL	Φ_K	= 1550 lb/Mw

References

1a Shepherd, L. R., and Cleaver, A. V., "The Atomic Rocket—1 and 2," *Journal of the British Interplanetary Society*, vol. 7, no. 5 and 6, 1948.

1b Tsien, H. S., "Rockets and Other Thermal Jets Using Nuclear Energy," Chap. 11 of "The Science and Engineering of Nuclear Power," vol. II, edit. by Clark Goodman, Addison-Wesley Press, Cambridge, Mass., 1949.

1c Bussard, R. W., and DeLauer, R. D., "Nuclear Rocket Propulsion," McGraw-Hill, New York, 1958.

2 Post, Richard F., "Controlled Fusion Research—An Application of the Physics of High Temperature Plasmas," *Review of Modern Physics*, vol. 28, no. 3, July 1956, pp. 338–362.

3 "Review of Fission Product Heat Sources for Power Generation in the 1–5 KW Range," Vitro Engineering Division, Vitro Corporation of America, KLX-1735, Office of Technical Services, Department of Commerce, Washington, D. C., Nov. 5, 1954.

4 Seifert, H. S., and Mills, M. M., "Problems in the Application of Nuclear Energy to Rocket Propulsion," Jet Propulsion Laboratory, Memo 3-4, Jan. 23, 1947, p. 2. Abstracted in *Physical Review*, vol. 71, 1947, p. 279.

5 Serber, Robert, "The Use of Atomic Power for Rockets," Project Rand, RAD-2, July 5, 1946, pp. 1–3.

6 Safonov, G., "The Criticality and Some Potentialities of Cavity Reactors," (abridged), Rand Corporation, RM-1835, July 17, 1955.

7 Shepherd, L. R., and Cleaver, A. V., "The Atomic Rocket—3," *Journal of the British Interplanetary Society*, vol. 8, Jan. 1949, pp. 23–24, 30–37.

8 Praining, O., "The Attainment of High Temperatures (up to 55,000°K) Under Laboratory Conditions," *Uspekhi Fiz. Nauk*, vol. 55, no. 4, 1955, pp. 595–608.

9 Brosan, G. S., "An Electrical Machine for Use in Extra-Terrestrial Environment," *Journal of the British Interplanetary Society*, vol. 14, no. 5, Sept. 1955.

10 Colgate, S. A., and Aamodt, R. L., "Plasma Reactor Promises Direct Electric Power," *Nucleonics*, vol. 15, no. 8, Aug. 1957, pp. 50–55.

Plasma Physics and Hypersonic Flight

J. W. BOND JR.[1]

Convair Division of General Dynamics Corporation, San Diego, Calif.

This paper reviews some of the effects of the presence of free electrons in a hypersonic shock layer. Shock front structure and boundary layer structure are briefly discussed and some of the differential plasma properties are mentioned.

Introduction

WHEN an object travels through air at altitudes below something like 200,000 ft and at Mach numbers greater than 12 to 15, the production of electrons in the shocked layer of air which surrounds the object has a significant effect on some of the properties of the shocked air. Above some altitude like 200,000 ft the influence of the electrons is felt at even lower Mach numbers, particularly in the ionosphere where the ambient electron density is no longer negligible.

The influence of electrons is felt not only on aerodynamic quantities such as heat transfer, drag and flow field, but also on physical quantities such as transport properties, radiative emission and absorption, and electromagnetic signal interaction. The main thesis of the present paper is to show how, and under what conditions, the electrons produced by the passage of a high speed missile through the atmosphere significantly affect both aerodynamic and physical quantities.

A plasma may be defined as a gas containing electrons in sufficient quantity to seriously affect the physical properties of the gas. Plasma physics then is simply the physics of such a gas. For example, the air in the shock layer surrounding a hypersonic missile may be in a plasma state if the missile is traveling at an extremely high velocity.

We will first discuss in general terms the structure of a hypersonic axially symmetric flow field. This will be followed by a more detailed discussion of the shock front and boundary layer with emphasis on the electron distribution. We will then show an example of an analysis of the Boltzmann equation and the relationship of the electron scattering cross section and the electron velocity distribution function.

Aerophysics

At hypersonic velocities a detached shock surrounds a blunt nosed object as it travels through the atmosphere, provided the ambient density is sufficiently high. For Mach numbers up to about 30 this density corresponds to altitudes below about 200,000 ft for hypersonic missiles. A schematic diagram of the flow of air about a hemisphere cylinder is shown in Fig. 1.

The *shock front* is a nonequilibrium region in which energy is being transferred from the translational degrees of freedom of the air molecules to various internal degrees of freedom. A more detailed discussion of the shock front is given below.

Immediately adjacent to the surface of the missile is the *boundary layer*. It is a narrow region in which the tangential gas velocity increases from zero at the surface to the local flow velocity in the shock layer.

In between the shock front and the boundary layer is the *shock layer*. At the lower altitudes it is a region of thermodynamic equilibrium; but at higher altitudes it can be a region of nonequilibrium due to the increase in relaxation times with decreasing density. In addition, at the higher altitudes the shock front and boundary layer thicknesses increase; and at some altitude they may overlap in such a way that the equilibrium shock layer disappears.

The wake, or afterflow region, contains the rocket exhaust; or, in the case of a ballistic missile, the wake is a region of low density, high temperature, turbulent flow.

The conditions which exist in the shock layer in the vicinity of the stagnation point in front of a blunt object traveling through the atmosphere at hypersonic speed are approximately the same as those which exist behind a normal shock front. Thus the one-dimensional shock relations may be used to compute the equilibrium conditions in the stagnation region. This has been done for a sphere entering the earth's atmosphere at about 24,000 fps and at an angle of about 20 deg to the horizontal (1).[2] The velocity and Mach number trajectories along with the corresponding values of the thermodynamic variables in the stagnation region of the shock layer are shown in Fig. 2. The shock compression η is the ratio of the density behind the shock to that in front of the shock, and the shock strength ξ is the corresponding pressure ratio.

The composition of the air in the stagnation region is shown for the trajectory in Fig. 3 along with corresponding values for the effective gamma (ratio of enthalpy to internal energy) and compressibility factor $g = pV/RT$. (Note that g is equivalent to the average number of particles into which an average initial air molecule has been dissociated or ionized.)

Before considering some of the details of the boundary layer and shock front the flow field will be discussed briefly. In the first approximation the shock front can be considered as negligibly thick compared to the shock layer. This is a good approximation at low altitudes. The flow field is then one of axial symmetry and varies from subsonic in the stagnation region to supersonic after about 40 deg about the hemisphere and to hypersonic along the cylinder. An analytic solution to

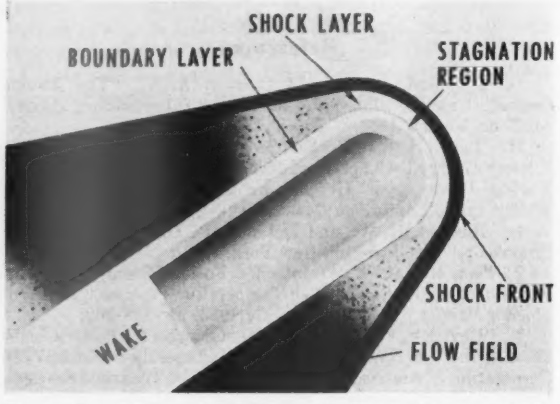

Fig. 1 Flow about a hemisphere cylinder moving through the atmosphere at hypersonic speeds

Received Sept. 12, 1957.

[1] Chief of Physics.

[2] Numbers in parentheses indicate References at end of paper.

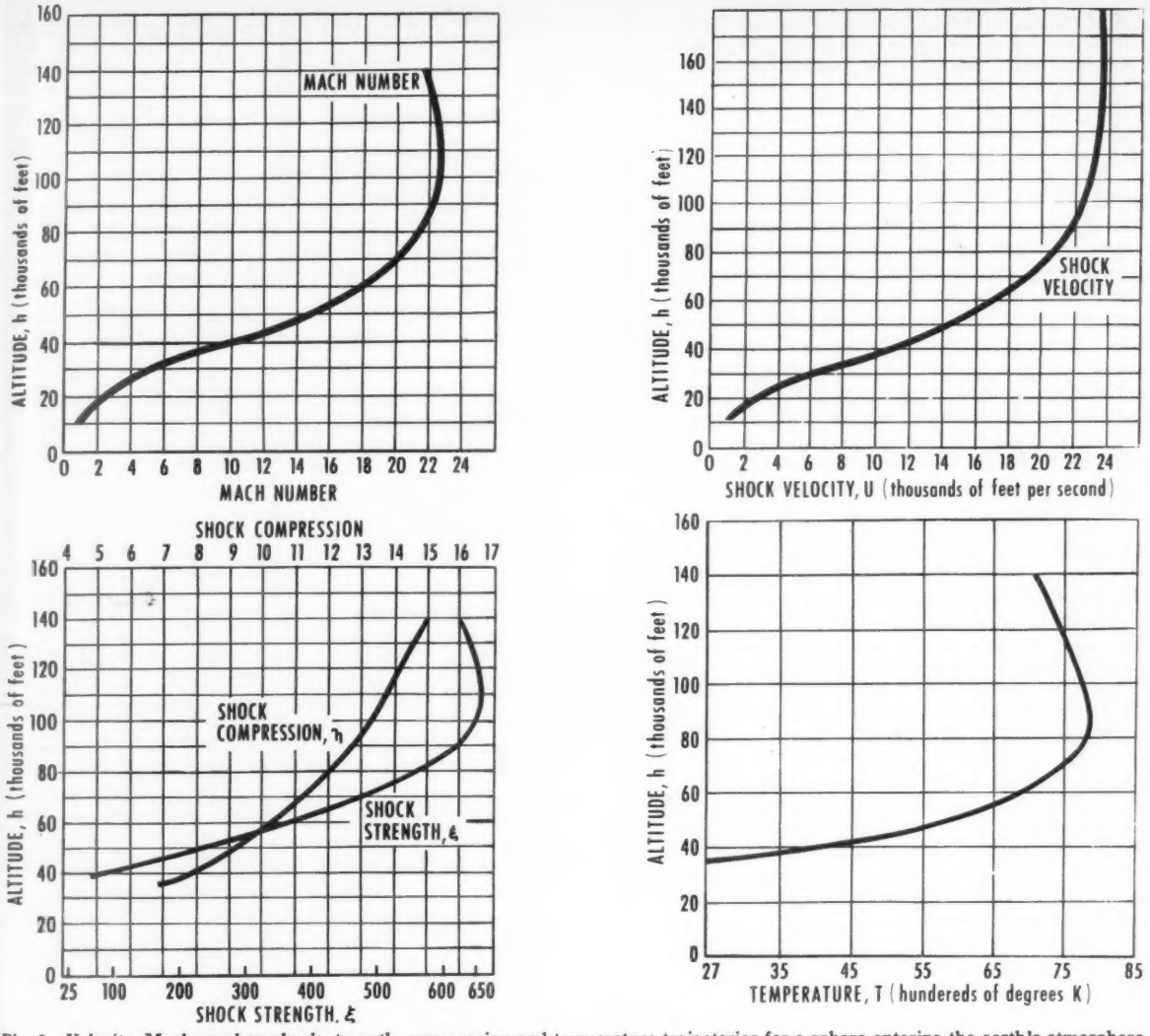

Fig. 2 Velocity, Mach number, shock strength, compression and temperature trajectories for a sphere entering the earth's atmosphere at 24,000 fps and an angle of 20 deg to the horizontal (stagnation region values)

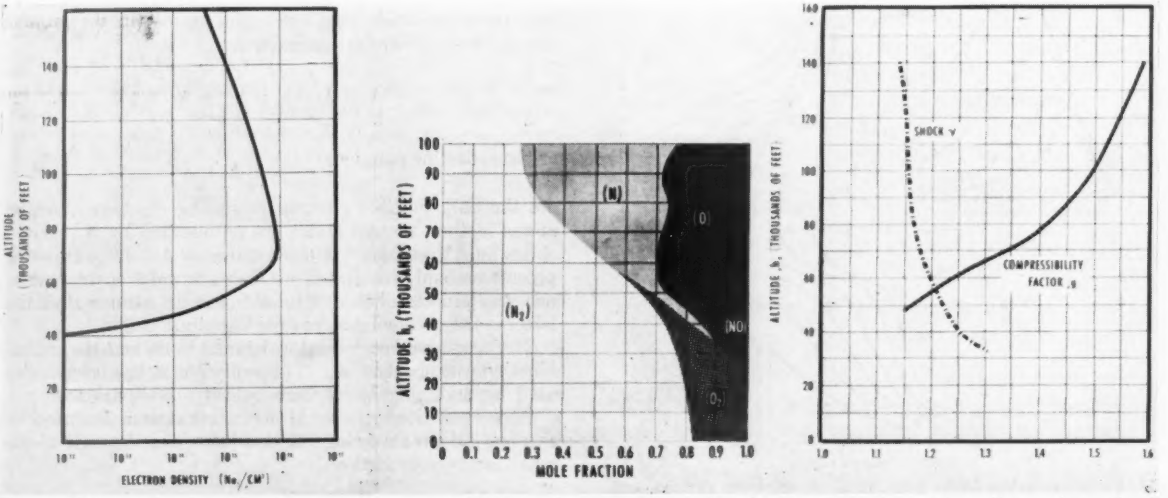

Fig. 3 Electron density, effective gamma, compressibility and composition trajectories for the sphere (stagnation region values)
NOTE: Electron densities were computed for a slightly different trajectory

such a flow field has not been obtained; however, numerous attempts have been made to obtain a good numerical solution. Most of these attempts have failed, primarily because of problems involving numerical instability near the sonic line. Even for the case of a constant gamma gas such as helium (below about Mach 25) a good numerical solution is difficult.

It is difficult to obtain a numerical solution because both the shock front and the sonic line are hard to locate. Also, when the shock front is assumed to be a discontinuity, it is difficult to integrate across it by ordinary methods. This difficulty can be circumvented by smearing the shock front out with the use of an artificial viscosity (2). Several mass points can then be located within the shock front and the integration carried out. The trouble with this method is inadequate machine storage space. Recently, a promising method has been developed by Harlow at the Los Alamos Scientific Laboratory (3, 4). It is called the "particle-in-the cell" method. The name follows from the representation of the hydrodynamic flow field by discrete particles that move in fixed cells.

Shock Front Structure in Air

We are concerned here primarily with the determination of electron densities rather than atom or molecule densities. However, since electrons are produced by ionizing collisions involving one or more of the heavier particles, it becomes necessary to determine the particle density of the atoms or molecules which are most directly concerned in the production of free electrons. In the case of air the situation is complicated by the formation of nitric oxide, NO. At the ambient conditions which exist in the atmosphere in front of the shock, the concentration of NO is completely negligible. However, behind the normal shock front the concentration may be as high as 10 per cent (cf. Fig. 4). The rate at which NO is formed in a shock front is difficult to calculate because the equilibrium concentration of NO is a maximum at about 5000 K and drops off rapidly for either higher or lower temperatures. In addition, there is a strong density dependence. Also plotted on Fig. 4 are the equilibrium values for γ and g as functions of density and temperature.

Corresponding to the previous definition, the shock front is the nonequilibrium region between the undisturbed air in front of the shock and the region in the shock layer behind the shock where thermodynamic equilibrium can first be assumed to exist. The "local" gas temperature inside the shock front

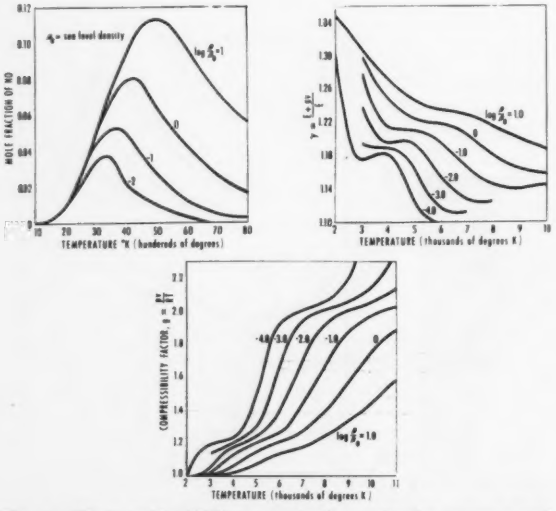

Fig. 4 Nitric oxide (NO) concentration, effective gamma and compressibility factor as functions of density and temperature for air

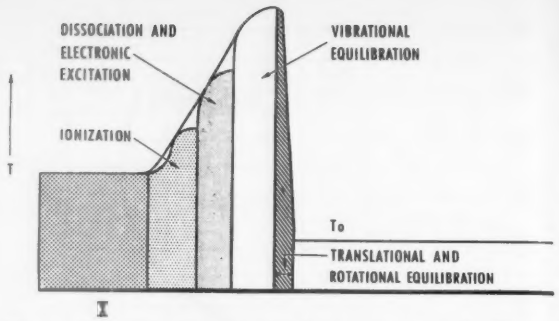

Fig. 5 Schematic diagram showing temperature distribution through a shock front in air

is considerably higher than the equilibrium temperature behind the shock front. A schematic diagram of the temperature distribution is shown in Fig. 5.

The ionization potential of NO is lower than any other major component of air in the temperature range of interest. Hence, most of the electrons present in the shock layer probably come from reactions involving NO or NO^+; for example

$$N + O \rightleftarrows NO^+ + e \quad \ldots\ldots [1]$$

is the most influential reaction in controlling the electron density.

In view of the complexity introduced into the structure of a shock front in air by the formation of NO, the structure of shock fronts, first in a monatomic gas, argon, and second in a pure diatomic gas, oxygen, will be considered. Let Δ_e be the distance between the front of the shock and the point behind the shock at which the electron density can be assumed to have (essentially) reached its equilibrium value. An estimate of Δ_e for argon, oxygen and air has been made for normal shocks as a function of density in front of the shock. The electron and plasma temperatures will be assumed to be equal for the three gases.

Consider a shock wave in pure argon. If an argon atom is initially at density and temperature ρ_1 and T_1, where the subscript 1 refers to conditions in front of the shock, then upon being struck by a strong shock the translational degrees of freedom are excited to conditions ρ' and T' within a distance of about two mean free paths $2L_1$. If T' is sufficiently high, energy will be transferred to other degrees of freedom such as electron excitation and ionization with resulting decrease in temperature and increase in density. At the peak of the shock front, represented by the conditions ρ', T', the only particles which exist are argon atoms (in the ground state); hence the ionization reaction

$$A + A \underset{\alpha_1}{\overset{\beta_1}{\rightleftarrows}} e + A^+ + A \quad \ldots\ldots [2]$$

or the excitation reactions

$$\left.\begin{aligned} A + A &\rightleftarrows A^* + A_{slow} \\ A + A^* &\rightleftarrows e + A^+ + A \end{aligned}\right\}$$

are the only possible electron producing reactions. Argon atoms in their ground states are represented by A, excited states by A*, and singly ionized states by A^+. The two-step process probably requires about the same order of time as the one-step process; hence, it is sufficient to assume that the latter is the predominant process initially.

The production coefficient is denoted by β_1 and the recombination coefficient by α_1. The coefficient β_1 has been evaluated by assuming Maxwellian velocity distributions (5).

Once a sufficient number of electrons has been produced by reaction [2] the following reaction takes over because of the much larger cross section

$$e + A \underset{\alpha_2}{\overset{\beta_2}{\rightleftarrows}} 2e + A^+ \quad \ldots\ldots [3]$$

The point where this reaction becomes predominant is called the *onset of ionization;* after this point is reached elections are produced at a much higher rate. In fact, the time required for the onset of ionization to occur probably represents over half of the shock front thickness; hence, it will be assumed that Δ_e is given to a sufficient degree of accuracy by the onset thickness.

If it is assumed that reactions [2 and 3] are the two predominant reactions up to the onset position, then the source term may be written as

$$\frac{dn_e}{dt} = \frac{\partial n_e}{\partial t} + \frac{\partial (un_e)}{\partial X} = S \quad \ldots\ldots [4]$$

In this relation n_e is the electron density, u the material velocity, X the Eulerian distance coordinate and

$$S = \beta_1 n_A^2 + \beta_2 n_e n_A \quad \ldots\ldots [5]$$

where (n_A is the atom density.) Recombination terms as well as other processes should be included in the expression for S; however, it is a good approximation to omit these terms in the region including and preceding the onset point.

In a Lagrangian system, where x' is the distance coordinate, Equation [5] becomes

$$\frac{dn_e}{dt} = \frac{\partial n_e}{\partial t}\Bigg)_{x'} = S - n_e \frac{\rho}{\rho_1} \frac{\partial u}{\partial x'}$$

If the equation of continuity

$$\rho_1 \frac{\partial V}{\partial t} = \frac{\partial u}{\partial x'} \qquad V = \frac{1}{\rho}$$

is inserted, the result is

$$\frac{d \ln (n_e V)}{dt} = \frac{S}{n_e} \quad \ldots\ldots [6]$$

Let the degree of ionization x be given by

$$x = \frac{n_e}{n_A + n_e} \quad \ldots\ldots [7]$$

In this relation it is assumed that the electron and ion densities are equal. Since $\rho = m(n_A + n_e)$ where m is the mass of an argon atom, then $n_e V = x/m$, and Equation [6] becomes

$$\frac{dx}{dt} = \frac{\beta_1 \rho}{m} + \frac{x\rho}{m}(\beta_2 - 2\beta_1) - x^2 \frac{\rho}{m}(\beta_2 - \beta_1) \quad \ldots\ldots [8]$$

Up to the onset point the density ρ is fairly constant and the degree of ionization extremely small; hence Equation [8] may be integrated to give

$$x = \frac{\beta_1}{\beta_2 - 2\beta_1}\left[e^{(\rho/m)\cdot(\beta_2 - 2\beta_1)\, t} - 1\right] \quad \ldots\ldots [9]$$

At the onset point the first two terms on the right of [8] are equal. From this and the assumption that the density does not change much up to the onset point, the (Eulerian) onset distance is given by

$$X'' = \frac{2.9 \times 10^{-24}\ \mathbf{U}}{\rho_1(\beta_2 - 2\beta_1)} \quad \ldots\ldots [10]$$

From this relation it is apparent that the shock front thickness goes, at least to a first approximation, inversely as the ambient density in front of the shock. The coefficients β_1 and β_2 are, of course, functions of the shock velocity $\mathbf{U}$.

The production coefficients β_1 and β_2 depend on the temperature and not on the density. The dependence of β_1 is on the atom, or plasma, temperature T, whereas β_2 depends on the electron temperature T_e. If the electron temperature is about the same as the plasma temperature, then $\beta_2 \gg \beta_1$ and X'' becomes

$$X'' = \frac{2.9 \times 10^{-24}\ \mathbf{U}}{\rho_1 \beta_2} \quad \ldots\ldots [11]$$

A few approximate values of X'' are given in Table 1.

Table 1 Approximate values for the thickness of an argon shock front (assuming $T_e = T$)

$\mathbf{U}$, cm/sec	$X''(\rho_1 = 1.3 \times 10^{-3}$ gm/cm^3)	$X''(\rho_1 = 1.3 \times 10^{-7}$ gm/cm^3)
5×10^5	3.4×10^{-4} cm	3 cm
6×10^5	1.6×10^{-4} cm	2 cm

Table 1 shows that if the density is decreased by a factor of 10^{-4} the shock front thickness becomes of the order of centimeters. If these values are extrapolated to the case of air, then at an altitude of about 200,000 ft the shock front thickness may be of the same magnitude as the shock layer thickness.

For argon the effective electron temperature inside the shock front is different from the plasma temperature (5). In order to estimate the electron temperature an additional relation is needed. This may be taken as an energy balance between ionizing collisions and Coulomb collisions. If this is done it is found that the shock front thickness for argon is considerably larger than the values noted in the table. However, for air, correspondence principle arguments may be used to show that the electron and plasma temperatures are probably about the same, although it should be pointed out that the concept of a "local" temperature inside the shock front is highly questionable.

A shock front in pure oxygen is considerably more difficult to analyze than one in pure argon. In the first place there are additional degrees of freedom of rotation, vibration, dissociation and molecular electronic excitation and ionization. In addition, both the oxygen molecule and, particularly, the oxygen atom have large electron affinities. Processes in which these various quantities are concerned involve cross sections which, for oxygen, are largely unknown.

It is obvious that the equilibration process occurs in such a way that the excitation of the various degrees of freedom occurs conjointly; however, the rates of excitation differ. In order to approximate the equilibrium process we may assume that vibrational equilibrium is achieved in times small compared to those for dissociation equilibration. The corresponding gamma used to compute the thermodynamic quantities is

$$\gamma = \frac{9}{7} = 1.223$$

For this value of γ

$$\eta_\infty = \frac{\gamma + 1}{\gamma - 1} = 8 \quad \ldots\ldots [12]$$

and (denoting onset values by a double prime)

$$\xi'' = \frac{2\rho_1 \mathbf{U}^2}{p_1(\gamma + 1)} - \frac{1}{\eta_\infty} = 1.1 \times 10^{-9}\ \mathbf{U}^2 - \frac{1}{\eta_\infty} \quad \ldots [13]$$

The corresponding compression is given by

$$\eta'' = \frac{\eta_\infty \xi'' + 1}{\xi'' + \eta_\infty} \quad \ldots\ldots [14]$$

and the temperature by

$$T'' = \frac{\xi'' T_1}{\eta''} \quad \ldots\ldots [15]$$

We have used the concept of onset for oxygen because of its usefulness in the argon analysis. Actually, the analogy with argon is not very good.

In addition to the internal degrees of freedom which oxygen has, there are many low-lying electronic states. Also, impact ionization is relatively unimportant in an oxygen shock front.

The predominant reactions are probably

$$\left.\begin{array}{ll} O_2 + O_2 \rightarrow 2O + O_2 & (\Delta E \sim 5.1 \text{ ev}) \\ O + O_2 \rightarrow 3O & (\Delta E \sim 5.1 \text{ ev}) \\ O + O \rightarrow O_2^+ + e & (\Delta E \sim 7.4 \text{ ev}) \end{array}\right\} \quad \ldots\ldots [16]$$

The production coefficients in the expression for the source terms S in Equation [5] are simply the Maxwellian averages $\overline{\sigma v}$; hence, from Equation [11]

$$\frac{\beta_2(O_2)}{\beta_2(A)} = \frac{\dfrac{\Delta E(O_2)}{kT(O_2)} \exp\left[-\dfrac{\Delta E(O_2)}{kT(O_2)}\right]}{\dfrac{I(A)}{kT(A)} \exp\left[-\dfrac{I(A)}{kT(A)}\right]} = \frac{X'(A)}{X'(O_2)} \quad \ldots [17]$$

This relation may be used to obtain an order-of-magnitude estimate for the oxygen shock front thickness. (It would be more correct to use the threshold energies which are somewhat higher than the ionization energies. Also, it is assumed in [17] that the difference between the ionization energy and the threshold energy may be scaled.)

Instead of doing a detailed analysis for oxygen we will consider the more complicated case of air. The complexity introduced into the computation of the shock front structure by the formation of nitric oxide has already been mentioned. The presence of NO will, because of its low ionization potential (9.5 ev), tend to make the onset distance less. However, there are processes other than impact ionization from which electrons may be obtained. For example, reaction [1] can easily go to the right but NO^+ is likely to dissociate before colliding with an electron; hence the recombination process [1] going to the left can be neglected prior to onset. Some other possible electron-producing reactions might be

$$N + O^- \rightarrow NO + e \quad \ldots\ldots [18]$$

$$O + O^- \rightarrow O_2 + e \quad \ldots\ldots [19]$$

In addition to the displacement type of reactions [1, 18 and 19], there are various impact ionization reactions.

Table 2 Some energy levels for air

Specie	Dissociation potential, ev	Ionization potential, ev	First electronic level, ev
N_2	9.7	15.51	6.0
O_2	5.08	12.5	0.9
N	...	14.54	2.38
O	...	13.61	1.96
NO	6.48	9.5	3.8
NO^+	10.6	...	...
O^+	...	35.15	...
N^+	...	29.61	...
N_2^+	8.72	...	...
O^-	...	−1.48	...
A	...	15.76	11.5

In order to obtain a feeling for the magnitude of the shock front thickness in air it seems reasonable to compare the relaxation times for the two (competing) processes

$$NO + M \xrightarrow{\beta_3} NO^+ + e + M \quad \ldots\ldots [20]$$

$$N + O \xrightarrow{\beta_4} NO^+ + e \quad \ldots\ldots [21]$$

In these reactions M represents any particle, β_3 is the production coefficient, and τ_3 the relaxation time for [20]; β_4, τ_4 are the corresponding quantities for [21]. If one of the relaxation times is much smaller than the other then the process corresponding to the longer time can be neglected. However, if

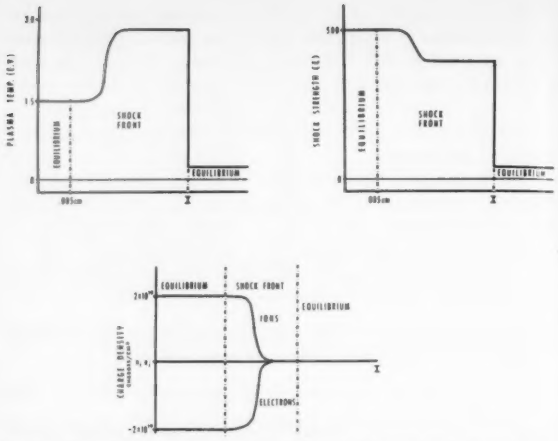

Fig. 6 Details of an argon shock front ($V \sim 6 \times 10^5$ cm/sec, $\rho_1 \sim 0.001$ gm/cm^3, $T_1 \sim 300$ K)

τ_3 and τ_4 are about equal, some sort of average relaxation time must be used. The energy balance for [20] is simply the ionization potential for NO, i.e., $\Delta E_3 = 9.5$ ev. For [21], the energy balance is $\Delta E_4 = 3$ ev.

The ratio of the relaxation times is, very roughly, given by

$$\frac{\tau_3}{\tau_4} = \frac{e^{-\Delta E_4/kT}}{e^{-\Delta E_3/kT}}$$

If the temperatures are equal then

$$\frac{\tau_3}{\tau_4} = e^{6.5/kT}$$

Since kT is about 1 ev or less, it follows that $\tau_3 \gg \tau_4$; hence reaction [21] should be the predominant reaction for the determination of Δ_e for air.

The analysis of the rate at which [21] proceeds inside a shock front in air depends upon the rates at which N and O are separately produced. The rate for the production of atomic oxygen can, to a good approximation, be computed from the coupled reactions

$$\left.\begin{array}{l} O_2 + O_2 \xrightarrow{\beta_5} 2O + O_2 \\ O + O_2 \xrightarrow{\beta_6} 3O \end{array}\right\} \quad \ldots\ldots [22]$$

(The rate for the production of atomic nitrogen can similarly be estimated.)

If x is the degree of dissociation, then for [22]

$$\frac{dx}{dt} = 6.10^{18} T^{1/2} e^{-5.1/kT} \left(\frac{5.1}{kT} + 1\right) \rho_1 \eta (1 - x) \ldots [23]$$

This equation, together with the equation of state and the Rankine-Hugoniot relations, can be numerically integrated across the shock front. An approximate integration of [23] along with the corresponding equations for the production of atomic nitrogen and for the production of electrons [21] indicates that between altitudes of 100,000 and 200,000 ft the shock front thickness is of the order of centimeters,[3] thus implying that the concept of an inviscid (or equilibrium) flow field above these altitudes may not be correct.

The above discussion should serve as an introduction to the general problem of shock front structure and the distribution of electrons through the shock front. However, it is not intended that a detailed analysis should be presented in this paper. Such an analysis has been made for argon and some

[3] Recent experimental results obtained at Princeton University by V. Blackman and his collaborators confirm this theoretical result (private communication).

numerical results are given below. In obtaining the argon results both the effect of an electron temperature different from the plasma temperature and the influence of various recombination processes were considered.

The numerical results for argon (see Fig. 6) have received some rough experimental confirmation by LaPorte and his students at the University of Michigan and by Kantrowitz and his collaborators at Cornell. In addition, some measurements were made at the Los Alamos Scientific Laboratory which also seem to confirm the argon results.

It has been difficult to obtain similar results for air because of the following reasons: Analytically the problem is complicated by the presence of additional degrees of freedom, the influence of low-lying excited electronic states, the numerous types of chemical species, and the lack of information on cross sections (or reaction rates). Experimentally, it has not been possible, until very recently, to produce sufficiently strong shocks in shock tubes to give the degree of ionization needed to make the same types of measurements as were made on the argon shock front, viz., measurements of electrical conductivity and of radiation.

Electric Potential in Gaseous Shock Fronts

With the above review of the flow structure about a hypersonic vehicle we are now in a position to discuss some of the plasma properties of the flow field. One such property is the positive electric potential that exists in strong gaseous shock fronts. Evidence of this potential was found about ten years ago by probe measurements made at the Los Alamos Scientific Laboratory.

These positive potentials come about as follows: In the argon shock front, once the onset point has been reached, there is a sudden increase in pressure and number density (including electron density), and a decrease in temperature. The resulting gradients exert a force on the electrons which is such as to cause a diffusion of electrons toward the front of the shock. The current may be symbolically written as

$$j\ (\text{total}) = j\ (\text{pressure}) + j\ (\text{density}) - j\ (\text{temperature}) - j\ (\text{Coulomb})$$

The first term on the right represents the current resulting from the positive pressure gradient, and the second term, that resulting from the positive gradient in the number density of the electrons. The third term is negative because the temperature gradient is negative. The fourth term results from the electric or Coulomb force between the electrons and the ions. The first three terms are shown schematically in Fig. 7. It is evident that the current due to the gradient in the electron density is by far the most important contribution to the total current.

In obtaining the currents the gas was treated as a binary mixture consisting of electrons n_1 and partially charged positive ions n_2 where $n = n_1 + n_2$. The equation used was

$$j = \frac{-n^2 e}{n_2} D_{12} \left\{ \frac{\partial}{\partial X}\left[\frac{n_1}{n}\right] + \frac{n_1}{np}\frac{\partial p}{\partial X} + \frac{k_T}{T}\frac{\partial T}{\partial X} \right\} + \frac{4\pi e^3 n_1 n^2 D_{12}}{n_2 p} \int (n_e - n_{A^+}) dX \quad \ldots\ldots [24]$$

The evaluation of the binary diffusion coefficient D_{12} and the thermal diffusion ratio k_T involves integrals containing the Coulomb force. Such integrals are usually divergent unless finite limits are assumed.

In our case the limit is the Debye shielding distance which is simply the relaxation distance which an electron can be expected to diffuse in a plasma. It is given by h where

$$h^2 = \frac{kT}{8\pi e^2 n_e}$$

and is contained in the electrostatic potential which must satisfy Poisson's equation, where the potential is given by

$$\phi = \frac{A}{r} e^{-r/h} \qquad (A = \text{const})$$

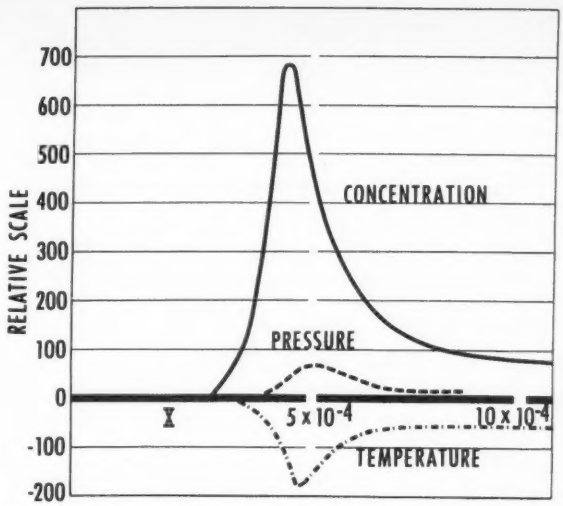

Fig. 7 Relative current densities due to electron diffusion in an argon shock front

The concept of plasma shielding implies that the density of free charges, i.e., ions and electrons, is sufficiently large so that electron collisions are collective rather than individual. This means that the electron sees the effective Coulomb field of a number of charges rather than that of each charge separately. Such a condition exists for electron densities sufficiently high to cause *onset* incidence.

Equation [24] was numerically evaluated to obtain the charge density resulting from the diffusion of electrons toward the front of the shock. This diffusion process causes a dipole or double layer to form in the shock front. If the charge distribution is integrated once the electric field is obtained, a second integration gives the electric potential. The numerical results are shown in Fig. 8.

The theoretical values given above for argon are in qualitative agreement with the experimental values obtained at Los Alamos. The corresponding theoretical values for air have not been worked out but experimental values have been obtained. The measured potential for air is considerably smaller than it is for argon, in accordance with the theory of the shock front given in the previous section.

Although the theory for air has been worked out, numerical values will be difficult to obtain until better values for some of the reaction cross sections are available. These cross sections are not as easy to compute for air as they are for argon because of the presence of diatomic molecules including nitric oxide NO and because of the many low-lying electronic states that occur in high temperature air.

Plasma Effects in Boundary Layers

The air in the shock layer about a Mach 20 missile may be ionized as high as 1 per cent. In this case there may be a sufficient number of electrons to diffuse through the boundary layer causing a negative potential within the boundary layer. Equation [24] should then be applicable. The second term on the right, which involves the pressure gradient, is negligible but the first and third terms both cause diffusion currents to flow toward the wall. (Note that in the shock front these two terms have opposite effects.)

In general, a missile flying at velocities where electron diffusion might become important will also have a reacting wall

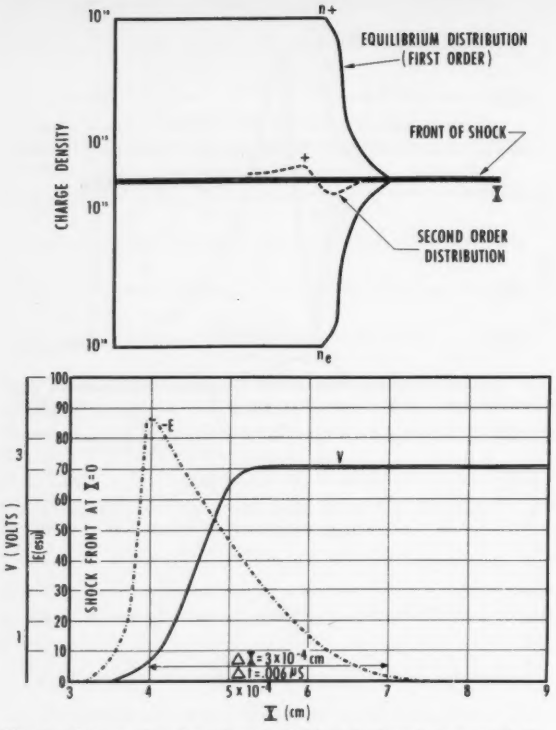

Fig. 8 Charge density, electric field and electric potential distribution in an argon shock front

which would submerge the effects of the electron diffusion. It is extremely difficult to predict what the wall effects may be and, although considerable work has been done on this problem in the study of probe potentials, the theory is far from being complete.

Another problem which may involve plasma effects is that of transport properties. For example, the thermal conductivity of air may be expected to increase with temperature up to the point where plasma effects must be considered. For air, this temperature is about 5000 K and, for nitrogen, somewhat higher. Theoretical and experimental values for the thermal conductivity of air and nitrogen are shown in Fig. 9 (6).

Boltzmann Equation Analysis

It has been implied in a foregoing section that one may compute the quantity $\overline{\sigma v}$ by simply averaging over a Maxwellian distribution. However, this is in general not true because the velocity distribution functions are probably non-Maxwellian inside a shock front—especially for the electrons (5). In addition, the cross sections are not well known.

The quantity $\overline{\sigma v}$ also enters into the dielectric coefficient of the shock layer plasma. The dielectric coefficient, in turn, affects the transmission of microwaves through the shock layer.

In both the computation of shock front reaction rates and microwave transmission the Boltzmann equation is used. (Of course, the hydrodynamic flow equations, with or without dissipation terms, may also be derived from the Boltzmann equation.) In order to show this, a brief discussion and application to microwave transmission is given below.

If $f_s(\vec{v}, \vec{r}, t)$ is the velocity distribution function for particle s, then the Boltzmann equation is

$$\frac{\partial f_s}{\partial t} + \vec{v} \cdot \frac{\partial f_s}{\partial \vec{r}} + \vec{F}_s \cdot \frac{\partial f_s}{\partial \vec{v}} = \left|\frac{\partial f_s}{\partial t}\right|_c \quad \ldots\ldots\ldots\ldots [25]$$

where $m_s \vec{F}_s$ is the force on a molecule of mass m_s and the right-hand side is the collision term which denotes the rate at which f_s is being altered by collisions. We have followed here the notation of Chapman and Cowling (7) so that

$$\vec{v} \cdot \frac{\partial f}{\partial \vec{r}} = u \frac{\partial f}{\partial x} + v \frac{\partial f}{\partial y} + w \frac{\partial f}{\partial z}$$

In case the distribution function is spatially independent, and in the presence of an electric field $E(t)$, Equation [25] reduces to

$$\frac{\partial f}{\partial t} + \frac{eE}{m} \frac{\partial f}{\partial v_y} = \left|\frac{\partial f}{\partial t}\right|_c \quad \ldots\ldots\ldots\ldots [26]$$

where the field is directed along the y-axis. If we now make the assumption that the plasma is weakly ionized so that the collision term contains only interactions between electrons and neutral particles, then the transport equation may be further reduced. This is done by using a suitable integrating multiplier and applying the equation of change (7). The result is

$$\frac{\partial \bar{v}_y}{\partial t} - n \int f(\bar{v}, t) v_y v \sigma(v) d\vec{v} = \frac{eE}{m} \quad \ldots\ldots\ldots [27]$$

In deriving this equation it has been assumed that the velocity distribution function of the neutral particles is Maxwellian. Hence, n is the number density of the neutrals. Also

$$\bar{v}_y = \int f v_y d\vec{v}$$

The total scattering cross section is given by $\sigma(v)$ and is equal to the momentum transfer cross section for low energy impact.

In order to solve [27] it is necessary to know both f and $\sigma(v)$. In practice the distribution function is usually assumed to be Maxwellian. In addition, it is often assumed that either $\sigma(v)$ is constant or that σv is constant. Both cases have received considerable attention. (It is easy to show that, under certain assumptions, Equation [27] may be further reduced to the standard wave equation for which many solutions are available.)

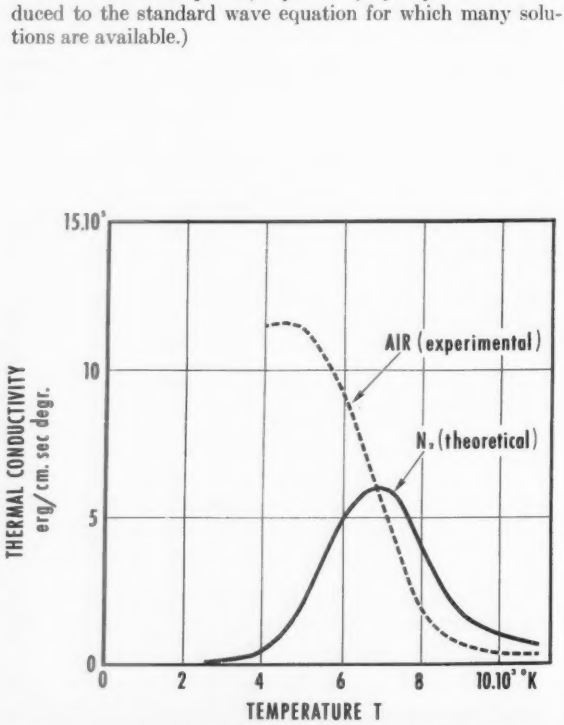

Fig. 9 Thermal conductivity of nitrogen and of air as a function of temperature

Electron Scattering Cross Sections

In the above analysis it has been shown that the total cross section $\sigma(v)$ plays an intimate role in the evaluation of reaction rates. Also, the cross section for the scattering of electrons from atomic or molecular systems is involved in the dielectric coefficient. In fact, the absorptivity of microwaves in plasmas is proportional to some power of the cross section. In case the electron and plasma temperatures are the same, as seems likely for an equilibrium shock layer in air, then the cross section involved is the elastic scattering cross section for electrons with the various atomic species. (This is probably true for missile velocities less than about Mach 20, although it is possible that some inelastic processes compete.)

In recent years there have been numerous attempts to compute or to measure the appropriate cross sections. Unfortunately, the results of the various efforts are not in agreement. In addition, the numerous theoretical evaluations appear to be incomplete or oversimplified. Experimentally, the difficulty is due to the lack of good environmental simulation. Theoretically, the difficulty is due to the presence of exchange and polarization effects at low energies. Exchange effects occur because of the Pauli principle; that is, the spins of each of the electrons involved in a collision can only have two orientations. Polarization effects occur because at the low energies concerned the orbital electrons can be perturbed by the presence of the incoming electron.

Velocity Distribution Functions

Another differential plasma property is the velocity distribution function $f(v)$. It has been assumed in most of the foregoing analysis that $f(v)$ is Maxwellian. This is a good assumption for the heavy particles, i.e., the atoms and ions, but it is probably a poor assumption for the most important plasma constituent, the electrons, in the missile velocity range with which we are concerned. This is because of the following reason: At low temperatures the electron density is low and atom-atom, atom-molecule, or molecule-molecule collisions predominate. In these collisions the masses involved are almost equal and energy transfer is large, thus providing a rapid means of temperature equilibration. At very high temperatures the electron density is large and electron-electron collisions predominate. Again, because of the equal masses involved the temperature equilibration is rapid. However, for intermediate temperatures where collisions between electrons and the various heavier particles are significant the temperature equilibration may be slow.

In most of the equation of state calculations that have been applied to air in the temperature range of interest to us, a modified Saha equation has been used to compute the equilibrium constant. This is simply the mass transfer law and assumes that the distribution functions are Maxwellian. If this is not the case, as seems likely for the electrons over a wide energy range, then the electron densities could be in error by a considerable factor.

For example, one of the factors implicit in the assumption of Maxwellian distributions is that the external energy is negligible. If this is not the case, as for externally applied electric and magnetic fields, then the distribution function for the electrons may well be highly non-Maxwellian.

Let us assume we have solved the Boltzmann equation and the resulting distribution is a Druyvesteyn function (this is the distribution function resulting when the thermal energy of the gas is much less than the externally applied electric energy). A simple analysis then shows that the electron density may be several orders of magnitude less than that obtained from application of the Saha equation (with Maxwellian distribution functions).

Magnetohydrodynamics

The above three sections have to do with differential plasma properties. The term magnetohydrodynamics (or hydromagnetics or magnetoaerodynamics) is primarily concerned with integrated plasma properties. The application lies in the simple fact that the air flowing in the shock layer about a hypersonic missile may be in a plasma state due to thermal agitation or due to artificially induced ionization such as sodium injection. If this plasma is then acted on by electromagnetic fields the plasma properties may be altered in various ways. Recently there have been numerous publications in this field, particularly in the Russian literature. Reference is here made to a few of the articles available in the American literature (8, 9, 10, 11).

References

1 Bond, J. W., Jr., "Equilibrium Conditions Behind a Normal Shock Front in the Atomsphere," Lockheed Aircraft Corp., MSD 1456, Dec. 1955.

2 Kolsky, H. G., "A Method for the Numerical Solution of Transient Hydrodynamic Shock Problems in Two Space Dimensions," Los Alamos Scientific Laboratory LA-1867, Sept. 1954.

3 Harlow, F. H., "A Machine Calculation Method for Hydrodynamic Problems," Los Alamos Scientific Laboratory, LAMS-1956, Sept. 1955.

4 Harlow, F. H., "The Particle-in-Cell Method for Two-dimensional Hydrodynamic Problems," Los Alamos Scientific Laboratory, LAMS-2082, Aug. 1956.

5 Bond, J. W., Jr., *Physical Review*, vol. 105, 1957, p. 1683.

6 Finkelnburg, W., and Maecker, H., *H. d. Physik*, Bd. XXII, Springer-Verlag, Berlin, 1956.

7 Chapman, S., and Cowling, T. G., "The Mathematical Theory of Non-Uniform Gases," Cambridge, The University Press, 1952.

8 Patrick, R. M., "Magnetohydrodynamics of Compressible Fluids," Ph.D. thesis, 1956, Cornell University, Ithaca, N. Y.

9 Rossow, V. J., "On Flow of Electrical Conducting Fluids Over a Flat Plate in the Presence of a Transverse Magnetic Field," NACA TN 3971, May 1957.

10 Pai, S. L., "Magnetohydrodynamics and Magnetogasdynamics," University of Maryland, TN BN-59, Sept. 1955.

11 Sears, W. R., "Recent Developments in Magnetoaerodynamics," IAS Summer Meeting, Los Angeles, June 1957.

A Practical Mathematical Approach to Grain Design

MAX W. STONE[1]

Rohm and Haas Co., Redstone Arsenal Research Division, Huntsville, Ala.

Equations were developed relating solid propellant grain geometry to the important ballistic parameters of cross-sectional loading density, sliver or tail-off fraction, progressivity ratio, initial surface and web. The equations were then solved by means of high speed computers and the results graphed in a readily usable form. If the loading fraction, sliver, progressivity ratio and web are given, grain designs which meet or most nearly meet given requirements can be found from the graphs. The graphs are useful in determining the effect of slight variations in design parameters. Illustrations of the use of the graphs are given for the internal-burning star and the internal-burning wagon wheel configurations. Calculations have also been made on a modified form of the wagon wheel[2] which permits one, two or three levels of thrust during burning.

Introduction

INTERIOR ballistic design is at times severely hampered by limiting boundary conditions. Generally, design is based on a set of performance criteria such as payload, burnt velocity, total weight, burning time and motor dimensions. Within these criteria, the designer is free to specify propellant, method of retaining the propellant charge in the motor, and charge configuration. Maximum performance depends on an optimum combination of these three variables.

An examination of the literature indicated that the opportunity to optimize charge design has not always been used to advantage, primarily because the designer has had no practical way to find the optimum geometry. Instead, charges have been designed empirically with compass and straightedge until workable designs were obtained; in many cases designs were not optimum. Such empirical technique is not in agreement with the increased demands for more effective ballistic systems.

In recent years several articles have been published on the mathematics of grain design (1, 2, 3).[3] Indeed, the contributions to this subject in the open and classified literature have been many and varied. However, a gap still existed between theoretical studies and practical usage. In an effort to bridge this gap, the mathematics of three representative charge designs have been reduced to usable form. The usefulness of this technique has been demonstrated by application to all internal-burning charges used by this Division. The simple, straightforward approach has been applied to the star, wagon wheel, and modified wagon wheel configurations.

The Internal-Burning Star

The goal was a mathematical analysis that could easily be used for the selection of grain designs. The techniques of geometry, algebra and trigonometry were chosen.

Because of its versatility and prominence as a charge configuration, the internal-burning star was chosen first for analysis. The star design shown in Fig. 1 may have desirable ballistic properties, but is not practical because thermal stresses will cause cracking of the grain at the points. Fig. 2 shows a star design with small circular arcs replacing the sharp points; this configuration will be considered here.

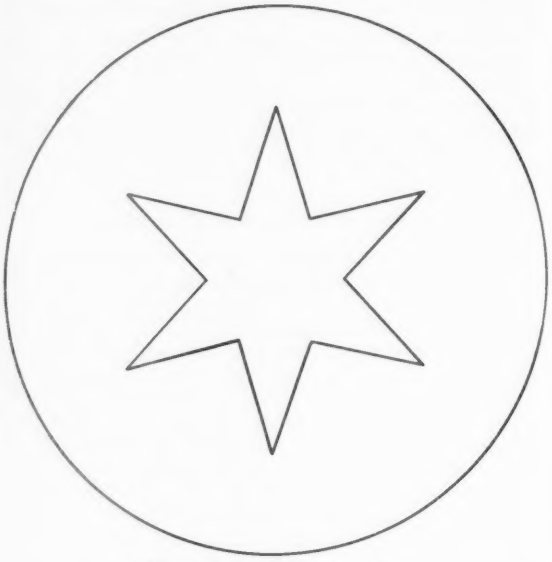

Fig. 1 Internal-burning star

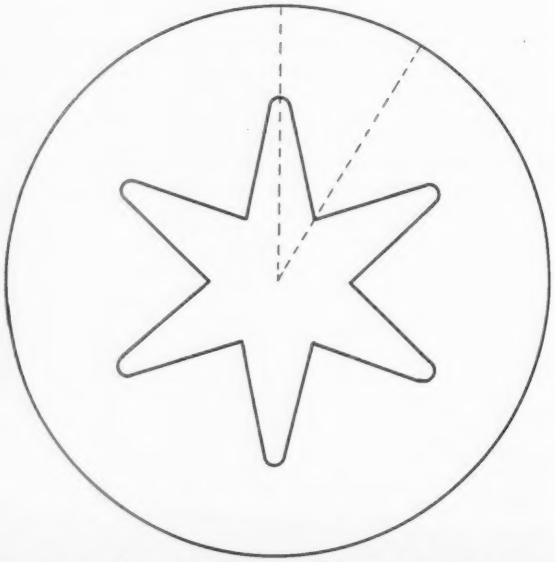

Fig. 2 Internal-burning star with stress-relief fillets

Presented at the ARS Semi-Annual Meeting, San Francisco, Calif. June 10–13, 1957.

[1] Mathematician.

[2] Also referred to as H-R design.

[3] Numbers in parentheses indicate References at end of paper.

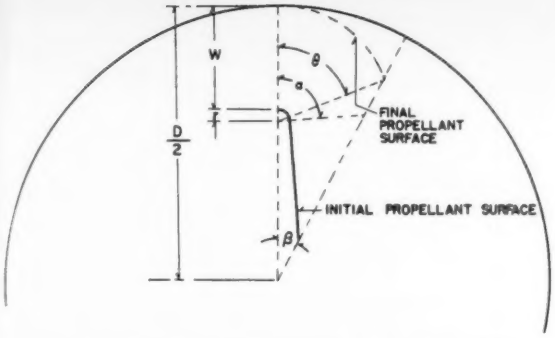

Fig. 3 Sector of internal-burning star-side burns out

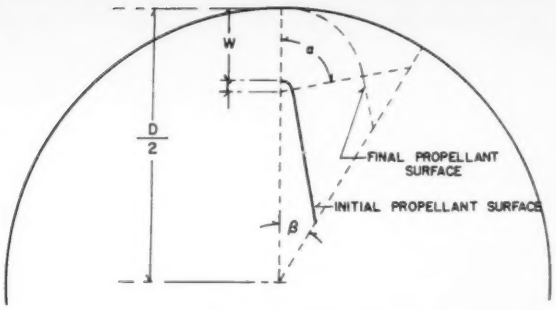

Fig. 4 Section of internal-burning star-side does not burn out

Assuming a constant cross section from one end of the propellant grain to the other, and neglecting the effect of erosive burning, it is convenient to use a cross section for all calculations. In addition, it is seen that there are $2N$ sectors symmetric with the one indicated by the dotted radii in Fig. 2, where N is the number of star points. Therefore, the geometric model, shown in Fig. 3, is the sector including one-half a star point with its attendant propellant mass. Because the author's experience has been with grains which were inhibited on the ends so that burning occurred only on the internal surfaces, this is the type burning considered here. The quantities to be used are defined in Fig. 3 and the following list. Final surface is understood to be the propellant surface existing at web burnout.

N = number of star points
D = outside diameter of the grain = inside diameter of the motor for case-bonded grain
w = web = shortest burning distance
r = radius of circular arc at star point
α = angle which subtends half the original arc of propellant at star point
θ = angle which subtends half the arc of propellant at web burnout
$\beta = \pi/N$

$$PR = \text{progressivity ratio} = \frac{\text{final propellant surface}}{\text{initial propellant surface}}$$

$$\epsilon = \text{loading fraction} = \frac{\text{total cross-sectional area of propellant}}{\text{cross-sectional area of motor}}$$

$$SF = \text{sliver or tail-off fraction} = \frac{\text{cross-sectional area of unburned propellant at web burnout}}{\text{cross-sectional area of motor}}$$

During burning the surface will regress in parallel layers, and, depending upon the initial shape, the final surface may be in an arc subtended by θ (Fig. 3) or an arc subtended by α plus a straight line segment (Fig. 4). Calculations concerning the configuration at burnout (SF and PR) will have to be treated separately for the two cases. The propellant present at web burnout may remain as sliver or it may burn at a reduced pressure to produce tail-off on the pressure-time trace.

It should be noted that loading fraction and sliver both have the motor area as their point of reference. If it is desired to know sliver as a fraction of the propellant, SF may be divided by ϵ.

The existence of thermal stresses in star-perforated grains (and others as well) is well known, and has resulted in much experimental work to determine their cause and the corrections needed. Since it has been demonstrated that star points having no fillets lead to cracked grains during curing and/or temperature cycling, it is now customary to replace with arcs all sharp indentions in the propellant surface. Thus, the stars used here have been equipped with circular arcs tangent to the sides of the point. All calculations made in this study use 0.03-in. as the arc radius for a 1-in.-diam grain. For larger grains the radius is linearly scalable. Other methods for relieving the stresses could be employed as well, as far as computational technique is concerned.

The equations relating grain geometry to the ballistic parameters of ϵ, SF and PR were written on the basis of geometrical considerations evident in Figs. 3 and 4. Thus, a series of equations[4] were obtained which relate the grain design parameters and the ballistic parameters of ϵ, SF and PR. Since the angle α has no ballistic significance, it will be preferable to specify values of the other parameters and solve for α. Although an analytical solution is not obtainable, the equations readily lend themselves to the iterative

[4] The equations are given in the Appendix.

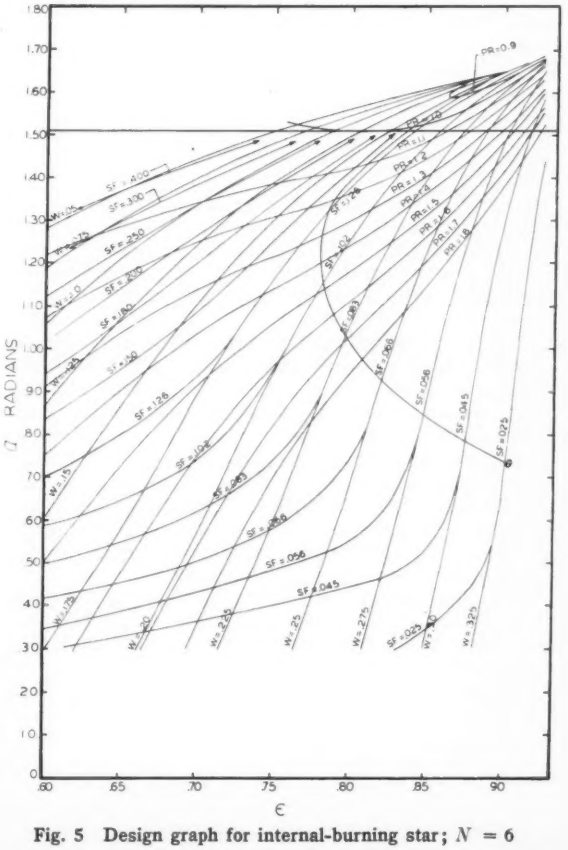

Fig. 5 Design graph for internal-burning star; $N = 6$

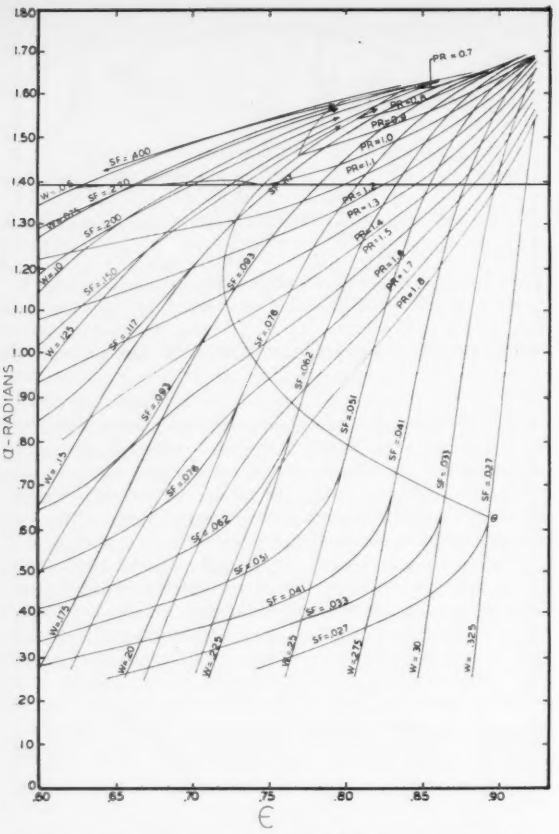

Fig. 6 Design graph for internal-burning star; $N = 7$

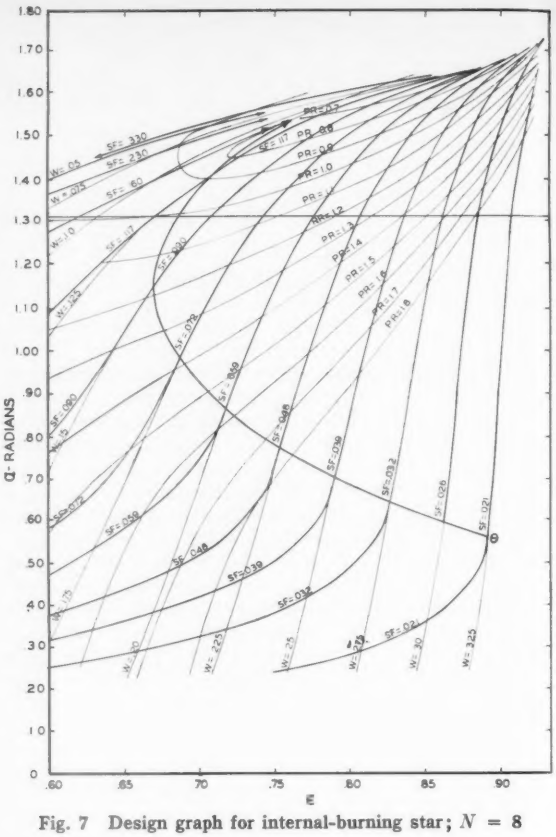

Fig. 7 Design graph for internal-burning star; $N = 8$

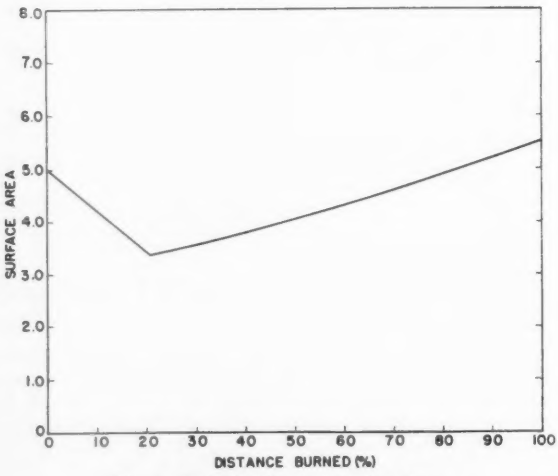

Fig. 8 Undesirable surface-time trace

procedures commonly used by large calculating machines.

The equations were programmed by the Redstone Arsenal Computation Laboratory[5] for the IBM 650 and computed for a wide range of the parameters N, w and PR. The results were graphed in the form shown in Figs. 5, 6 and 7, with a different graph for each value of N from 2 through 16 (4). All calculations were based on $D = 1$ in. and $r = 0.03$ in.; however, the results may be extended to any size motor by scaling on the diameter. All angles and ratios are unchanged while linear distances are multiplied by the diameter.

There are two lines on the graphs which must be explained further. The theta curve represents the locus of points for which $\theta = \alpha$, the point at which the straight line part of the star point disappears. The value of θ is read on the α scale. Designs chosen from the concave side of the theta curve will be such that the straight side of the star point will disappear before web burnout. Conversely, designs from the convex side of the curve will have the straight side remaining at web burnout. Because the graph is crowded near the top, the theta curve ends in an arrow, indicating that it does not cross the next web line as it continues upward.

The other unexplained line on the graphs is a horizontal straight line. In the case $N = 7$ (Fig. 6), for example, it appears at $\alpha = 1.3992$ radians. This line has to do with the shape of the surface-time trace for a particular design. For example, from the design graph, a design can be chosen which seems to be ideal, yet the surface-time history may be as in Fig. 8. This may happen in the case where the straight sides of the star point burn out before the web does, so that there are two distinct phases of the surface progression with each having its own separate progressivity ratio. Equations have been written to determine the value of α required to give a certain PR, all other parameters being known, but the equations are too complex to be readily used because the second phase is nonlinear. A compromise solution was obtained by calculating the value of α required to raise the first portion of the surface-time trace to neutrality ($PR = 1.0$). This condition is simply $\alpha = \tan(\alpha - \beta)$, a constant for each N. This is the value represented by the horizontal line on each design graph. Now, for example, with that particular value of α just mentioned and a $PR = 1.1$, the surface-

[5] Now part of Army Ballistic Missile Agency.

time trace will be as shown in Fig. 9. Dropping below the horizontal line increases the progressivity ratio for the first phase, going above the line decreases it. This information yields a qualitative picture of the pressure-time trace which can be checked by actually plotting the surface-time history.

Surface as a function of x, the distance burned, can be plotted by means of the following equations

$$S_x = 2NDl \times \left[(r + x)\,\alpha + \frac{\left(\frac{D}{2} - r - w + \frac{r + x}{\cos \alpha}\right) \sin \beta}{\cos (\alpha - \beta)} - (r + x) \tan \alpha \right] \quad \ldots [1]$$

where l is length of grain. Equation [1] is applicable until the second term becomes equal to the last (third) term, indicating that the side has disappeared. Then Equation [2] is valid.

$$S_x = 2NDl\,(r + x) \left[\beta + \text{arc sin} \frac{\left(\frac{D}{2} - r - w\right) \sin \beta}{r + x} \right] \quad \ldots [2]$$

If only the shape of the trace is desired, the multiple $2NDl$ may be omitted.

It should be noted that the pressure-time trace will not necessarily have the same progressivity ratio as the surface-time trace because of the effect of the pressure exponent (6, 7). In addition, erosive burning, if present, will change the burning pattern.

There is a minimum value for α, shown in Fig. 10. This means that the inner projection (the base) of the star point is the same distance from the motor wall as the star point itself. Since the result is $2N$ points with only alternate ones possessing the stress relief fillet, a more practical minimum is shown in Fig. 11. This is outside the region of normal interest, as seen from Figs. 5, 6 and 7, and is of no real concern. The maximum value for α is indicated in Fig. 12. These limits were observed in the construction of the graphs.

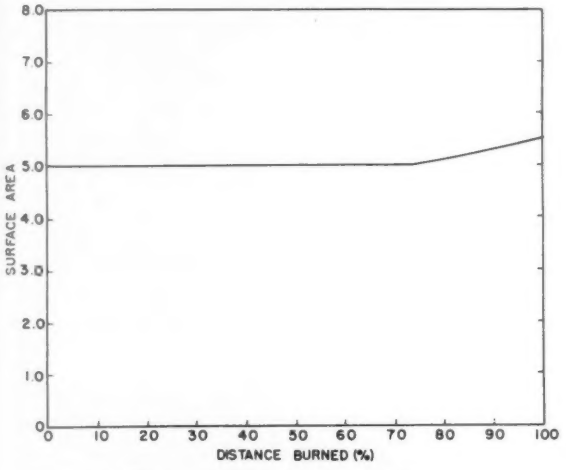

Fig. 9 Improved surface-time trace

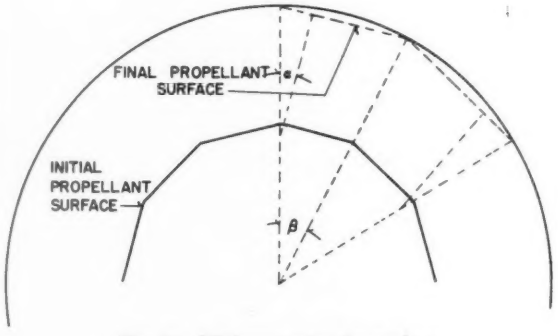

Fig. 10 Minimum value for angle α

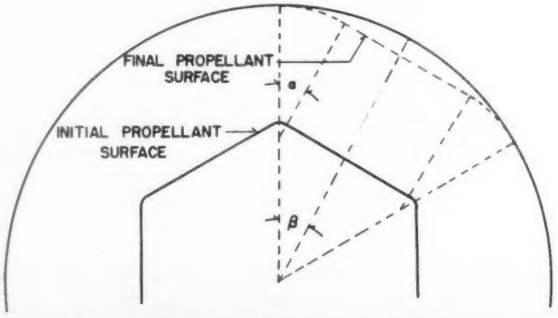

Fig. 11 Practical minimum value for angle α

Example 1

Required:

PR—neutral, no dip or peak in surface-time trace
ϵ —approximately 75 per cent
SF—low as possible
w —thin web, exact value not critical

Solution: There is only one design for each value of N that gives a completely neutral trace; that design is found at the intersection of the horizontal line with the curve $PR = 1.0$. From Figs. 5, 6 and 7, it is immediately apparent that only at $N = 7$ is the ϵ requirement satisfied. At that point *SF* is $12\frac{1}{2}$ per cent and $w = 0.144$ in.

Example 2

Required:

PR—nearly neutral, slight progressivity acceptable
ϵ —high, over 85 per cent
SF—low as possible
w —fairly thick web, in the neighborhood of $0.2D$

Solution: From the graphs the following design was chosen: $N = 6$, $PR = 1.05$, $\epsilon = 85.1$ per cent, $SF = 11.1$ per cent, $w = 0.19$ in. The surface-time trace is neutral for about 80 per cent of the burning distance and then becomes slightly progressive.

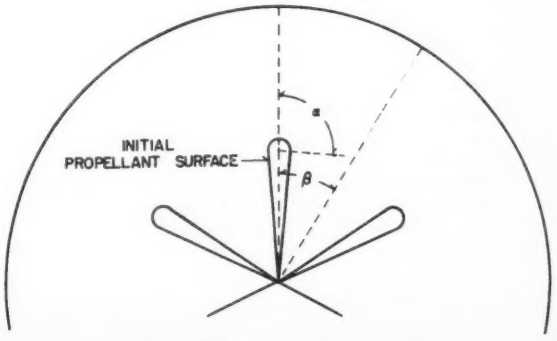

Fig. 12 Maximum value for angle α

Fig. 13 Internal-burning wagon wheel design

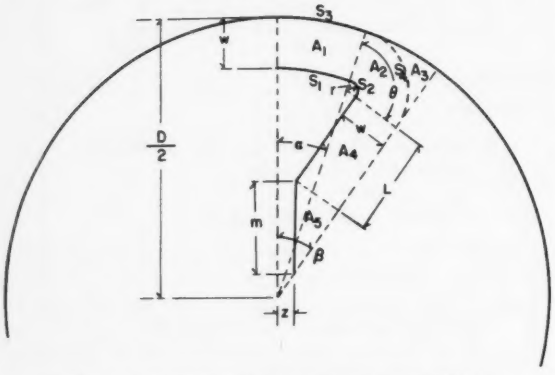

Fig. 14 Sector of internal-burning wagon wheel

The Internal-Burning Wagon Wheel Design

Another basic configuration that has proved useful in several slightly differing forms is the wagon wheel design, shown in Fig. 13. The thickness of the spear of propellant is twice the web, that is, twice the shortest distance between inner and outer surfaces of the grain. The two corners of the spokes (the port) are circular arcs tangent to the sides of the spears and to the short arc between them, which is concentric with the grain perimeter.

This configuration received the same treatment as the star. Many of the same definitions and designations apply; the new ones may be seen in Fig. 14. It would be possible to calculate the length of line L if z were specified, but it seems more reasonable to include L in the equation for progressivity ratio, specify a desired PR and solve for L. This was the procedure followed in the calculations that have been performed.

The equations for the wagon wheel were programmed for the Redstone IBM 650 and solved for a wide range of values of N, w and PR. As before, D and r were constant at 1 and 0.03 in., respectively.

The equation for the line L indicates that there is no wagon wheel design giving a neutral surface-time trace ($PR = 1.0$) because the quantity ($PR - 1$) is used as a divisor. For all practical purposes a neutral design can be obtained because values of PR very close to 1.0, e.g., 1.01, were used successfully.

The computer results were plotted in the form shown in Figs. 15 and 16 for values of N from 2 through 16 (5). Use

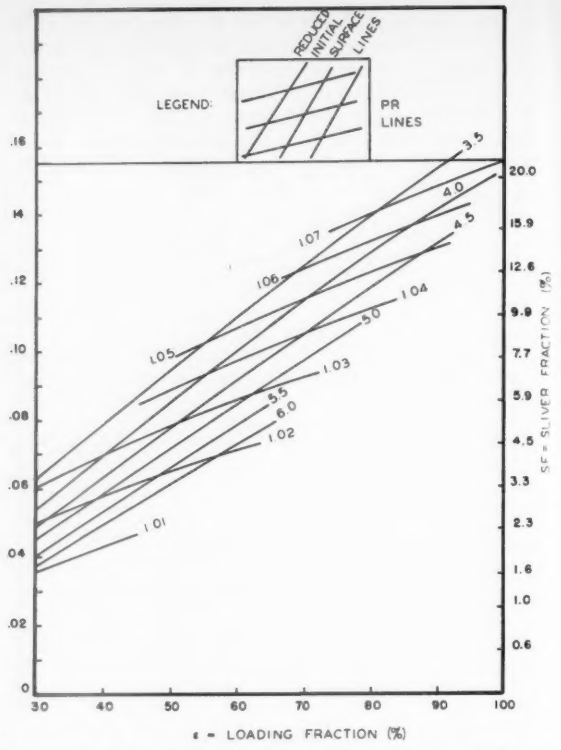

Fig. 15 Design graph for internal-burning wagon wheel; $N = 5$

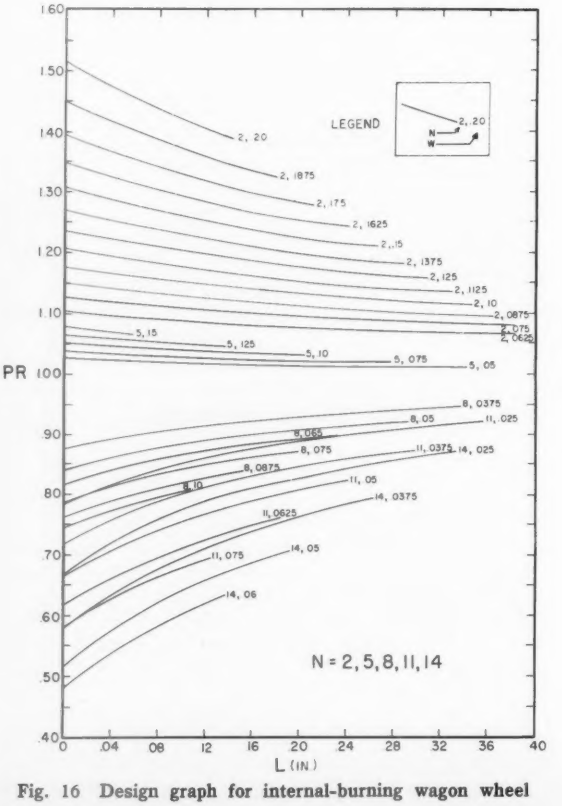

Fig. 16 Design graph for internal-burning wagon wheel

of the graphs is the same as with the star, with the exception that L must be found from the second graph or hand computed from the equation after the design is chosen. The wagon wheel is a thin-web design, with its maximum being about $0.2D$, while the star can go up to about $0.33D$. In both designs sliver fraction increases with web; the star sliver fraction decreases with increasing N while the wagon wheel sliver fraction increases. Thus, of the two, only the wagon wheel provides small values of SF for small N.

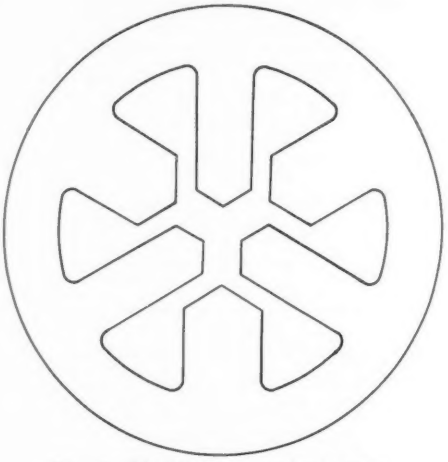

Fig. 17 Modified wagon wheel design

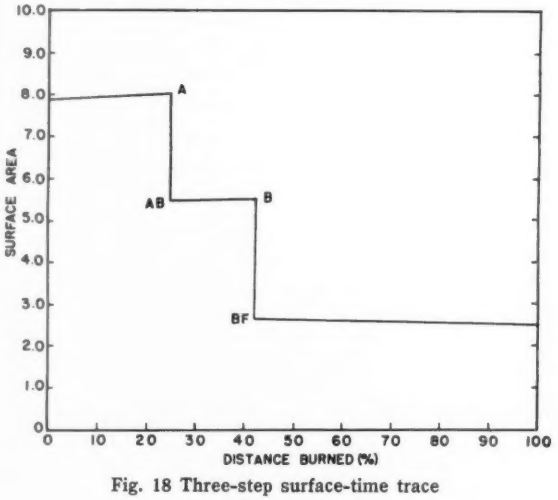

Fig. 18 Three-step surface-time trace

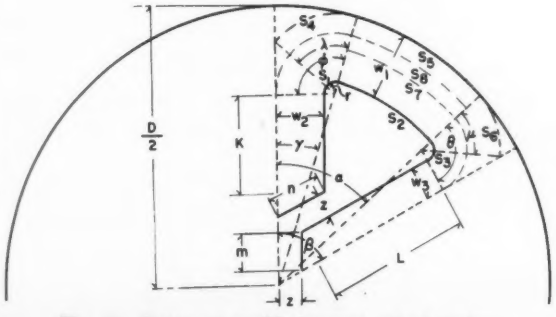

Fig. 19 Sector of modified wagon wheel design

As one would expect, there is a maximum value of web that can be put into a motor. This value can be found from

$$w_{max} = \frac{\left(\frac{D}{2} - r\right)\sin\beta - r}{\sin\beta + 1} \quad \ldots\ldots\ldots\ldots [3]$$

Example 3

Required:

PR—nearly neutral, slight progressivity acceptable
ϵ —80 per cent
SF—low as possible
w —thin web

Solution: Although only the graph for $N = 5$ is reproduced here, all traces for $N = 6$ and above will be regressive; for values of N less than 5, traces become increasingly progressive. Therefore, the only chance for a high loading fraction in a nearly neutral design is at $N = 5$. Thus from Fig. 15 is chosen the design $N = 5$, $\epsilon = 80.2$ per cent, $SF = 9.8$ per cent, $w = 0.112$ in., $PR = 1.04$, and from Fig. 16 the line L is found to be 0.15 in.

Modified Wagon Wheel

This useful design (Fig. 17) is a wagon wheel design with alternately long and short spears of propellant. In this analysis N will refer to the number of long spears (equal to the number of short spears) but not the total number of spears.

A major innovation in the analysis of this design is the treatment of the three burning distances as not necessarily being equal. The three burning distances are determined by the thickness of the long and of the short spears and by the shortest distance from inner to outer propellant surfaces. This gives the possibility of a one-level (all burning distances equal), two-level (two burning distances equal) or three-level (all burning distances unequal) thrust operation (Fig. 18). (The wagon wheel could be treated in this way also.) The relative heights of the levels in the second and third cases can be adjusted somewhat by the choice of the long spear with its larger mass of propellant for the first step, or the short spear with its smaller mass, or by choosing which of the webs are to be equal.

Some new lines and angles are added in this analysis; they are indicated in Fig. 19. Because of the web treatment, the equations arrived at are more numerous and appear more formidable than previous ones. A compromise to practicality was made in defining the configuration so that the distance z (Fig. 19) applies between two spears as it does between the long spear and the center lines. Thus, the spear with K as its side is always the short one.

In the same manner as before, equations were written to relate the grain geometry to ϵ, *SF* and *PR*. These equations were then programmed for solution on the IBM 704 at the Redstone Arsenal Computation Laboratory, and solutions obtained for a wide range of values of w_1, w_2, w_3, N and *PR*. This work has just been completed and the results will be graphed in a form similar to the other design graphs.

Acknowledgment

The author wishes to thank W. D. Hand, now with the Chrysler Corporation at Redstone Arsenal, for his help and encouragement during the early part of this work. The original idea and impetus for the study was provided by H. M. Shuey, head of the Ballistics Section, Rohm and Haas Co.

Appendix. Equations for Grain Designs

Internal-Burning Star

The equations are derived directly from the geometry of

the design (Figs. 3 and 4) in terms of the definitions given in the text of the article. For the case where the straight sides of the star point disappear before web burnout, the following equations are true

$$\epsilon = 1 - \frac{4N}{\pi D^2}\left[\frac{\left(\frac{D}{2} - r - w + \frac{r}{\cos\alpha}\right)^2 \sin\beta\cos\alpha}{\cos(\alpha-\beta)} + r^2(\alpha - \tan\alpha)\right] \quad \ldots [A\text{-}1]$$

$$PR = \frac{(r+w)\theta}{r(\alpha - \tan\alpha) + \frac{\left(\frac{D}{2} - r - w + \frac{r}{\cos\alpha}\right)\sin\beta}{\cos(\alpha-\beta)}} \quad \ldots [A\text{-}2]$$

where

$$\theta = \beta + \arcsin\frac{\left(\frac{D}{2} - r - w\right)\sin\beta}{r+w} \quad \ldots [A\text{-}3]$$

$$SF = 1 - \frac{4N}{\pi D^2}\left[(r+w^2)\,\theta + (r+w)\left(\frac{D}{2} - r - w\right)\sin\theta\right] \quad \ldots [A\text{-}4]$$

In the case where the side does not disappear during burning (Fig. 4), Equation [A-1], along with the following equations for progressivity ratio and sliver fraction apply

$$PR = \frac{r(\alpha - \tan\alpha) + w[\alpha - \tan(\alpha-\beta)] + \frac{\left(\frac{D}{2} - r - w + \frac{r}{\cos\alpha}\right)\sin\beta}{\cos(\alpha-\beta)}}{r(\alpha - \tan\alpha) + \frac{\left(\frac{D}{2} - r - w + \frac{r}{\cos\alpha}\right)\sin\beta}{\cos(\alpha-\beta)}} \quad \ldots [A\text{-}5]$$

$$SF = \epsilon - \frac{8N}{\pi D^2}\left[rw(\alpha - \tan\alpha) + \frac{w^2}{2} \times [\alpha - \tan(\alpha-\beta)] + \frac{\left(\frac{D}{2} - r - w + \frac{r}{\cos\alpha}\right) w\sin\beta}{\cos(\alpha-\beta)}\right] \quad \ldots [A\text{-}6]$$

Internal-Burning Wagon Wheel Design

From the geometry of the grain as seen in Fig. 14, the following equations can be written

$$\alpha = \beta - \arcsin\frac{r+w}{\frac{D}{2} - r - w} \quad \ldots [A\text{-}7]$$

$$\theta = 90^\circ + \beta - \alpha \quad \ldots [A\text{-}8]$$

$$m = \frac{w}{\sin\beta} \quad \ldots [A\text{-}9]$$

$$PR = \frac{S_3 + S_4 + L + \frac{w}{\tan\beta} - m}{S_1 + S_2 + L + m} \quad \ldots [A\text{-}10]$$

Actually, the final surface is $S_3 + S_4$, but up until the instant of burnout the spear of propellant remains. A separate equation for line L cannot be written without also specifying z; it is more desirable to specify PR and solve for L in Equation [10].

$$L = \frac{S_3 + S_4 + \frac{w}{\tan\beta} - m - (S_1 + S_2 + m)\,PR}{PR - 1} \quad \ldots [A\text{-}11]$$

Expressions for the arc lengths are easily obtained and will be omitted here. The area ratios are found by

$$\epsilon = \frac{\sum_{i=1}^{5} A_i}{\frac{1}{2N}\frac{\pi D^2}{4}} = \frac{4\alpha(Dw - w^2) + 8Lw + \frac{4w^2}{\tan\beta} + D^2(\beta - \alpha) - 4r^2\theta}{\frac{\pi D^2}{N}} - \frac{\frac{4(r+w)^2}{\tan(\beta-\alpha)}}{\frac{\pi D^2}{N}} \quad \ldots [A\text{-}12]$$

and

$$SF = \frac{A_3}{A_{\text{motor}}} = \frac{D^2(\beta - \alpha) - 4(r+w)^2\theta - \frac{4(r+w)^2}{\tan(\beta-\alpha)}}{\frac{\pi D^2}{N}} \quad \ldots [A\text{-}13]$$

Modified Wagon Wheel Design

Again the equations are found in a straightforward fashion. The angles appearing in Fig. 17 can be calculated by

$$\alpha = \beta - \arcsin\frac{r + w_3}{\frac{D}{2} - r - w_1} \quad \ldots [A\text{-}14]$$

$$\gamma = \arcsin\frac{r + w_2}{\frac{D}{2} - r - w_1} \quad \ldots [A\text{-}15]$$

$$\theta = 90^\circ + \beta - \alpha \quad \ldots [A\text{-}16]$$

$$\phi = 90^\circ + \gamma \quad \ldots [A\text{-}17]$$

$$\mu = \theta - \arccos\frac{r + w_3}{r + w_1} \quad \ldots [A\text{-}18]$$

$$\lambda = \phi - \arccos\frac{r + w_2}{r + w_1} \quad \ldots [A\text{-}19]$$

The arc lengths S_1 through S_8 are calculated simply as the product of angle and radius so those equations will not be printed here.

The length of the line L will be determined from the PR equations which follow, similar to the wagon wheel design. Since K is a function of L, it can be found by Equation [A-20].

$$K = L - m + \frac{r + w_2}{\tan\gamma} + \frac{w_3}{\tan\beta} - \frac{w_2}{\tan\beta} - \frac{r + w_3}{\tan(\beta - \alpha)} \quad \ldots [A\text{-}20]$$

In order to distinguish practical values of L, the following equations must be solved. The maximum value occurs when $z = 0$.

$$L_{max} = \frac{r + w_3}{\tan(\beta - \alpha)} - \frac{w_3}{\tan\beta} \quad \text{[A-21]}$$

and the minimum at $k = 0$

$$L_{min} = m + \frac{w_2}{\tan\beta} + \frac{r + w_3}{\tan(\beta - \alpha)} - \frac{r + w_2}{\tan\gamma} - \frac{w_3}{\tan\beta} \quad \text{[A-22]}$$

In a multistep thrust or pressure trace, it is obvious that PR as previously defined is inadequate. To be meaningful, a separate PR must be calculated for each step. Thus, from Fig. 16 the following definitions present themselves

$$PR_a = \frac{\text{surface at } A}{\text{initial surface}} \quad \text{[A-23]}$$

$$PR_b = \frac{\text{surface at } B}{\text{surface at } AB} \quad \text{[A-24]}$$

$$PR_c = \frac{\text{final surface}}{\text{surface at } BF} \quad \text{[A-25]}$$

The equation used to calculate PR_a for any particular case will depend upon the relationship of the webs to each other. The following equations give PR_a for each case and also the intermediate surfaces from which PR_b and PR_c can be calculated by Equations [A-24 and A-25]. The denominator of the PR_a equation is the initial surface (S_i) and is the same in every case.

$w_1 = w_2 = w_3$

$$PR_a = PR_b = PR_c = \frac{K + L - 2n + 2(r + w_1)\,\phi + \frac{2\,w_1}{\tan\beta} + S_5}{m + n + K + L + S_1 + S_2 + S_3} \quad \text{[A-26]}$$

$w_1 = w_2 > w_3$

$$PR_a = \frac{1}{S_i}\left[K + L - m + \frac{w_1 - w_3}{\sin\beta} - \frac{w_3}{\tan\left(90° - \frac{\beta}{2}\right)} + (r + w_3)\,(\theta + \phi) + \frac{w_3}{\tan\beta} + S_7\right] \quad \text{[A-27]}$$

$$\text{surface } AB = \text{surface } BF = K + \frac{w_1 - w_3}{\sin\beta} - \frac{w_3}{\tan\left(90° - \frac{\beta}{2}\right)} + (r + w_3)\,(\theta + \phi) + S_7 \quad \text{[A-28]}$$

$$\text{surface } B = \text{final surface} = K - n + (r + w_2)\,\phi + \frac{w_2}{\tan\beta} + S_5 + S_6 \quad \text{[A-29]}$$

$w_1 = w_3 > w_2$

$$PR_a = \frac{1}{S_i}\left[K + L - n + \frac{w_2}{\tan\beta} + (r + w_2)\,(\theta + \phi) + \frac{w_1 - w_2}{\sin\beta} - \frac{w_2}{\tan\left(90° - \frac{\beta}{2}\right)} + S_8\right] \quad \text{[A-30]}$$

$$\text{surface } AB = \text{surface } BF = L + \frac{w_1 - w_2}{\sin\beta} - \frac{w_2}{\tan\left(90° - \frac{\beta}{2}\right)} + (r + w_2)\,(\theta + \phi) + S_8 \quad \text{[A-31]}$$

$$\text{surface } B = \text{final surface} = L - m + \frac{w_3}{\tan\beta} + (r + w_3)\theta + S_4 + S_5 \quad \text{[A-32]}$$

$w_1 > w_2 = w_3$

$$PR_a = \frac{1}{S_i}\left[K + L - 2m + \frac{2w_2}{\tan\beta} + 2(r + w_2)\theta + S_8\right] \quad \text{[A-33]}$$

$$\text{surface } AB = \text{surface } A = \text{surface } B = \text{bracketed term of Equation [A-33]} \quad \text{[A-34]}$$

$$\text{surface } BF = (r + w_2)\,(\theta + \phi) + S_8 \quad \text{[A-35]}$$

$$\text{final surface} = S_4 + S_5 + S_6 \quad \text{[A-36]}$$

$w_1 > w_2 > w_3$

$$PR_a = \frac{1}{S_i}\left[K + L - m + \frac{w_2 - w_3}{\sin\beta} - \frac{w_3}{\tan\left(90° - \frac{\beta}{2}\right)} + (r + w_3)\,(\theta + \phi) + \frac{w_3}{\tan\beta} + S_7\right] \quad \text{[A-37]}$$

$$\text{surface } AB = K + \frac{w_2 - w_3}{\sin\beta} - \frac{w_3}{\tan\left(90° - \frac{\beta}{2}\right)} + (r + w_3)\,(\theta + \phi) + S_7 \quad \text{[A-38]}$$

$$\text{surface } B = K - n + \frac{w_2}{\tan\beta} + (r + w_2)\,(\phi + \theta - \psi) + S_8 \quad \text{[A-39]}$$

where

$$\psi = \text{arc tan}\,\frac{\sqrt{(r + w_2)^2 - (r + w_3)^2}}{r + w_3} \quad \text{[A-40]}$$

$$\text{surface } BF = (r + w_2)\,(\theta + \phi - \psi) + S_8 \quad \text{[A-41]}$$

$$\text{final surface} = S_4 + S_5 + S_6 \quad \text{[A-42]}$$

$w_1 > w_3 > w_2$

$$PR_a = \frac{1}{S_i}\left[K + L - n + \frac{w_2}{\tan\beta} + (r + w_2) \times (\theta + \phi) + \frac{w_3 - w_2}{\sin\beta} - \frac{w_2}{\tan\left(90° - \frac{\beta}{2}\right)} + S_8\right] \quad \text{[A-43]}$$

$$\text{surface } AB = L + \frac{w_3 - w_2}{\sin\beta} - \frac{w_2}{\tan\left(90° - \frac{\beta}{2}\right)} + (r + w_2)\,(\theta + \phi) + S_8 \quad \text{[A-44]}$$

$$\text{surface } B = L - m + \frac{w_3}{\tan\beta} + (r + w_3)\,(\theta + \phi - \Omega) + S_7 \quad \text{[A-45]}$$

where

$$\Omega = \text{arc tan}\,\frac{\sqrt{(r + w_3)^2 - (r + w_2)^2}}{r + w_2} \quad \text{[A-46]}$$

$$\text{surface } BF = (r + w_3)\,(\theta + \phi - \Omega) + S_7 \quad \text{[A-47]}$$

$$\text{final surface} = S_4 + S_5 + S_6 \quad \text{[A-48]}$$

Although not necessary in the calculations, the value of z will aid in drawing the design.

$$z = (\sin\beta)\left[\frac{r + w_3}{\tan(\beta - \alpha)} - \frac{w_3}{\tan\beta} - L\right] \quad \text{[A-49]}$$

The area ratios are

$$\epsilon = \frac{4N}{\pi D^2}\left[\frac{w_2^2 + w_3^2}{\tan\beta} + 2Kw_2 + 2L\,w_3 - r^2\,(\theta+\phi) + \frac{D^2\beta}{4} - \frac{(r-w_2)^2}{\tan\gamma} - \frac{(r+w_3)^2}{\tan(\beta-\alpha)} - \left(\frac{D}{2} - w_1\right)^2(\alpha-\gamma)\right] \ldots [A\text{-}50]$$

$$SF = \frac{4N}{\pi D^2}\left[\frac{D^2\gamma}{4} - (r+w_1)^2\,\lambda - (r+w_2)^2\tan(\phi-\lambda) + \frac{D^2\,(\beta-\alpha)}{4} - \frac{(r+w_2)^2}{\tan\gamma} - \frac{(r+w_3)^2}{\tan(\beta-\alpha)} - (r+w_1)^2\,\mu - (r+w_3)^2\tan(\theta-\mu)\right] \ldots [A\text{-}51]$$

References

1 Price, E. W., "Charge Geometry and Ballistic Parameters for Solid Propellant Rocket Motors," JET PROPULSION, vol. 24, Jan.-Feb. 1954, p. 16.

2 Vogel, J. M., "A Quasi-Morphological Approach to the Geometry of Charges for Solid Propellant Rockets: The Family Tree of Charge Designs," JET PROPULSION, vol. 26, Feb. 1956, p. 102.

3 Epstein, L. I., "The Design of Cylindrical Propellant Grains," JET PROPULSION, vol. 26, Sept. 1956, p. 757.

4, 5 These graphs, though unclassified, appear in classified reports. Copies may be obtained from the author.

6 Wimpress, R. N., "Internal Ballistics of Solid-Fuel Rockets," McGraw-Hill, New York, 1950.

7 "Rocket Fundamentals," OSRD 3992.

Design, Fabrication and Testing of the Vanguard Satellite[1]

ROBERT C. BAUMANN[2]

Naval Research Laboratory, Washington, D. C.

Flight and orbital environmental conditions exert a great influence on satellite design. As information on these conditions changed and became firm the satellite design went through numerous stages. Material selected for the satellite shell and structure is magnesium alloy FS-1. Design and operation of the structure and shell, antennas and separation mechanism are discussed. Methods for control of satellite temperatures are thermal isolation of the inner package, shell coatings and thermal switches. From a circular blank disk, a near-perfect hemisphere, only 0.026 in. thick, is formed to make the satellite shell. Tubes are formed and welded to make up the "bird cage" internal structure. Fitting and assembly of the satellite involve jewelers' precision on the part of several groups. Satellite structural components are design-tested individually at first. The assembly is then tested to the expected environmental conditions of acceleration, vibration, vacuum and temperature.

Introduction

IN JULY 1955, President Eisenhower formally announced that the United States would undertake the launching of artificial satellites as a part of the research program for the International Geophysical Year. One satellite has already been launched by the U. S. Army. To place the Navy's small 20-in.-diam 21½-lb satellite in an orbit around the earth takes a three-stage rocket vehicle approximately 72 ft long, weighing over 10 tons. Such a vehicle (Fig. 1) may be described as follows: The first stage is a liquid-fueled rocket with a 27,000-lb-thrust rocket motor. The second stage, also a liquid propellant rocket, attaches to the forward end of the first stage and houses the third stage and satellite during its flight. The second stage contains the "brains" for the entire launching vehicle. The third stage is a solid propellant rocket. The satellite, mounted on the separation mechanism, is attached to the third stage rocket.

[1] Revised edition of paper presented at the ARS Spring Meeting, April 4–6, 1957, Washington, D. C.

[2] Head, Satellite Structures Group, Project Vanguard. Mem. ARS.

Flight Environmental Conditions

The flight events that precede the ejection of the satellite from the third stage may be described as follows (Fig. 2).

Fig. 1. Vanguard launching vehicle

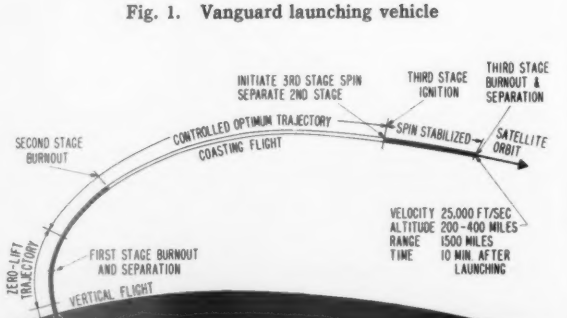

Fig. 2. Vehicle trajectory

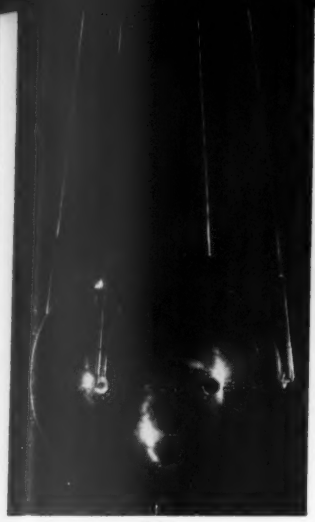

(a)

(b)

Fig. 3 (a) Satellite with antennas in the folded position. (b) Satellite with antennas in the radial position

(a) The vehicle goes through a short vertical flight and then starts a zero-lift trajectory. (b) Approximately midway through this zero-lift phase the first stage burns out, separation of the second stage from the first stage occurs, and the second stage is ignited. (c) The second stage is controlled for optimum trajectory through part of its powered and all of its coasting flight. (d) The third stage is spun and the second stage is separated. (e) When the second stage is clear the third stage ignites and is spin-stabilized throughout its burning period. (f) At burnout, approximately 10 min after launching, the satellite and the third stage will have a velocity of approximately 25,000 fps, an altitude of 200 to 400 miles, and a range of approximately 1500 miles.

The satellite must survive vibrations imposed by three individual rocket motors. It must survive the shocks of rocket starts. In addition, it must withstand steady state accelerations up to 35 g, aerodynamic heating to 300 F and rotation to 150 rpm.

Orbital Environmental Conditions

The difficulty encountered in trying to design for orbital environmental conditions lies mostly in the uncertainty of these conditions. One of the major roles of the satellite is to get measurements of these conditions. Not much is known about ambient temperatures, meteors, space dust, cosmic rays, x-rays, etc., at altitudes from 200 to 1400 miles, the space in which the satellite must travel. Of the unknowns, temperature seems to stand out as the major problem. The batteries and transistors to be used can only operate in a comparatively narrow temperature range (0 to 60 C). The orbit, the time of year of firing and the hour of firing contribute to the variations in temperatures expected. The satellite skin will fluctuate through a wide range of temperatures. It will become extremely cold when the earth is between the satellite and the sun. It will become hot when it is on the sunny side.

Design

General

Design criteria had to be determined on the basis of preliminary estimates of the magnitude of the powered flight forces. Design factors of safety to be used in the design calculations were then established. Before actual design could begin, the basic shape of the satellite had to be established. Some of the contributing factors that determined the size and shape were the maximum size that would fit into the vehicle with a minimum weight penalty for the second stage, minimum size needed to allow effective optical tracking in the orbit, and minimum weight of shell and structure.

Material Selection

The most important factor, other than reliability, that controls design is weight. For every pound the satellite weighs it takes approximately 1000 lb of rocket vehicle to give the necessary velocity to orbit. Every gram of satellite structural weight decreases the scientific payload the same amount. It was necessary, therefore, to make a very thorough study of materials for use in the satellite shell and structure. FS1 magnesium alloy was chosen as a shell and basic structure material because of its light weight and also because it is one of the most commonly used and easily worked magnesium alloys. Calculations indicate that adequate strength could be obtained from FS1 in minimum thicknesses to be used for fabrication.

Structure and Shell

The various loads incurred by the structure during the ascending trajectory may be analyzed as follows (Fig. 9): The major concentrated load which is the internal package is carried directly through the Kel-F support to the main hub at the base of the structure. This hub rests on the separation mechanism and the load is transmitted directly into the top of the third stage. The side loads incurred by vibration are transmitted from the internal package through the four Kel-F side rods. These rods transmit the load to the circumferential rim on the major axis of the satellite. Part of the side loads are taken up by the vertical bow-shaped tube, and part is transmitted around the ring into the shell of the satellite itself at the antenna supports. The major antenna load is carried by the structure but a portion of the load is transmitted through the shell. The load of the shell is picked up at the top ring of the structure, at the major or equatorial axis and also at the base. The highest stresses in the shell are located near the base of the satellite; hence the skin is thicker there. This section covers about $10\frac{1}{2}$ in. in diam at the base of the sphere and is 0.050 in. thick. Thinner skins (i.e., approximately 0.025) show an oil-canning effect when being vibrated in the horizontal direction and fatigue quite rapidly. The frame is designed to take up to $6\frac{1}{2}$-in. maximum diam by $13\frac{1}{4}$-in.-long internal package. This affords a considerable amount of flexibility for the internal package design. The method of base support and side support is such that it is relatively easy to incorporate different shapes and sizes of internal packages.

Antennas

The antennas are 29 in. long and constructed primarily of $\frac{1}{4}$-in. OD by 0.024-in. wall aluminum tubing 6061ST6. They

Fig. 4 Satellite in Coating Facility at ERDL, Fort Belvoir, Va.

are operated by a spring which is a tension. The antennas are folded forward while the nose cone is on the second stage (Fig. 3 (a)). When the nose cone is jettisoned the antennas will rotate more than 90 deg to the radial position and lock on a tapered surface (Fig. 3 (b)).

Temperature Control

The shell temperature can be controlled to a degree by its surface coating. The satellite coating must satisfy two fundamental requirements. It must be highly reflective, in the visible, and it must emit absorbed solar energy to stabilize its temperature. Such a coating has been developed.[3] An evaporative coating of aluminum provides high reflectance while an outer coating of silicon monoxide, transparent in the visible, provides the required emissivity in the infrared. Fig. 4 shows the coating facility of ERDL, Fort Belvoir, Va.

The internal package containing the electronics and batteries must be thermally isolated from the shell. Only two methods of heat transfer are involved—radiation and conduction. Radiation transfer is minimized by using gold-plated surfaces (low thermal emissivity) and conduction is minimized by using low thermal conductance structural supports to connect the internal package to the shell. The isolation achieved in this manner will keep the internal package temperature within 1 C of the mean orbital temperature. The shell temperature will fluctuate ±15 C about its mean orbital temperature after equilibrium has been reached.

A very thorough analytical and experimental program is being conducted on the thermal phase in order to get the best heat balance possible. If by chance estimates of orbital temperature conditions are extremely far off the result would be that instead of the two-week designed life for the electronics we might get data for only a few days. These data would, however, tell us where the estimates were in error and give the next unit a far greater chance for a full life.

The Satellite Separation Mechanism

Fig. 5 shows the separation mechanism which is a completely self-contained unit that fits in a socket at the base of the satellite. It uses the characteristics of the third stage as a method of arming and operation. The mechanism operates as follows: If approximately 12 g or more are applied for over 2 sec, the clock will be allowed to run for 10 sec more to a stop on the g-weight arm; if 12 g or more is applied for less than 2 sec, the unit will reset itself. Then after the g level is reduced below the 12-g level at third stage burnout the timer will start to run and run approximately 26 sec. At the end of this period the timer arm closes circuits to the caterpillar motors, which expand, pulling the hold-down pins in and rotating the spring release. The spring exerts a force which imparts a differential velocity of approximately 3 fps between the third stage and the satellite. The unit is designed with two completely independent circuits. Two RM-1 batteries are used. One caterpillar motor is fired by each battery independently. Upon closing of the circuit by the timer arm, the batteries furnish enough voltage to the wire wound squibs in the caterpillar motors to cause them to ignite the charge and the expanding gases do the work of pulling the pins and rotating the spring release. Either of these circuits is capable of firing and releasing the satellite. The purpose of the duplication is to insure a higher degree of reliability.

Fabrication[4]

Shells

A circular blank disk 0.091 in. thick is cut out of sheet stock. This disk is then drawn with one die in one stroke of the press with the material heated to 650 F. After the flash is trimmed off, the drawn hemisphere is placed on a spinning lathe. The metal hemisphere is spun hot (600 F approximately) to give exact internal dimensions required. The inner segment of the pressure zone is spun from a flat circular blank of magnesium.

[3] Bradford, A. P., Cox, J. T., and Hass, G., "Coatings for Infrared Optics of the Satellite," U. S. Army Engineer Research and Development Laboratories, Fort Belvoir, Va.

[4] "Manufacturing the Earth Satellite," *The Magazine of Magnesium*, May 1957 edition.

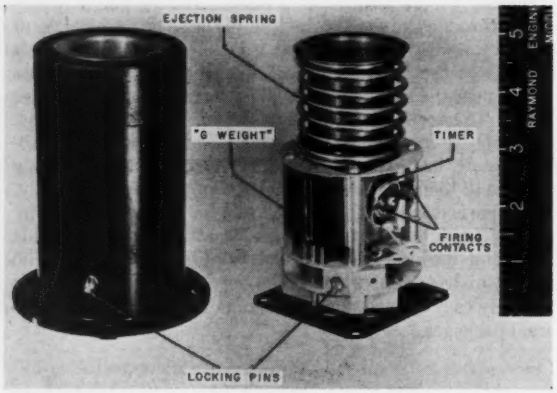

Front View

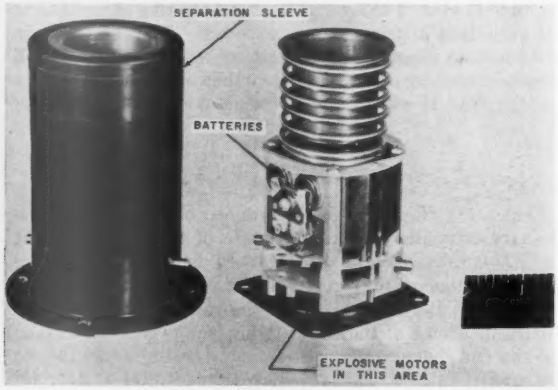

Rear View

Fig. 5 Satellite separation mechanism

The desired section is trimmed out of the spinning. The two pressure connection fittings are welded in position and then the inner segment is welded onto its proper location in the interior of the hemisphere. Fig. 6 shows the resulting pressure cavity. The unit is then stress-relieved and hydrostatically pressure-tested for leaks. When the unit is found to be leak-free it is placed on a mandrel and the outer surface is machined to give a skin thickness of 0.026 in. except at base section where it is 0.050 in. thick. The hemispheres are then trimmed and all drilling, tapping and other machine work is done. The hemispheres are then ready for finishing and plating.

The Structure

The tubular sections that make up the structure are first bent into the shape desired. These pieces are then machined as necessary in order to obtain the proper fits. The entire assembly is fitted to a special jig and positioned so that it will meet specifications and tolerances as to the concentricity, dimensions, etc. The tubular structure is then welded together while clamped in place on the jig (Fig. 7). With the structure still on the jig the spherical surfaces at the top, bottom and where the antennas are located are then machined to fit the inside dimensions of the shell halves (Fig. 8).

Assembly

After completion of the structure the shell halves are then mounted onto the structure and secured in place by rivets and screws. After the shells are assembled to the structure and inspected the unit is then ready for shipment to NRL where further assembly of the scientific equipment and the coating of the shell will take place.

The "Kel-F" support pieces are made at NRL and are on hand when the unit arrives. The shells are taken off the structure and sent to Fort Belvoir for the silicon monoxide coating process. The internal structure is sent to the NRL shops for fitting of the internal package with the Kel-F supports and the assembly of the antennas. Upon return of the shells from coating, the lower half of the shell is assembled to the structure. Gages, such as erosion gages, temperature gages, pressure gages, and so forth, are mounted on the lower hemisphere. The internal package is assembled; the antenna connections are made; the wiring is done on the lower half of the sphere and the upper half of the sphere terminating in the plugs previously mentioned. There is an extensive inspection and test procedure performed on each and every unit prior to, and after, the assembly procedure.

Testing

Shells with Pressure Zones

1 Hydrostatic. Each hemisphere is tested hydrostatically as it is received from the contractor. The zone is filled with distilled water and the pressure is increased gradually until a pressure of 25 psig is reached. This test is for the purpose of determining the structural adequacy of the zone and also to locate any leaks.

2 Dry Gas. After completion of the hydrostatic tests the hemisphere is dried and filled with freon gas to approximately 20 psig. A leak detector is employed to locate minute leaks. Leaks, if any, are marked and the zone is then flushed with nitrogen gas.

3 Vacuum. The zone is connected to a vacuum system and the pressure is reduced to 0.5 mm Hg vacuum. A sealer is introduced into any small holes for sealing the leaks. The hemisphere is then oven dried again. Steps 2 and 3 are repeated until no leaks can be detected.

Satellite Separation Mechanism

In general the purpose of the tests on the satellite separation

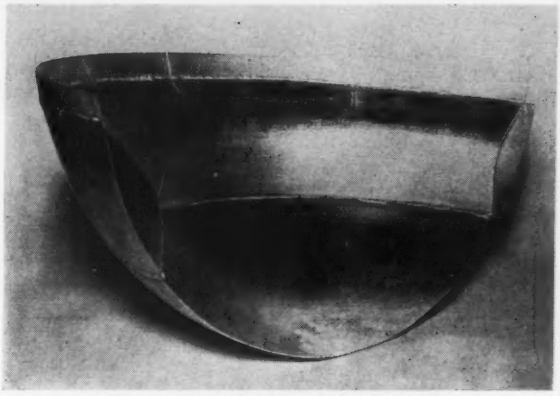

Fig. 6 Cross section of pressure zone

Fig. 7 Welding satellite structure

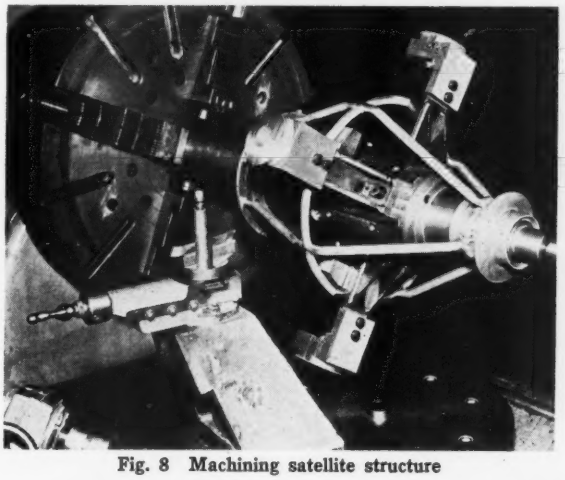

Fig. 8 Machining satellite structure

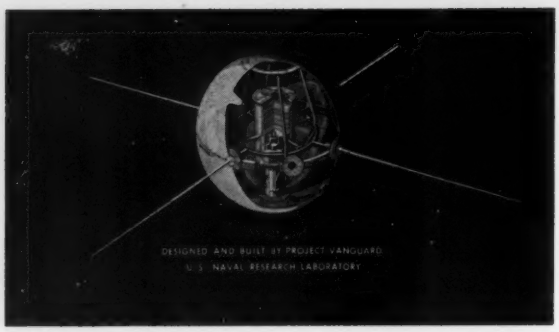

Fig. 9 Scientific earth satellite

mechanisms were to determine their suitability as separation units for separating the satellite after completion of third stage burning. The units must withstand the environmental conditions of the launching vehicle, provide sufficient delay and sufficient force to separate the satellite from the third stage after third stage burnout.

Antennas

The tests on the antennas were for two purposes. First, to check out the antenna design to insure that the antenna will survive the environment which exists during flight, such as aerodynamic heating, vibration, and acceleration. The second set of tests are checks to determine whether or not the antennas have been fabricated properly and have the strength as required, i.e., checking the heat-treatment of the antennas.

Assembly Design and Final Acceptance Tests

Design acceptance tests and final acceptance tests are made independently under test conditions outlined by the Environmental Subcommittee of the Science Program Committee at NRL. The design acceptance tests consist of: (a) Random vibration up to 25 g parallel to thrust from 10 to 2000 cps and up to 20 g from 10 to 2000 cps traverse to thrust; (b) steady state acceleration to 75 g in the thrust direction; (c) extensive thermal-vacuum life tests between 0 and 60 C (internal package temperature) on the completely instrumental satellite. The final acceptance tests of flight units consist of the following tests: (a) Random vibration up to 10 g from 10 to 2000 cps; (b) steady stage acceleration to 35 g in the thrust direction; and (c) thermal and vacuum tests as follows: simulation of initial heating of shell to 300 F, temperature cycling similar to design acceptance tests, and life test of one week under vacuum and thermal conditions.

Two complete satellites, identical to flight units, are used for thermal testing. These units are instrumented with all gages, electronics and batteries. The assembly is placed in a vacuum chamber which is housed in a high altitude chamber. The environment in this chamber can be controlled. The temperature is cycled in a manner which simulates the expected orbital temperature fluctuations. The pressure is reduced to 0.1 mm of mercury for these tests. The temperature of the shell, the inner package and electronics are continually monitored. The equipment is operated as it will be in orbit and monitored constantly. Such a test as this takes about three weeks if no failures of equipment occur.

Summary

After the results of the many and varied tests have been studied and analyzed and the design is considered satisfactory to meet all requirements, the resultant satellite (Fig. 9) may be described as follows: The highly polished silicon monoxide coated 20-in.-diam magnesium sphere has four antennas mounted 90 deg apart at the equator. These antennas are fastened by tubular rods to a tubular ring which is concentric with the cylindrical inner package. This ring is also supported by four bow-shaped vertical tubular members spaced 90 deg apart at angles of 45 deg to the antenna supports. These vertical members are fastened to the support ring of the access port at the top and to the main support column which houses the separation mechanism at the bottom. The cylindrical internal package is mounted on the main support column and is also secured to the concentric tubular ring by four low thermal conductivity radial supports spaced 90 deg apart and angularly positioned between the antenna supports and the vertical members. The sphere is girdled by two pressure zones or bands, one below the equator and one above. On the shell are three microphones, a Lyman Alpha solar cell and two Lyman Alpha ion chambers. In addition to the microphones and the Lyman Alpha experiment, there are experiments which consist of erosion gages and temperature gages, which are located both at the north pole area and around the equator. There is a pressure gage located on the concentric tubular ring. Also included in the internal package are five $\frac{3}{4}$-in.-thick modules; of these one module is for the Minitrack transmitter and associated electronics; one module is for the Lyman Alpha electronics and batteries; one for the coding 48 channel telemetering system; one for the peak memory orbital switch unit; and one for the meteor counter. Below these five $\frac{3}{4}$-in.-thick modules are the battery packages. One battery package is $1\frac{5}{16}$ in. thick; the other battery package is $2\frac{1}{2}$ in. thick. These seven modules are held to the top cover of the internal package through two $\frac{1}{4}$-in.-diam rods. On the top cover of the internal package are several connectors. One 36-pin connector; one 14-pin connector; one 50-ohm microdot connector and two standoffs for the Lyman alpha experiment. The connectors serve two purposes—not only do they connect the gages on the skin to the electronics, but they also connect the batteries with the electronics, thus acting as a turn-on switch.

Conclusion

When the Vanguard launching vehicle places the small IGY earth satellite sphere into orbit, it will have placed a reliable laboratory into space. This laboratory together with the Sputniks and the Explorer will be instrumental in unlocking some of the hidden secrets of our planet and the space which surrounds us. Perhaps it will be an important instrument by which man can insure his survival when he first attempts to venture into the darkness beyond.

A Recording Sodium-Line Reversal Pyrometer

W. M. BROBECK,[1] R. E. CLEMENSEN[2] and W. E. VORECK[3]

Radiation Laboratory, University of California, Livermore, Calif.

An instrument for the measurement of flame temperatures from 1500 to 2700 C by the sodium-line reversal method is described in which the eye and hand of a trained operator are replaced by a closed-loop electromechanical system. The advantages are in continuous recording of varying flame temperatures, increased accuracy, and measurement on flames that would be dangerous to an observer.

Introduction

THE sodium-line reversal method of measuring high gas temperatures (1)[4] has been widely used and accepted. In this method a sodium salt is introduced into the hot gas, and the brightness of the characteristic D lines of the sodium spectrum is compared with the background formed by the continuous spectrum of a lamp filament observed through the same gas. With a fixed gas temperature, as the filament temperature is raised the sodium lines are first brighter and then darker than the background. At the "reversal point," at which the lines and background have the same brightness, the temperature of a black body having the same brightness as the filament is equal to the gas temperature. By observing the filament with an optical or thermopile pyrometer, the equivalent black body temperature that equals the sodium-line reversal (SLR) temperature of the gas can be obtained.

The temperature reading is independent of the path length or concentration of sodium in the gas over a wide range. The effect of insufficient light is to make the location of the reversal point less definite but not to move the reversal temperature, since the reversal point depends on the ratio of excited to unexcited sodium atoms. Detailed discussion of the method and its accuracy are given in (2, 3, and 5).

In the usual application of this method to steady temperatures, the reversal point is observed by an operator looking through a spectroscope and adjusting the lamp filament manually. Methods have been devised for displaying the reversal temperature on film (3) and of following the temperature in the combustion chamber of an engine (4).

Design

In the application to be described it was desired to present the gas temperature on a conventional self-balancing potentiometer having a full scale travel in the order of 1 sec.

The arrangement used is shown diagrammatically in Fig. 1. Light from the filament B passes through condensing lens C and through the gas stream E. From the gas stream the light passes through the collimating lens G, slit H, prism I, and objective lens J of the spectroscope to the vibrating mirror K. From K the light, now consisting of the spectrum in the region of the sodium D lines, passes through the exit slit M into the photomultiplier tube N. A block diagram of the electrical circuit is shown in Fig. 2. The output of the phototube is commutated by the chopper and fed through the amplifier to the two-phase motor which adjusts the brightness of the lamp filament to match the brightness of the sodium D lines from the flame.

Operation

The spectrum and electrical signals are shown in Fig. 3. The two sodium lines are not resolved by the photocell. When the lamp is cooler than the gas the spectrum appears as in (a). As the mirror sweeps the line back and forth across the exit slit the phototube output appears as in (b). When chopped, the signal (c) is produced, having the necessary 60-cycle component to drive the two-phase motor in the increase direction. At (d), (e), and (f) are shown the corresponding signals for the case in which the lamp filament is too bright and the sodium lines appear dark against the brighter background.

The 60-cycle component in the bright light shown in (e) and (f) of Fig. 3 is due to nonlinearity in photocell response and difference in energy content of light of different colors. It is caused by scanning the spectrum in the area of the sodium lines as shown in (g). The 60-cycle component can be reduced by reducing the mirror amplitude, and by use of a 60-cycle filter on the photocell output. The chopper phase is adjusted to make any residual 60-cycle component cancel out as shown in (f). The signals in (b), (c), (e), (f) are obtained with no filter on the photocell output. With the filter installed, input to the chopper is a smooth sine wave which decreases to zero at balance, and then increases 180 deg out of phase when the balance point is passed. If the vibrating mirror were driven at 30 cycles instead of 60, the chopper would evidently not be required. However, this arrangement has not been tried.

The temperature is observed by the radiation pyrometer

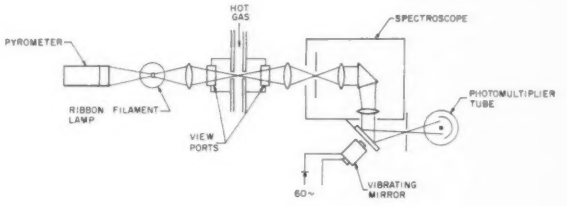

Fig. 1 Diagram of optical system

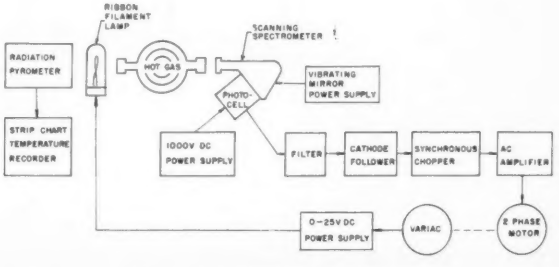

Fig. 2 Electronic block diagram

Received Sept. 27, 1957.

[1] Assistant Director, in charge of mechanical engineering.
[2] Electronic Engineer.
[3] Chemical Engineer.
[4] Numbers in parentheses indicate References at end of paper.

(A, Fig. 1) focused on the lamp filament and driving the recording potentiometer. It had been planned to record the lamp filament voltage but changes observed in the characteristics of the filament made the use of the radiation pyrometer preferable. The recorder is located several hundred feet from the optical system. Controls, not shown, are provided for adjusting the amplitude and phase of the mirror vibration. The effect of these adjustments is observed by a cathode-ray oscilloscope displaying the amplifier input.

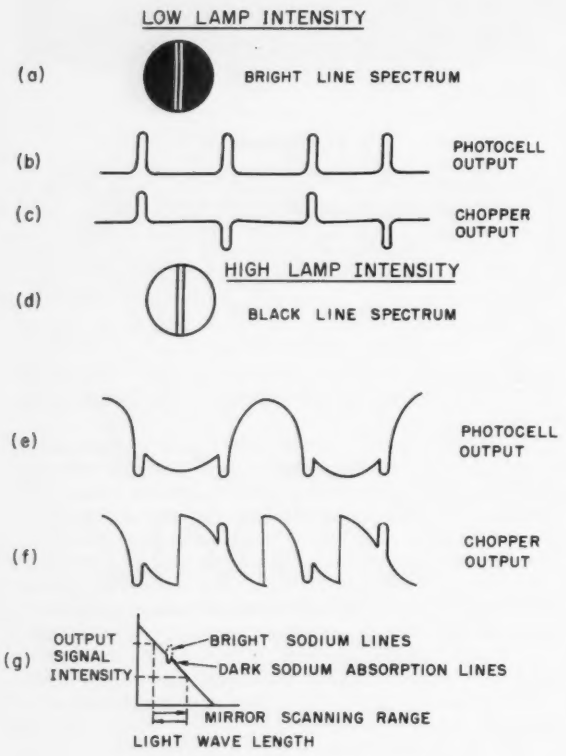

Fig. 3 Optical and electrical signals

The walls of the test section, in which the pressure is a few hundred psi, are protected by a graphite tube. The windows D and F (Fig. 1) can become obscured by carbon or metal vapor released in the test section. Deposits on the window F are important only as they affect the sharpness of the balance point, but changes in the transmission of D will affect the recorded temperature. For this reason, the radiation pyrometer has been calibrated by observing the filament with an optical pyrometer through the glass of window D before and after several runs. In the present application, the change during a 5-min run has not been appreciable. The correction for absorption in the glass between the lamp and the flame is approximately related by $k = \Delta T/T^2$. For a typical lens and viewport, k equals 4×10^{-6} for the lens C, and 9×10^{-6} for the viewpoint D. Using these correction factors, the pyrometer can be calibrated by an optical pyrometer looking directly at the lamp.

Sodium vapor is introduced into the gas at a point of low velocity by a sodium "bubbler," in which coiled nichrome wire filament is used to heat sodium chloride to its boiling point in a ceramic cup. Sodium vapors from the cup are swept into the flame to provide the concentration of sodium necessary in the hot gas.

The usable range of the instrument is limited to from 1500 to 2700 C. The lower limit is reached when the signal strength is so low that the photocell cannot pick it up. The upper limit is determined by the maximum usable filament temperature. Although tungsten does not melt until it reaches 3370 C, excessive vaporization causes obstruction of the light and rapid failure of the filament above 2700 C.

Results

Peformance of the instrument has been quite satisfactory. The balance point of the instrument agrees with that obtained by eye. Calibrations of repeated balance points agree to within the accuracy of the optical pyrometer, which is ±5 C. The hysteresis as determined by the return to balance after a disturbance is ±5 C, as shown in Figs. 4 and 5. The observed flame temperatures in Figs. 4 and 5 agree quite well with temperatures reported in the literature of 1737 C for ethane in air and 2067 C for acetylene in air (5). Fluctuations in the base lines are due to variations in flame temperature. The deflections up and down scale were deliberately introduced to check hysteresis and recovery time of the instrument. As can be

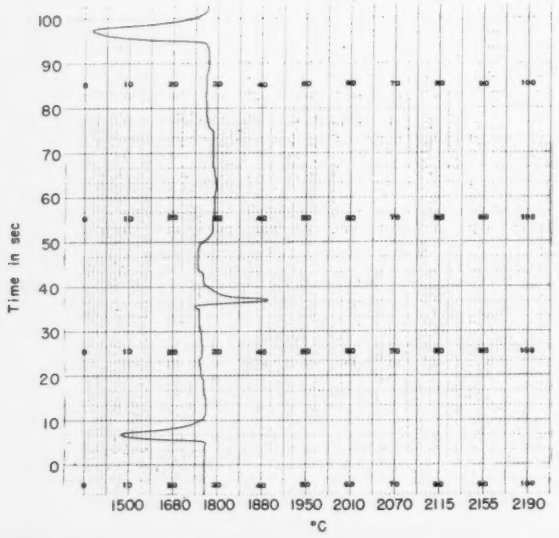

Fig. 4 Hysteresis of temperature measurement, propane-air flame

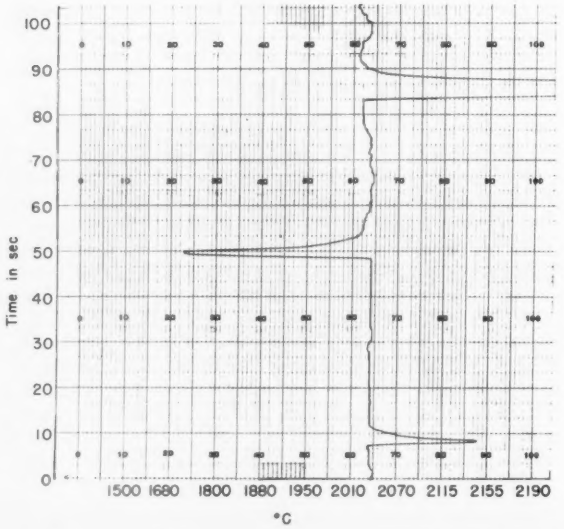

Fig. 5 Hysteresis of temperature measurement, acetylene-air flame

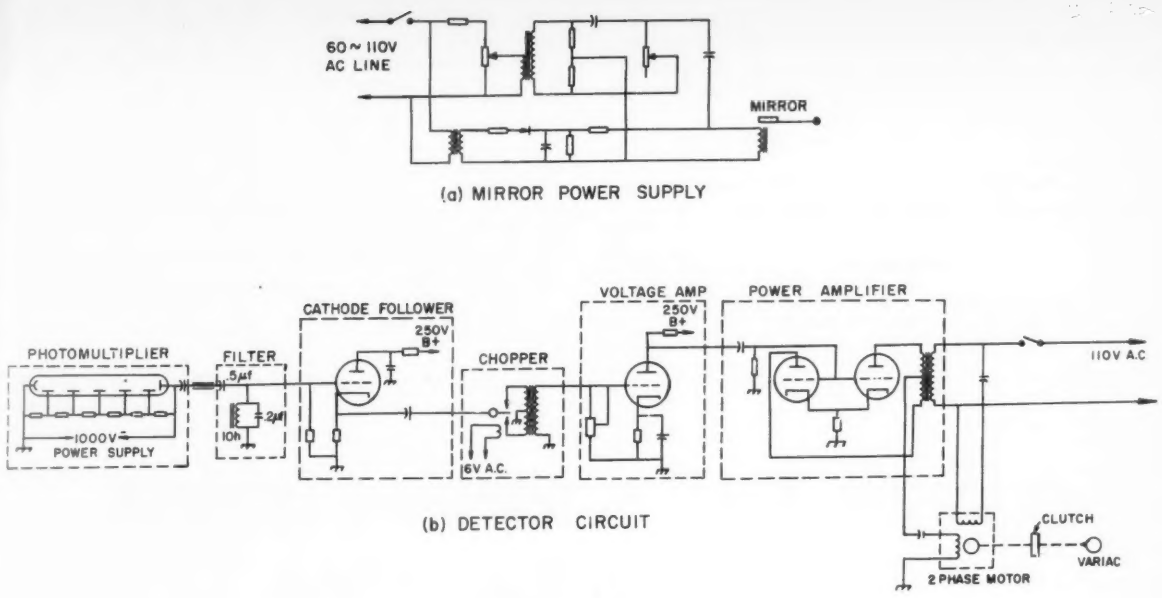

Fig. 6 Electronic circuits

seen, the speed of the motor drive limits use of this instrument to flames whose rate of temperature variations does not exceed 50 C per sec.

Calibration

The recorder is calibrated by observing the lamp filament from the same position as the recording pyrometer with an optical pyrometer. Several temperatures are checked, and the millivolt output of the recorder is correlated against the optical pyrometer readings corrected for the effect of lens C, viewport D_1, and the difference in tungsten emissivity between 6650 Å, where the pyrometer is calibrated, and 5893 Å where the sodium D lines are located (7). The combined correction is obtained from

$$\Delta T = 0.000117 T_{op}^{1.63}$$

Acknowledgments

The authors wish to acknowledge the valued assistance of R. A. Heckman, who initiated the project; also J. G. Bolger, R. N. Clark and A. C. Griffin for assistance with the mechanical design, the electrical construction and the mechanical construction, respectively.

This work was sponsored by the U. S. Atomic Energy Commission.

Appendix A. Electronic Balancing Circuit

The over-all operation of the electronic part of the instrument has been described, and is shown in the block diagram of Fig. 2. Circuit details of the unique components in the system are shown in Fig. 6.

The signal output is generated by an oscillating mirror which sweeps a small portion of the spectrum, including the sodium D lines at 5890 and 5896 Å across the slit in front of the photomultiplier. The mirror power supply shown in Fig. 6(a) produces a half-wave 60-cycle component to the mirror magnet. This causes the mirror to vibrate at a 60-cycle rate, producing a 120-cycle component of the sodium lines in the photomultiplier output. Amplitude of the mirror is adjusted to sweep a range from 5887 to 5899 Å to produce a balanced 120-cycle component. Phase of the mirror is adjusted to produce maximum sensitivity to 120 cycles and minimum response to the 60-cycle component.

Light leaving the exit slit enters the photomultiplier of the detector circuit shown in Fig. 6(b). Most of the 60-cycle component, produced by the nonlinearity of the spectral sensitivity of the photomultiplier and any high frequency interference, is shorted to ground in the filter, which is tuned to pass only 120 cycles.

Appendix B. SLR Scanning Spectroscope

Preliminary work was done using a conventional Bausch and Lomb (6) spectroscope, with a vibrating mirror and photocell system substituted for the eyepiece. Since this arrangement was not portable and was difficult to keep in alignment, a compact instrument has been designed and is being constructed.

An assembly drawing of the proposed instrument is shown in Fig. 7. Light path and general operation have been described previously. The spectroscope design has been simplified by the addition of a front surface mirror A behind the prism B which produces a constant deviation of light beams regardless of prism position. Light is focused by lens C on the entrance slit D. Light leaving the entrance slit is

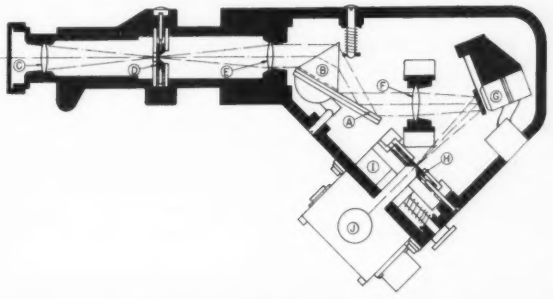

Fig. 7 Scanning spectroscope

made parallel by lens E. After passing through the prism B it is reflected from mirror A through lens F. Light from lens F is reflected from the vibrating mirror G and is focused on the exit slit H. Normally it passes through a hole in slide I into a photocell in box J. For spectrum and slit adjustment, a mirror on slide I can be pulled into position to reflect light into an eyepiece.

Since construction of this improved instrument has not been completed, its operation has not been tested.

References

1 Féry, Ch., *Comptes Rendus Hebdomadaires des Séances de l'Académie des Sciences*, vol. 137, 1903, p. 909.

2 Lewis, B., and von Elbe, G., "Combustion, Flames and Explosions of Gases," Academic Press, New York, 1951.

3 Landenberg, R. W., Lewis, B., Pease, R. N., and Taylor, H. S., editors, "Physical Measurements in Gas Dynamics and Combustion," Princeton University Press, Princeton, N. J., 1954.

4 El Wakil, M. M., Myers, P. S., and Uyehara, O. A., "An Instantaneous and Continuous Sodium-Line Reversal Pyrometer," *Trans. ASME*, vol. 74, 1952, p. 255.

5 Gaydon, A. C., and Wolfhard, H. G., "Flames, Their Structure, Radiation and Temperature," Chapman and Hall Ltd., London, 1953.

6 Bausch and Lomb Optical Company, laboratory spectroscope, Cat. 33-82-05.

7 Worthing and Halliday, "Heat," John Wiley and Sons, Inc., New York, 1948.

An Iterative Method of Determining Equilibrium Compositions of Reacting Gases

S. T. CHU[1]

Ohio State University, Columbus, Ohio

Introduction

NUMEROUS papers have been published in the past on the determination of equilibrium compositions for reacting gases. A comprehensive but brief review on this subject can be found in (1).[2] The governing equations, upon which the solutions of equilibrium compositions may be obtained are mainly of two kinds—the material balance equations and the equilibrium equations. Because of the nonlinear algebraic form of the latter equations, solutions of closed form are not obtained.

In (1) the various approximate methods were classified into four categories: (a) Trial and error methods, (b) iterative methods, (c) graphical methods and use of published tables and (d) punched-card or machine methods.

The iterative method presented here is somewhat different in nature from those previously published in that category in that the efficiency of iteration should be independent of whether the mixture is far from or close to the stoichiometric proportions. Furthermore, this method has the merit of providing explicit correction terms for each succeeding iteration; that is, the solutions of each iteration may be obtained by simple algebraic operations whose forms remain invariant for all orders of iterations. Convergence criterion for this method may be established mathematically for a simple problem of dissociation of diatomic gases which is employed mainly as a testing case for convergence. It indicates that the results for this case will converge even when the zeroth order of approximation involves an error of one hundred per cent in magnitude.

Analysis

The equilibrium compositions of a mixture of perfect gases having chemical reactions are dictated by Dalton's law and the conditions of equilibrium. For simplicity, we shall take the case of stoichiometric reaction of water vapor as an illustration, which is represented by the following equations

Dalton's law

$$p_{H_2O} + p_{H_2} + p_{O_2} + p_{OH} + p_O + p_H = p \quad [1]$$

Conservation of atomic elements

$$p_{H_2O} + 2p_{O_2} + p_{OH} + p_O - \beta(2p_{H_2O} + p_{OH} + 2p_{H_2} + p_H) = 0 \quad [2]$$

where β is the ratio of (N_O/N_H).

Equilibrium conditions

$$p_O(p_{O_2})^{-1/2} = K_O \quad [3]$$

$$p_H(p_{H_2})^{-1/2} = K_H \quad [4]$$

$$p_{H_2}(p_{O_2})^{1/2}(p_{H_2O})^{-1} = K_{H_2O} \quad [5]$$

$$p_{OH}(p_{H_2})^{1/2}(p_{H_2O})^{-1} = K_{H_2O}^* \quad [6]$$

In these equations, all the equilibrium constants are known functions of temperature. For a given set of values of pressure and temperature, this system is sufficient for the determination of the six unknown partial pressures. However, because of nonlinear algebraic equations involved, solutions of closed form have not been obtained. A method based on successive approximation has been given by R. Edse (2). Various other methods may be found in (1).

In the following, an alternative method is suggested which has the merit of providing correction terms for the next iteration. Convergence criterion of this iteration process may be established.

In the above algebraic system, Equations [1–6], the first two equations are linear while the other four are nonlinear. However, the last four equations are of such a form that their

Received Sept. 18, 1957.

[1] Assistant Professor, Aeronautical Engineering Department.

[2] Numbers in parentheses indicate References at end of paper.

logarithmic differentials are related by linear equations; that is

$$(dp_O/p_O) - (\tfrac{1}{2}dp_{O_2}/p_{O_2}) = 0 \quad [7]$$

$$(dp_H/p_H) - (\tfrac{1}{2}dp_{H_2}/p_{H_2}) = 0 \quad [8]$$

$$(dp_{H_2}/p_{H_2}) + (\tfrac{1}{2}dp_{O_2}/p_{O_2}) - (dp_{H_2O}/p_{H_2O}) = 0 \quad [9]$$

$$(dp_{OH}/p_{OH}) + (\tfrac{1}{2}dp_{H_2}/p_{H_2}) - (dp_{H_2O}/p_{H_2O}) = 0 \quad [10]$$

For given values of p and T, the values of p_{O_2} and p_{H_2O} are first chosen and they are denoted by

$$p_{O_2}^{(o)} \qquad p_{H_2O}^{(o)}$$

Then the values of $p_O^{(o)}$, $p_H^{(o)}$, $p_{OH}^{(o)}$, $p_{H_2}^{(o)}$ can be readily obtained from Equations [3, 4, 5, 6]. Now let us denote the first approximation to be given by

$$p_i^{(1)} = p_i^{(o)} + \delta p_i^{(o)} \quad [11]$$

where the subscript i denotes any one of the components. From Equations [1 and 2], we have

$$\sum_i p_i^{(o)} + \sum_i \delta p_i^{(o)} = p \quad [12]$$

$$p_{H_2O}^{(o)} + 2p_{O_2}^{(o)} + p_{OH}^{(o)} + p_O^{(o)} + \delta p_{H_2O}^{(o)} + 2\delta p_{O_2}^{(o)} + \delta p_{OH}^{(o)} + \delta p_O^{(o)} \quad [13]$$

$$- \beta(2p_{H_2O}^{(o)} + p_{OH}^{(o)} + 2p_{H_2}^{(o)} + p_H^{(o)} + 2\delta p_{H_2O}^{(o)} + \delta p_{OH}^{(o)} + 2\delta p_{H_2}^{(o)} + \delta p_H^{(o)}) = 0$$

In terms of the difference form of zeroth approximation, Equations [7–10] may be written as

$$(\delta p_O^{(o)}/p_O^{(o)}) - (\tfrac{1}{2}\delta p_{O_2}^{(o)}/p_{O_2}^{(o)}) = 0 \quad [14]$$

$$(\delta p_H^{(o)}/p_H^{(o)}) - (\tfrac{1}{2}\delta p_{H_2}^{(o)}/p_{H_2}^{(o)}) = 0 \quad [15]$$

$$(\delta p_{H_2}^{(o)}/p_{H_2}^{(o)}) + (\tfrac{1}{2}\delta p_{O2}^{(o)}/p_{O_2}^{(o)}) - (\delta p_{H_2O}^{(o)}/p_{H_2O}^{(o)}) = 0 \quad [16]$$

$$(\delta p_{OH}^{(o)}/p_{OH}^{(o)}) + (\tfrac{1}{2}\delta p_{H_2}^{(o)}/p_{H_2}^{(o)}) - (\delta p_{H_2O}^{(o)}/p_{H_2O}^{(o)}) = 0 \quad [17]$$

Now, we can eliminate all $\delta p_i^{(o)}$ except $\delta p_{O_2}^{(o)}$ and $\delta p_{H_2O}^{(o)}$ from Equations [12, 13] by using [14, 15, 16, 17]. The resulting equations from [12 and 13] read

$$\begin{cases} (p_{H_2O}^{(o)} + \tfrac{1}{2}p_{OH}^{(o)} + \tfrac{1}{2}p_H^{(o)} + p_{H_2}^{(o)})(\delta p_{H_2O}^{(o)}/p_{H_2O}^{(o)}) \\ \quad + (p_{O_2}^{(o)} - \tfrac{1}{2}p_{H_2}^{(o)} + \tfrac{1}{4}p_{OH}^{(o)} + \tfrac{1}{2}p_O^{(o)} - \tfrac{1}{4}p_H^{(o)}) \times \\ \qquad (\delta p_{O_2}^{(o)}/p_{O_2}^{(o)}) = p - \sum_i p_i^{(o)} \end{cases} \quad [18]$$

$$\begin{cases} [(1-2\beta)p_{H_2O}^{(o)} + \tfrac{1}{2}(1-2\beta)p_{OH}^{(o)} - 2\beta p_{H_2}^{(o)} - \tfrac{1}{2}\beta p_H^{(o)}] \\ \quad (\delta p_{H_2O}^{(o)}/p_{H_2O}^{(o)}) + [2p_{O2}^{(o)} + \tfrac{1}{4}(1-2\beta)p_{OH}^{(o)} + \tfrac{1}{2}p_O^{(o)} \\ \quad + \beta p_{H_2}^{(o)} + \tfrac{1}{4}\beta p_H^{(o)}]\,(\delta p_{O_2}^{(o)}/p_{O_2}^{(o)}) = [2\beta p_{H_2}^{(o)} + \beta p_H^{(o)} \\ \qquad - (1-2\beta)p_{H_2O}^{(o)} - 2p_{O_2}^{(o)} \\ \qquad\qquad - (1-2\beta)p_{OH}^{(o)} - p_O^{(o)}] \end{cases} \quad [19]$$

These two equations may be expressed as

$$A^{(o)}\delta p_{H_2O}^{(o)} + B^{(o)}\delta p_{O_2}^{(o)} = p - \sum_i p_i^{(o)} \quad [20]$$

$$C^{(o)}\delta p_{H_2O}^{(o)} + D^{(o)}\delta p_{O_2}^{(o)} = E^{(o)} \quad [21]$$

from which the quantities $\delta p_{H_2O}^{(o)}$ and $\delta p_{O_2}^{(o)}$ can be evaluated.

In turn, we can obtain the first approximations $p_{H_2O}^{(1)}$ and $p_{O_2}^{(1)}$ from Equation [11]. Using Equations [3, 4, 5, 6], the first approximations for all partial pressures are determined.

Succeeding iterations are to be performed in exactly the same fashion. The starting equations are

$$A^{(n)}\delta p_{H_2O}^{(n)} + B^{(n)}\delta p_{O_2}^{(n)} = p - \sum_i p_i^{(n)} \quad [22]$$

$$C^{(n)}\delta p_{H_2O}^{(n)} + D^{(n)}\delta p_{O_2}^{(n)} = E^{(n)} \quad [23]$$

where

$$A^{(n)} = (p_{H_2O}^{(n)} + \tfrac{1}{2}p_{OH}^{(n)} + \tfrac{1}{2}p_H^{(n)} + p_{H_2}^{(n)})/p_{H_2O}^{(n)}$$

$$B^{(n)} = (p_{O_2}^{(n)} - \tfrac{1}{2}p_{H_2}^{(n)} + \tfrac{1}{4}p_{OH}^{(n)} + \tfrac{1}{2}p_O^{(n)} - \tfrac{1}{4}p_H^{(n)})/p_{O_2}^{(n)}$$

$$C^{(n)} = [(1-2\beta)p_{H_2O}^{(n)} + \tfrac{1}{2}(1-2\beta)p_{OH}^{(n)} - 2\beta p_{H_2}^{(n)} - \tfrac{1}{2}\beta p_H^{(n)}]/p_{H_2O}^{(n)}$$

$$D^{(n)} = [2p_{O_2}^{(n)} + \tfrac{1}{4}(1-2\beta)p_{OH}^{(n)} + \tfrac{1}{2}p_O^{(n)} + \beta p_{H_2}^{(n)} + \tfrac{1}{4}\beta p_H^{(n)}]/p_{O_2}^{(n)}$$

$$E^{(n)} = [2\beta p_{H_2}^{(n)} + \beta p_H^{(n)} - (1-2\beta)p_{H_2O}^{(n)} - 2p_{O_2}^{(n)} - (1-2\beta)p_{OH}^{(n)} - p_O^{(n)}]$$

The process is always to determine first $\delta p_{H_2O}^{(n)}$ and $\delta p_{O_2}^{(n)}$ from the known values of nth approximations of all the partial pressures. Knowing $\delta p_{H_2O}^{(n)}$ and $\delta p_{O_2}^{(n)}$, the values of $(n+1)$-th approximations for other partial pressures are then obtained by using Equations [3, 4, 5, 6]. It is obvious that iteration may be terminated as soon as the right-hand sides of Equations [22 and 23] become insignificantly small.

Generalization of this method to other chemically reacting systems may be easily made in a straightforward fashion as soon as the number of independent chemical reactions in the system can be ascertained and the governing equations of equilibrium are formulated.

In the following, we will study the convergence criterion of the above iteration scheme. The method is applied to the simple case of dissociation of diatomic gases whose exact solution of equilibrium composition can easily be determined. The reason for choosing this particular example is the simplicity in establishing the convergence criterion for this case. Similar criteria may be established for more complex cases. However, they will require tedious algebraic manipulation.

The governing equilibrium equations for the dissociation of diatomic gases, $(1/2)Y_2 \rightleftharpoons Y$, are

$$p_Y + p_{Y2} = p \quad [24]$$

$$p_Y(p_{Y_2})^{-1/2} = K \quad [25]$$

In applying the present iteration method to this case, we write

$$\delta p_Y^{(o)} + \delta p_{Y_2}^{(o)} = p - p_Y^{(o)} - p_{Y2}^{(o)} \quad [26]$$

$$(\delta p_Y^{(o)}/p_Y^{(o)}) - (\tfrac{1}{2}\delta p_{Y_2}^{(o)}/p_{Y_2}^{(o)}) = 0 \quad [27]$$

First we choose a value of $p_{Y_2}^{(o)}$; then the value of $p_Y^{(o)}$ is obtained from Equation [25], i.e.

$$p_Y^{(o)} = K(p_{Y_2}^{(o)})^{1/2} \quad [28]$$

Substituting this into [26 and 27], we have

$$\delta p_Y^{(o)} + \delta p_{Y_2}^{(o)} = p - K(p_{Y_2}^{(o)})^{1/2} - p_{Y_2}^{(o)} \quad [29]$$

$$\delta p_Y^{(o)} - \tfrac{1}{2}K(p_{Y_2}^{(o)})^{1/2}\delta p_{Y2}^{(o)} = 0 \quad [30]$$

Eliminating $\delta p_Y^{(o)}$ from [29 and 30], we obtain

$$[1 + \tfrac{1}{2}K(p_{Y_2}^{(o)})^{-1/2}]\delta p_{Y_2}^{(o)} = p - K(p_{Y_2}^{(o)})^{1/2} - p_{Y_2}^{(o)} \quad [31]$$

Since $p_{Y_2}^{(1)} = p_{Y_2}^{(o)} + \delta p_{Y_2}^{(o)}$, we can rewrite Equation [31] as

$$(p_{Y_2}^{(1)}/p_{Y_2}^{(o)}) = 1 + [(p - p_{Y_2}^{(o)} - K\sqrt{p_{Y_2}^{(o)}})/(p_{Y_2}^{(o)} + \tfrac{1}{2}K\sqrt{p_{Y2}^{(o)}})] \quad [32]$$

By induction, the following general relation may be derived

$$(p_{Y_2}^{(n+1)}/p_{Y2}^{(n)}) = 1 + Q^{(n)} \quad [33]$$

where

$$Q^{(n)} = \left[(p - p_{Y_2}^{(n)} - K\sqrt{p_{Y_2}^{(n)}}) \Big/ \left(p_{Y_2}^{(n)} + \frac{K}{2}\sqrt{p_{Y_2}^{(n)}} \right) \right]$$

In Equation [32], we see that if $p_{Y2}^{(o)}$ is estimated to be larger than the correct answer, the second term on the right-hand side of that equation will be negative; thus $p_{Y_2}^{(1)}$ will be smaller than $p_{Y2}^{(o)}$. On the other hand, if $p_{Y_2}^{(o)}$ is estimated to be smaller than the correct answer, the second term on the right-hand side of that equation will be positive; thus $p_{Y_2}^{(1)}$ will be larger than $p_{Y_2}^{(o)}$. The same characteristic is also exhibited by the general equation [33]. Therefore, qualitatively we see the trend of this iteration scheme proceeds in the right direction. Furthermore, it is seen that the iteration will be automatically terminated as soon as the second term on the right-hand side of Equation [33] approaches zero.

It follows from this discussion that the convergence of this iteration method can be proved if the following two conditions are shown to be valid

$$|Q^{(n)}| > |Q^{(n+1)}| \quad [34]$$

$$\{Q^{(n)}\}_{n \to N} \to 0 \quad [35]$$

To prove condition [34] is equivalent to requiring

$$\left| \left(p_{Y_2}^{(n+1)} + \frac{K}{2}\sqrt{p_{Y_2}^{(n+1)}} \right) \left(p - p_{Y_2}^{(n)} - K\sqrt{p_{Y_2}^{(n)}} \right) \right| > \left| \left(p_{Y2}^{(n)} + \frac{K}{2}\sqrt{p_{Y_2}^{(n)}} \right) \left(p - p_{Y2}^{(n+1)} - K\sqrt{p_{Y_2}^{(n+1)}} \right) \right|$$

or

$$\left| p_{Y_2}^{(n+1)} \left(p - p_{Y_2}^{(n)} - K\sqrt{p_{Y_2}^{(n)}} \right) \right| > \left| (p_{Y_2}^{(n)} \left(p - p_{Y_2}^{(n+1)} - K\sqrt{p_{Y_2}^{(n+1)}} \right) \right|$$

By using Equation [33], the term on the left-hand side of the above inequality, after rearranging, may be written as

$$\left| p_{Y_2}^{(n)} \left(p_{Y_2}^{(n)} + \frac{K}{2}\sqrt{p_{Y_2}^{(n)}} \right) Q^{(n)}(1 + Q^{(n)}) \right|$$

Similarly, the term on the right-hand side of the inequality may be written as

$$\left| p_{Y_2}^{(n)} \left\{ \left(p_{Y_2}^{(n)} + \frac{K}{2}\sqrt{p_{Y_2}^{(n)}} \right) Q^{(n)}(1 + Q^{(n)}) - p_{Y_2}^{(n)} Q^{(n)}(1 + Q^{(n)}) - K\sqrt{p_{Y_2}^{(n)}}(1 - \sqrt{1 + Q^{(n)}}) - \frac{K}{2}\sqrt{p_{Y_2}^{(n)}}\,(Q^{(n)})^2 \right\} \right|$$

Examining these expressions closely, we see that the above inequality holds provided that

$$|Q^{(n)}| < 1 \quad [36]$$

To prove condition [35] is equivalent to showing

$$\left(p_{Y_2}^{(n+1)} + K\sqrt{p_{Y_2}^{(n+1)}} \right)_{n \to N} \to p$$

because the denominator of $Q^{(n+1)}$ is always positive. Now, we will express the above quantity in terms of $Q^{(n)}$ as follows

$$\left(p_{Y2}^{(n+1)} + K\sqrt{p_{Y2}^{(n+1)}} \right) = p_{Y_2}^{(n)}(1 + Q^{(n)}) + K\sqrt{p_{Y2}^{(n)}(1 + Q^{(n)})}$$

The last term on the right-hand side can be expanded by binomial series when $|Q^{(n)}| < 1$

$$p_{Y2}^{(n+1)} + K\sqrt{p_{Y2}^{(n+1)}} = p_{Y2}^{(n)}(1 + Q^{(n)}) + K\sqrt{p_{Y2}^{(n)}}\,[1 + \tfrac{1}{2}Q^{(n)} - \tfrac{1}{8}(Q^{(n)})^2 + \ldots]$$

As a consequence of [34], the absolute value of $Q^{(n)}$ will successively decrease as n increases, higher order terms involving square of $Q^{(n)}$ or higher may be dropped from the above expression when n approaches large integer N. That is

$$p_{Y2}^{(n+1)} + K\sqrt{p_{Y2}^{(n+1)}})_{n \to N} \to p_{Y2}^{(n)}(1 + Q^{(n)}) + K\sqrt{p_{Y2}^{(n)}}\,(1 + \tfrac{1}{2}Q^{(n)}) \equiv p$$

Therefore, [35] is verified under the proviso of [36].

Consequently, the condition $|Q^{(n)}| < 1$ may be taken as the criterion of convergence of this iterative method for the case of dissociation of diatomic gases. In terms of the initial choice, zeroth order approximation, this condition reads

$$\left| \frac{p - p_{Y_2}^{(o)} - K\sqrt{p_{Y_2}^{(o)}}}{p_{Y_2}^{(o)} + \frac{K}{2}\sqrt{p_{Y_2}^{(o)}}} \right| < 1$$

which is not at all stringent. For example, the zeroth order estimation involving ± 100 per cent error will still satisfy this condition.

It should be emphasized here that the study for the case dissociation of diatomic gases is mainly for the purpose of illustration since exact solution of the equilibrium composition for this case can be explicitly obtained. Furthermore, the rate of convergence is not established. Numerical computations, however, indicate fast convergence; first or second order approximations will provide accurate results in most cases.

For many cases where the mixture is far from the stoichiometric proportions, judicious selection of the zeroth order approximations may be made along the line suggested in (2) which will shorten the number of required iterations.

In view of the invariance of the form of the iteration formula for a given reacting system, this method should be particularly well adaptable to automatic machine computation.

References

1 Lewis, B., Pease, R. N., and Taylor, H. S., Editors, "Combustion Processes," vol. II of High Speed Aerodynamics and Jet Propulsion Series, Princeton University Press, 1956.

2 Edse, R., "Calculations of Detonation Velocities in Gases," WADC TR 54-416, March 1957.

Technical Notes

Ignition of Electrolytic Monopropellants by Submerged Electrical Discharge[1]

MARJORIE W. EVANS,[2] FRANK I. GIVEN[3] and G. M. MULLER[4]

Stanford Research Institute, Menlo Park, Calif.

ELECTROLYTIC liquid monopropellants can be ignited in the liquid phase by submerged high voltage electrical discharge. The authors have studied the nature of high voltage discharge in electrolytic liquids, the factors controlling the ignition or failure to ignite of monopropellants, and the propagation rate and shape of the reaction front following ignition. Experimental techniques included measurements of current through, and potential drop across, a submerged gap as a function of time, with a precision of ±10 per cent. Simultaneously, a modified Beckman and Whitley Model 189 Framing Camera was used to obtain time sequence pictures at a rate of 0.25 frame/μsec.

Upon sudden (rise time = 5 μsec) application of 1.5 to 4 kilovolts from a storage condenser to a localized electrode submerged in the monopropellant, a corona of finite lifetime is formed in the neighborhood of the electrode. This corona grows and then fades, disappearing at 30 to 40 μsec. If the anode-cathode geometry is such that the corona dies before a continuous path is formed through the corona from anode to cathode, no arcing occurs, and the remaining portion of the energy on the condenser may be discharged through the electrolytic liquid, the current being carried by the ions in electrolytic conduction. If, however, a continuous plasma path

Received Nov. 26, 1957.

[1] This work was supported in part by the Department of the Army, Ordnance Corps, through Ballistic Research Laboratories, under Contract DA-04-200-ORD-320.

[2] Senior Physical Chemist. Mem. ARS.

[3] Now Engineer, Aerojet-General Corp., Sacramento, Calif. Mem. ARS.

[4] Mathematician.

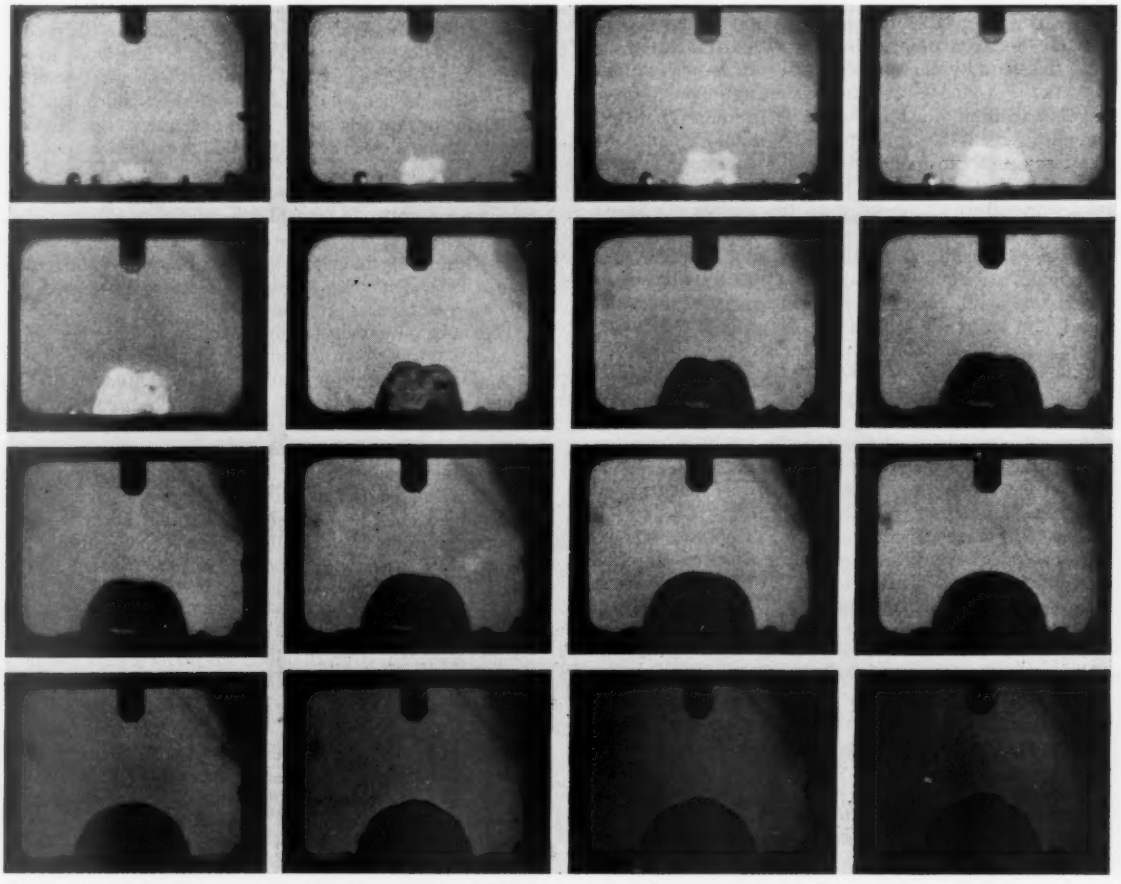

Fig. 1 Corona discharge and ignition in hydrazine, hydrazine nitrate monopropellant—voltage, 3500 v; condenser capacitance, 55 μf; framing rate, 0.25 frame/μsec; exposure time, 1.3 μsec

EDITOR'S NOTE: The Technical Notes and Technical Comments sections of JET PROPULSION are open to short manuscripts describing new developments or offering comments on papers previously published. Such manuscripts are published without editorial review, usually within two months of the date of receipt. Requirements as to style are the same as for regular contributions (see masthead page).

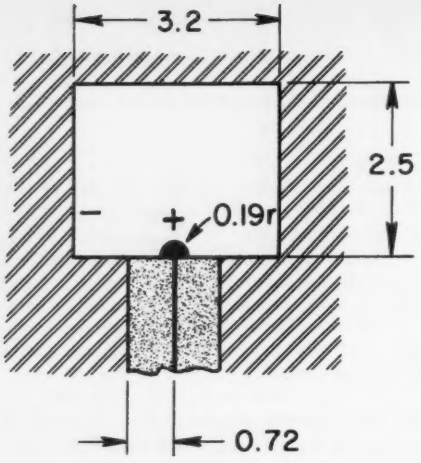

Fig. 2 Cross section reaction vessel; width of chamber = 5.1 cm; all dimensions are in centimeters

is effected during the corona lifetime, arcing occurs and the condenser rapidly discharges through the low resistance path provided by the arc.

For proper conditions of geometry and voltage, the monopropellants can be ignited either by arc or corona discharge, and the initial reaction occurs within the region affected by the arc or by the corona. A study of corona ignition for a variety of anode-cathode geometries and voltages showed that ignition is a function of energy density within the corona. By suitably controlling the geometry and voltage, ignition can occur upon delivery to a corona of as little as 1 to 10 joules. Criteria for effecting ignition with the lowest total expenditure of energy from the storage condenser were tentatively established.

Upon successful ignition, a self-propagating reaction zone moves through the liquid at the rate of 70 to 100 meters per sec for as long a time as the vessel walls remain intact and hold the liquid together. For a hemispherically growing reaction zone, this propagation velocity means that, within 100 μsec of the initial application of voltage to the electrode, reaction begins in approximately 2 cc of liquid; and, within 250 μsec, 8 cc of liquid have undergone at least partial reaction. Assuming very fast chemical reaction, the 65–30–5 (per cent weight) hydrazine, hydrazine nitrate, water propellant used in these experiments will produce in 250 μsec as much as 0.5 mole of gaseous products.

A series of framing camera pictures of monopropellant ignited by a corona discharge is shown in Fig. 1. A cross section of the reaction chamber is given in Fig. 2. Plexiglas windows 1 in. thick bolted to a heavy metal vessel formed two sides of the chamber. The protruding finger from the top of the vessel in Fig. 1 was floating at electrolyte potential and had no significance in the experiment. The vessel was completely filled with monopropellant. The first seven frames show the growth and decay of the corona. Ignition occurred within the corona during that time (28 μsec). The remaining frames show the self-propagation of the reaction zone into the liquid for 36 μsec more. According to other data taken simultaneously, the reaction zone propagated for a total of 230 μsec, at which time the Plexiglas windows shattered under the pressure of the products of reaction. Ignition for this particular geometry (not by any means the optimum geometry for economy of energy) required delivery to the corona-electrolyte system of 115 joules, of which 35 were delivered to the corona itself and were instrumental in igniting the monopropellant.

A detailed description of the behavior of electrical discharges in electrolytic monopropellants and an analysis of the function played by anode-cathode geometry and condenser voltage in ignitibility of electrolytic monopropellants is to be presented at the Seventh Combustion Symposium, Oxford, 1958.

A Note on Sonic Sudden Enlargements

R. H. PAGE[1]

Stevens Institute of Technology, Hoboken, N. J.

Introduction

FIGURE 1 has been found quite useful in estimating pressure ratios across choked abrupt area changes followed by *short* tubes. Since the permissible range of pressure ratios across a sonic sudden enlargement can be ascertained from this chart, problem solutions may often be expedited by its use.

Use of Fig. 1

The geometry considered in this paper and a typical pressure profile are shown in the figure. How the acoustic state at section 1 is approached (e.g., Fanno line or isentropic expansion) does not influence these results. For a given area ratio A_2/A_1, the maximum value (curve A), probable minimum value (curve B), and absolute minimum value (curve C), of the static pressure ratio P_2/P_1 are plotted. Curve B is called the probable minimum because it is more likely to occur than curve C. The curve C solution is somewhat analogous to the strong shock solution for angle shock since it must be forced on the flow to apply. (However, curve B represents a larger entropy change across the sudden expansion than curve C.)

The small charts at the top of the figure present the stagnation pressure ratio, P_{0_2}/P_{0_1} (maximum and minimum values), and the length of the "recovery zone" L/D_2 (where D_2 is the downstream tube diameter). Since the length of the recovery zone is dependent on a number of factors, the dashed curve only represents an approximation.

The maximum values, curve A, are independent of the geometry of the expansion and may be used for both outward-expanding and inward-expanding axially symmetric and two-dimensional sonic sudden enlargement. The minimum values, curves B and C, are, strictly speaking, only applicable to outward expanding axially symmetric configurations (the most frequently encountered geometry). However, minimum values calculated for two-dimensional sudden enlargements and sudden enlargements around abrupt central bodies in circular conduits fall within 10 per cent of these curves. Thus, Fig. 1 may be used, with some reservations, for configurations other than axially symmetric ones.

The top chart emphasizes that this figure is restricted to expansions followed by a short tube or to the short portion of a longer tube. The over-all pressure ratio for a sonic sudden enlargement followed by a rather long tube includes the downstream pressure ratio P_3/P_2 which must be calculated from the downstream flow path (e.g., Fanno or Rayleigh line). For *long* tubes acoustically choked at section 1, the over-all pressure ratio P_3/P_1 (where P_3 is the pressure at tube exit) may become rather low, limited by section 3 becoming sonic. For that case: $P_3/P_1 = P_{0_3}/P_{0_1} = A_1/A_2$. If the tube is very long, a double throat problem may exist, and it will be necessary to check (1)[2] to see if acoustic flow will ever be reached at section 1. For, if in the transient starting operation, section 3 (the end of the pipe) chokes before section 1, the sudden enlarge-

Received Nov. 25, 1957.

[1] Professor of Mechanical Engineering.

[2] Numbers in parentheses indicate References at end of paper.

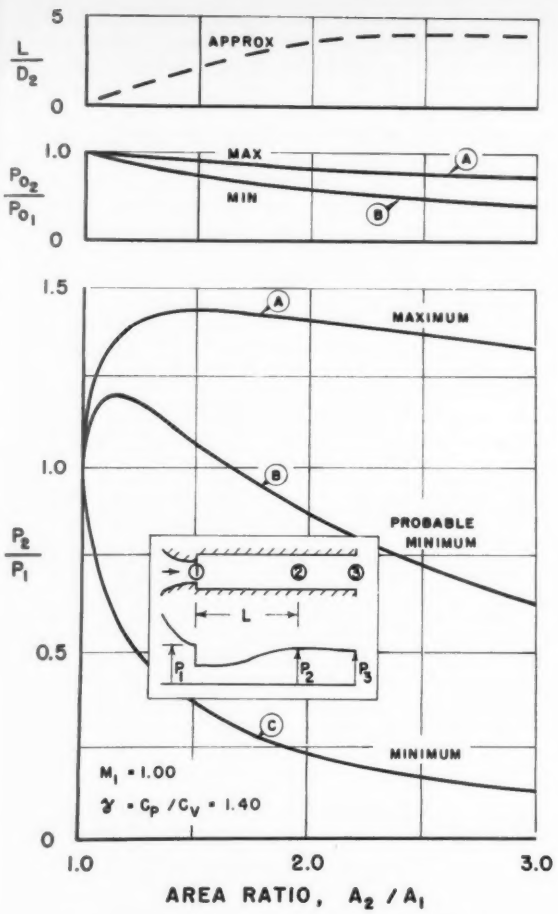

Fig. 1 Pressure ratios for axially symmetric flow

ment will remain subsonic. (Subsonic sudden enlargements are solved by well-known procedures (2, 3) for which convenient charts are available (4).)

Origin of Curves

A modified one-dimensional adiabatic analysis in which the shear stress at the wall is neglected has been used for the calculations. In applying the momentum principle, the force acting on the annular area or "base area" (A_2-A_1) is computed from the pressure acting on the base area. This "base pressure" is treated two ways:

1 For curve A, the base pressure was set equal to the sonic pressure P_1 and thus, in the manner of previous investigators (2, 3), a maximum pressure regain curve was calculated. This approaches unity asymptotically as the area ratio A_2/A_1 is increased. Of course large values of A_2/A_1 invalidate the one-dimensional assumption and, therefore, the curve is not continued for areas ratios larger than three.

2 For curves B and C, the minimum pressure ratios were desired. Low pressure ratios P_2/P_1 are obtained (2, 5) when the pressure acting on the annular area (base pressure) becomes less than the sonic pressure P_1. Indeed, the lowest pressure ratios, P_2/P_1, occur when the base pressure is at a minimum. Lowest limiting base pressure values are available (6) and were used in the analysis to calculate curves B and C. In this way the rather complex axially symmetric analysis (6) was merged into a one-dimensional treatment.

The recovery zone length is not subject to a simple definition and depends upon parameters not included in this note. This provisional curve was constructed as a compendium of experimental observations (2,7,8). It is not accurate, but is intended to present the order of magnitude of the recovery length.

Further Details

For most engineering purposes the maximum and minimum values of the pressure ratio P_2/P_1 will provide sufficient design information. The exact determination of the pressure ratio P_2/P_1, rather than the determination of maximum and minimum values, is much too involved to be considered in this note. However, detailed studies have been conducted (6, 9). W. L. Chow in a private communication indicates that further investigations are being carried out and that a comprehensive report may be forthcoming.

References

1 Shapiro, A. H., "The Dynamics and Thermodynamics of Compressible Fluid Flow," vol. 1, Ronald Press, New York, 1953, pp. 143–203.

2 Cole, B. N., and Mills, B., "The Theory of Sudden Enlargements Applied to the Poppet Exhaust-Valve, with Special Reference to Exhaust-Pulse Scavenging," *Proceedings of the Institution of Mechanical Engineers*, vol. 1B, no. 8, 1952–1953, pp. 364–377.

3 Hall, W. B., and Orme, E. M., 'Flow of a Compressible Fluid Through a Sudden Enlargement in a Pipe,' *Proceedings of the Institution of Mechanical Engineers*, vol. 169, no. 49, 1955, pp. 1007–1015.

4 Unterberg, W., "Communication on 'Flow of a Compressible Fluid Through a Sudden Enlargement in a Pipe' by Hall, W. B., and Orme, E. M.," *Proceedings of the Institution of Mechanical Engineers*, vol. 169, no. 49, 1955, p. 1018.

5 Wick, R. S., "The Effect of Boundary Layer on Sonic Flow Through an Abrupt Cross-Sectional Area Change," *Journal of the Aeronautical Sciences*, vol. 20, no. 10, 1953, pp. 675–682. "Further Comments on the Effect of Boundary Layer on Sonic Flow Through an Abrupt Cross-Sectional Area Change," *Journal of the Aeronautical Sciences*, vol. 22, 1955, pp. 135–137.

6 Korst, H. H., Page, R. H., and Childs, M. E., "A Theory for Base Pressures in Transonic and Supersonic Flow," University of Illinois, Engineering Experiment Station, ME-TN-392-2, OSR-TN-55-89, 1955.

7 Hall, W. B., and Orme, E. M., "Authors' Reply—Communication on 'Flow of a Compressible Fluid Through a Sudden Enlargement in a Pipe'," *Proceedings of the Institution of Mechanical Engineers*, vol. 169, no. 49, 1955, p. 1020.

8 Kochendorfer, F. D., and Rousso, M. D., "Performance Characteristics of Aircraft Cooling Ejectors Having Short Cylindrical Shrouds," NACA RM E51E01, 1951.

9 Korst, H. H., Chow, W. L., Zumwalt, G. W., and Smith, S. J., "Some Investigations of the Effect of Approaching Flow Boundary Layer on the Base Pressure Solution for Axi-Symmetric Sudden Expansion," University of Illinois, Internal Report, Mechanical Engineering Department, 1956.

Mach Reflections in Two-Dimensional Diffusers From Hydraulic Analogy Experiments

E. V. LAITONE[1] and J. E. STOUT[2]

University of California, Berkeley, Calif.

The separation distance required to prevent the formation of a Mach reflection between two wedges, representing either a two-dimensional diffuser or a Busemann biplane, is obtained by assuming that the normal shock wave could not have been created if the first expansion wave from the shoulder of the wedge would intersect it. This hypothesis

Received Jan. 15, 1958.

[1] Professor of Mechanical Engineering.

[2] Now at Douglas Aircraft Co., Santa Monica, Calif.

is verified experimentally for the special case corresponding to a specific heat ratio of $\gamma = 2$ by means of the shallow water hydraulic analogy.

FIGURE 1 gives an indication of the range of validity of the shallow water flow hydraulic analogy (see (1, 2 or 3)[3]) to two-dimensional gas dynamics for the particular cases occurring when either determining the minimum Mach number that must be attained in order to prevent a detached normal shock wave from forming in front of a given stream-tube deflection of $\theta_s(N = 1)$, or when determining the Mach number that must be exceeded in order to prevent the formation of a Mach reflection ($N = 2$). The usefulness of the direct analogy to two-dimensional compressible flow is limited to the regime wherein the oblique shock wave relations are approximated to the desired degree of accuracy by the isentropic compression values. As pointed out in (1 and 2), no hydraulic analogy exists for the mixed problem of transonic flow (having both subsonic and supersonic domains interacting), or whenever isentropic domains interact with the shock wave, unless the entropy increase through the shock wave can be neglected. That is, the direct analogy fails whenever the exact relations depicted in Fig. 1 are not sufficiently accurate approximations to one another.

[3] Numbers in parentheses indicate References at end of paper.

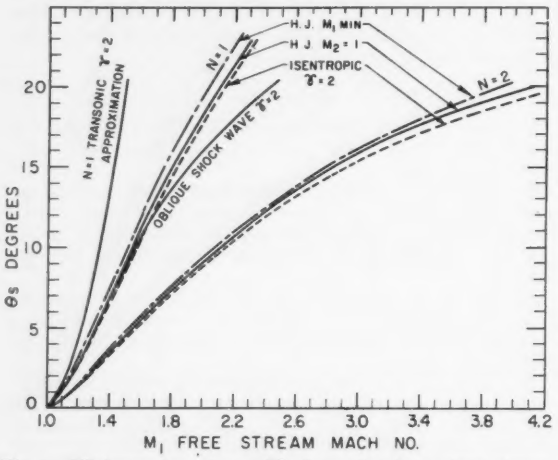

Fig. 1 Minimum free stream Mach number for a given stream tube deflection, $N = 1$, or for a reflection from a plane wall, $N = 2$

It is obvious from Fig. 1 that the model laws determined by the transonic similarity approximation, which are generally used to convert hydraulic analogy experimental results (3) from a specific heat ratio equivalent to $\gamma = 2$ to the usual gas dynamic case of $\gamma = 7/5$, cannot have as large a range of validity as the hydraulic analogy itself possesses in checking the fundamental equations of motion with $\gamma = 2$. Consequently, as pointed out in (1 and 2), the hydraulic analogy is more limited when used as a direct model test than it is when used as a check on any theoretical derivations or hypotheses concerning the behavior of the fundamental nonlinear equations of motion. Even when the hydraulic analogy to two-dimensional compressible flow completely breaks down, the shallow water tests are still useful for checking various methods used to develop approximate mathematical solutions of the boundary value problems, similar to the type occurring

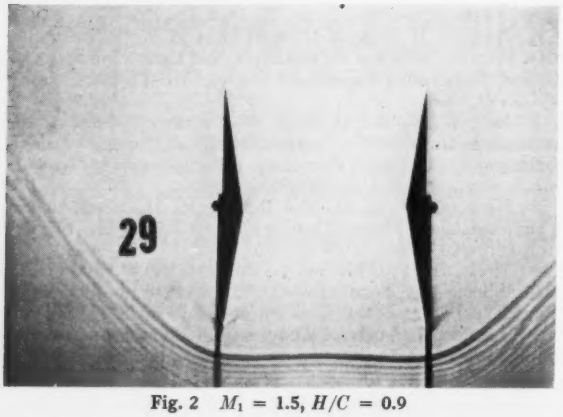

Fig. 2 $M_1 = 1.5$, $H/C = 0.9$

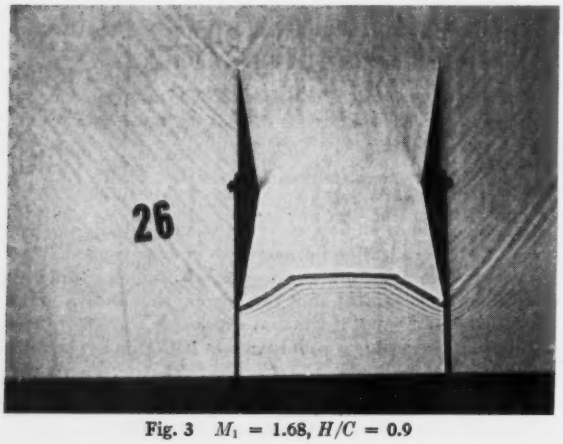

Fig. 3 $M_1 = 1.68$, $H/C = 0.9$

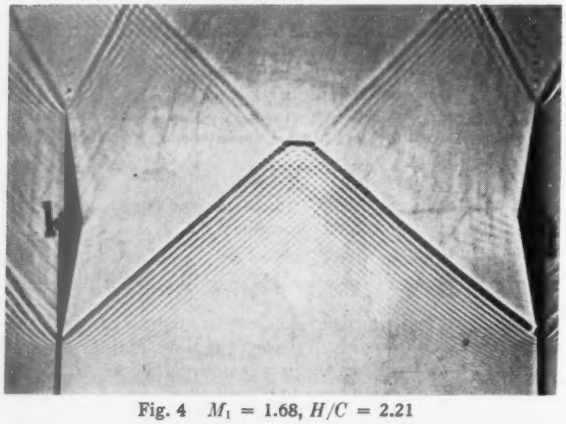

Fig. 4 $M_1 = 1.68$, $H/C = 2.21$

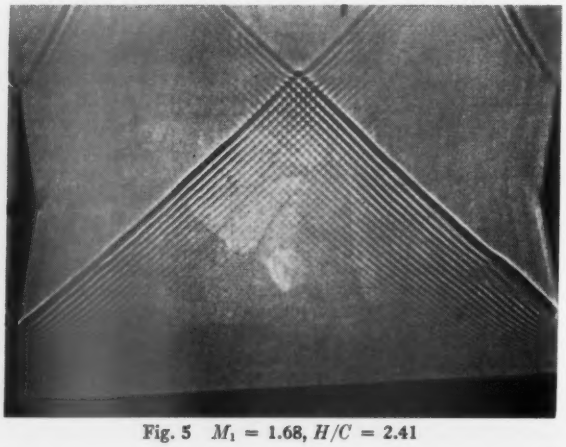

Fig. 5 $M_1 = 1.68$, $H/C = 2.41$

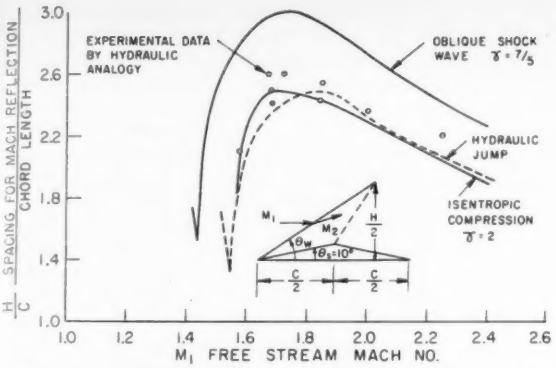

Fig. 6 Minimum separation distance which prevents Mach reflection between two wedge profiles

in gas dynamics, arising from the nonlinear equations defining the hydraulic jump and the potential shallow water theory. The only restrictions then are that the vertical accelerations outside the hydraulic jumps be negligible, and that all pressures be approximately hydrostatic. As shown in (1 and 2), these restrictions are satisfied, at least at transonic conditions, if the water depth everywhere remains less than $^1/_4$-in. and the model size is suitably large.

As an example of the application of shallow water experiments in formulating a theoretical solution valid for the gas dynamics case, even though the hydraulic analogy itself would fail as a direct model test, we shall determine a criterion for the necessary separation distance between two wedge profiles (simulating either a Busemann biplane or a two-dimensional diffuser) that would prevent the formation of a normal shock wave in between them; that is, the separation distance that would eliminate a Mach reflection.

Figs. 2 and 3 show typical cases of a normal shock wave producing a choking in the internal flow between two wedges. The photographs were taken by towing two 10-in. chord, 10-deg nose angle wedges at constant velocity through still water at a depth of 0.2 in. in a tank 20 ft long and 4 ft wide as described in (1). Fig. 2 shows the normal shock wave in front of both wedges since the free stream or towing Mach number is 1.50 which is less than the minimum value of 1.51 corresponding to a detached hydraulic jump for a 10 deg nose angle in Fig. 1 ($N = 1$).

In Figs. 3, 4 and 5, the free stream or towing Mach number is 1.68, which is greater than that defined by $N = 1$ in Fig. 1, but is still less than that given by $N = 2$. Therefore, a Mach reflection occurs whenever the attached nose shock waves intersect before they are met by the expansion waves arising from the wedge shoulders. That is, as the separation distance is increased, the expansion waves from the shoulder must eventually cancel the normal wave as in Fig. 5. Since the flow is everywhere supersonic, the nose shock waves form straight lines; consequently the minimum separation distance H, in order to have the first expansion wave arising at the shoulder meet the shock wave intersection point as shown in Fig. 6, is easily evaluated as

$$\frac{H}{C} = \left[\frac{\tan(\theta_s + \arcsin 1/M_2) - \tan\theta_s}{\tan(\theta_s + \arcsin 1/M_2) - \tan\theta_w}\right]\tan\theta_w = \left[\cos(\theta_w - \theta_s) - \sqrt{M_2^2 - 1}\sin(\theta_w - \theta_s)\right]^{-1}\left(\frac{\sin\theta_w}{\cos\theta_s}\right) \quad [1]$$

Fig. 6 presents Equation [1] for both the shallow water theory and the ideal gas flow having $\gamma = 7/5$. The experimental data given in Fig. 6 were obtained from the hydraulic analogy tests, the minimum separation distance which would eliminate the normal wave or hydraulic jump being determined from photographs similar to Figs. 4 and 5. The data indicate that a separation distance only slightly greater than that given by Equation [1] for shallow water theory will prevent the occurrence of a normal wave. It would now be of great interest to compare Equation [1] with corresponding experimental data in gas dynamics. Such tests would determine the range of validity of Equation [1], and, at the same time, should verify the similarity in the physical behavior between a shallow water flow and a two-dimensional compressible gas flow, even though the hydraulic analogy itself is not directly applicable as a model test for the entire range of the experimental data shown in Fig. 6.

References

1 Laitone, E. V., "A Study of Transonic Gas Dynamics by the Hydraulic Analogy," *Journal of the Aeronautical Sciences*, vol. 19, April 1952, pp. 265–272.

2 Laitone, E. V., "Developments in Gas Dynamics by the Hydraulic Analogy," Jubile Scientifique de M. Dimitri P. Riabouchinsky, "Memoires sur la Mecanique des Fluides," *Publications Scientifiques et Techniques du Ministére de l'Air, Paris*, 1954, pp. 203–217.

3 Harleman, D. R. F., and Ippen, A. T., "The Range of Application of the Hydraulic Analogy in Transonic and Supersonic Aerodynamics," Jubile Scientifique de M. Dimitri P. Riabouchinsky, "Memoires sur la Mecanique des Fluides," *Publications Scientifiques et Techniques du Ministére de l'Air, Paris*, 1954, pp. 91–112.

Friction and Heat Transfer in a Rough Tube at Varying Prandtl Numbers

R. C. HASTRUP,[1] R. H. SABERSKY,[2] D. R. BARTZ[3] and M. B. NOEL[4]

California Institute of Technology, Pasadena, Calif.

A set of experiments was carried out with the purpose of extending the available data on heat transfer in rough tubes as well as the information concerning the relationship between heat transfer and friction. The results are presented in terms of the heat transfer coefficient C_h and the friction coefficient C_f. Particular attention was paid to the effect of Prandtl number. The experiments were carried out in an electrically heated tube with water as a working fluid. By using water at various temperatures experiments could be performed over a continuous range of Prandtl numbers from about 1 to 7. For the tube and the type of roughness used in this experiment the results confirm that roughness increases the heat transfer as well as the friction coefficient, but that the ratio C_h/C_f decreases with increasing roughness. The latter effect seemed slightly more pronounced at the lower Prandtl numbers.

Nomenclature

c = specific heat
C_f = friction coefficient
C_h = heat transfer coefficient
d = tube diameter
d_e = equivalent diameter for rough tubes
g = gravitational constant
k = conductivity of tube wall
L = length of tube section
p = pressure
q = heat transfer rate per unit area

Received Jan. 16, 1958.

[1] Graduate Student. Now with Aerojet-General Corp., Sacramento, Calif. Mem. ARS.

[2] Associate Professor of Mechanical Engineering.

[3] Senior Research Engineer, Jet Propulsion Laboratory.

[4] Test Engineer, Jet Propulsion Laboratory.

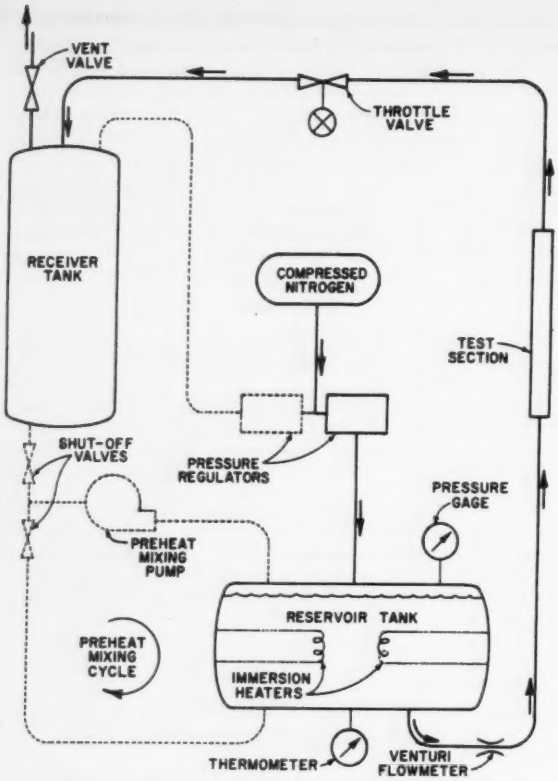

Fig. 1 Schematic diagram of test installation

Re = Reynolds number = Vd/ν
s = thickness of tube wall
t = temperature
t_b = bulk temperature of fluid
t_{wi} = temperature at inside of tube wall
t_{wo} = temperature at outside of tube wall
u = local velocity
V = average fluid velocity
ϵ_f = turbulent exchange coefficient for friction
ϵ_h = turbulent exchange coefficient for heat transfer
ν = kinematic viscosity
ρ = density
σ = Prandtl number = $c\mu/k$
τ = shear per unit area

Introduction

THE effect of wall roughness on friction in circular pipes has been well known for a long time. The most extensive set of experiments is perhaps that due to Nikuradse (1).[5] In these experiments Nikuradse prepared pipes of different degrees of roughness by means of sand grains of various sizes. For each pipe the friction drop was measured and the results were presented in a graph of the friction factor vs. Reynolds number. The experiments covered a range of relative roughness up to $^1/_{15}$, where the relative roughness was defined as the ratio of the sand grain diameter to the pipe diameter.

A similar set of experimental data for the heat transfer coefficient in tubes of different roughness would be equally useful. It would be of theoretical interest as well as of practical importance, for example, in the design of heat exchanger surfaces. In contrast to the rather complete data available on the friction coefficient, the information on the heat transfer coefficient in rough tubes is still relatively scarce. Of course, some work has been done in this field—one of the most valuable studies perhaps being the work recently published by Nunner (2).

[5] Numbers in parentheses indicate References at end of paper.

The lack of information becomes particularly apparent when it is realized that much more data are required for a proper representation of the heat transfer coefficient than for the representation of the friction coefficient. This results from the fact that the friction coefficient is determined adequately by two parameters: the relative roughness and the Reynolds number. At least one additional parameter, the Prandtl number, is, however, required for the proper determination of the heat transfer coefficient. For a complete investigation of heat transfer in rough tubes it is, therefore, not sufficient to represent the heat transfer coefficient as a function of Reynolds number for various relative roughnesses, in analogy with Nikuradse's graph. A graph of this type will have to be obtained for various Prandtl numbers. It was the purpose of these experiments to contribute to the information necessary for a complete survey of the heat transfer in rough tubes. The phase which was selected for this investigation was the effect of Prandtl number on the heat transfer coefficient in a tube of given roughness.

Test Equipment and Procedure

In order to conduct the desired experiments it was decided to use water as the working fluid. Water has the characteristics convenient for this experiment; that is, its Prandtl number is markedly affected by temperature, and its density is essentially constant. At room temperature the Prandtl number is approximately 7, and it can be made to decrease to unity by raising the temperature to about 300 F. By changing the temperature, therefore, a continuous variation of the Prandtl number could be effected without having to change fluids.

The experimental installation is shown schematically in Fig. 1. The water is contained in a reservoir and heated under pressure to the desired temperature; it is then forced out of the reservoir by pressure from a nitrogen supply tank. The water then flows through the test section into a receiver tank. The pressurized system produces a very steady flow and allows accurate flow and pressure measurements. The tank capacity was sufficiently large for run durations of the order of 5 min. This time interval was adequate for establishing equilibrium operating conditions.

The test section itself consisted of a stainless steel tube (Type 321) of $^3/_8$ in. diam. The wall thickness of the tube was 0.010 in. The length of the complete tube was 39 in. Of this, only 18 in. at the downstream end were heated, and this portion represented the actual test section. The upstream portion of the tube, corresponding to about 50 diameters, served as entrance length to establish an equilibrium velocity profile. The entire test section together with about 15 diameters of the entrance length were artificially roughened by knurling from the outside. During the knurling operation the inside of the tube was filled with a low melting point alloy ("Cerro bend") which was melted out after completion of the operation. The knurl pattern used was diamond shaped and relatively coarse. The diagonals of the diamond were approximately 0.10 and 0.05 in., and the depth of impressions produced on the inside of the tube was approximately 0.008 in. Immediately upstream and downstream of the 18-in. test section, a small length of tube was left smooth. These smooth regions were provided so that static pressure taps could be located at points where there would be no local disturbances due to surface roughness.

In addition to the rough tube a smooth test section with a smooth entrance section was also procured. The smooth test section was used because it seemed desirable to conduct experiments with such a tube first, so that the results could be compared with those of other experimenters as well as with the results of the rough tube.

Heat transfer to the 18-in. section of both the rough and the smooth tube was provided by electrical means. Alternating

current was passed through the stainless steel tube, the thin wall of the tube itself serving as a resistance heater. Electric heating has proved to be quite convenient in experiments of this type, as it allows rapid adjustment and accurate determination of heat flow rates.

The principal measurements that were made consisted of (a) the temperature of the water entering the test section, (b) the surface temperature at two places on the outside of the test section, 9 and 16 in. from the entrance, (c) the pressure drop across the test section and (d) the electric power dissipation in the test section. In addition the flow rate was determined by means of a Venturi meter. The dimensions of the test section were, of course, also required. In the case of the rough tube an effective tube diameter was defined on the basis of the volume of the tube as

$$d_e = \sqrt{\frac{\text{vol}}{L}\frac{4}{\pi}} \quad \ldots\ldots [1]$$

where vol is the volume of the tube and L the corresponding length. The volume was determined by measuring the amount of water required to fill the tube.

The quantities which we sought in these experiments were the friction coefficient C_f and the heat transfer coefficient C_h. These coefficients are given by

$$C_f = \left(-\frac{dp}{dx}\right)\frac{d}{2\rho V^2} \quad \ldots\ldots [2]$$

$$C_h = \frac{q}{\rho c V(t_{wi} - t_b)} \quad \ldots\ldots [3]$$

where t_{wi} is the temperature on the inside surface of the tube wall and t_b is the bulk temperature of the fluid. Both C_f and C_h may be computed from the aforementioned measurements. In computing C_f, the pressure gradient dp/dx was assumed to be constant along the test section. It was therefore set equal to $\Delta p/L$ where Δp is the pressure drop across the test section and L is its length. The velocity V was obtained from the volume flow rate and the cross-sectional area of the tube. In the case of the rough tube the diameter was taken to be equal to the effective diameter and the cross-sectional area was also based on this diameter. The heat transfer rate per unit area in Equation [3] was obtained assuming uniform power consumption along the tube. This assumption was justified as the specific electrical resistance of the tube was practically constant for the temperature changes which occurred in the tests. The inside wall temperature t_{wi} was calculated from the temperature measurement at the outside of the wall t_{wo}, correcting for the temperature drop through the wall by the expression

$$t_{wi} = t_{wo} - \frac{qs}{k}\left(\frac{1}{2} - \frac{s}{6d}\right) \quad \ldots\ldots [4]$$

The bulk temperature at any point along the tube was computed by adding to the temperature of the fluid entering the test section, the temperature increase caused by the total heat transfer to the fluid from the tube wall up to the section in question. With these data and knowing the fluid properties, the coefficients C_f and C_h were computed. It may be pointed out that the coefficients thus obtained represent local values applying to a particular section of the tube and that they are not averages over the length of the tube.

Great care was taken in making all the measurements. Particular attention was given to the problem of temperature measurements. In order to obtain satisfactory accuracy it was found necessary to calibrate each thermocouple in place. With precautions of this type it was possible to obtain reproducibility of the experimental coefficients C_f and C_h within 1 and 2 per cent, respectively. This reproducibility was also achieved in cases where a given Reynolds number was obtained in different ways, i.e., by means of different sets of values of velocity and viscosity.

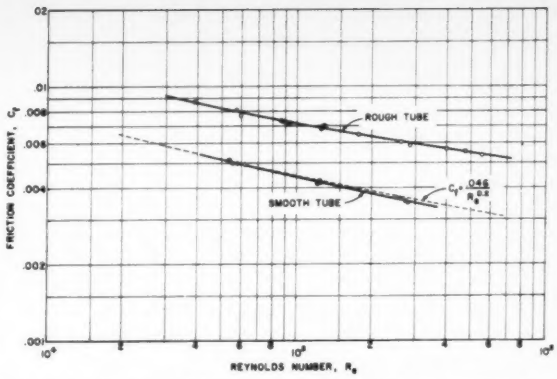

Fig. 2 Friction coefficients for the rough and the smooth tube as a function of Reynolds number

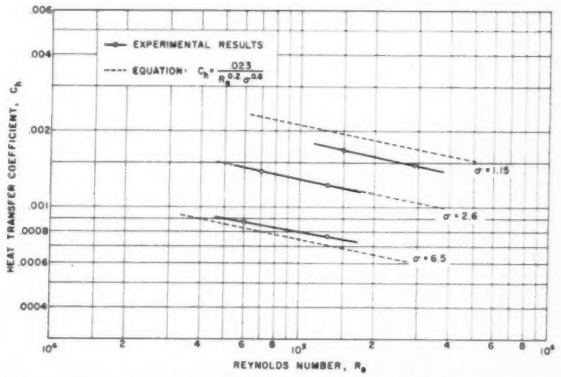

Fig. 3 Heat transfer coefficient for the smooth tube as a function of Reynolds number

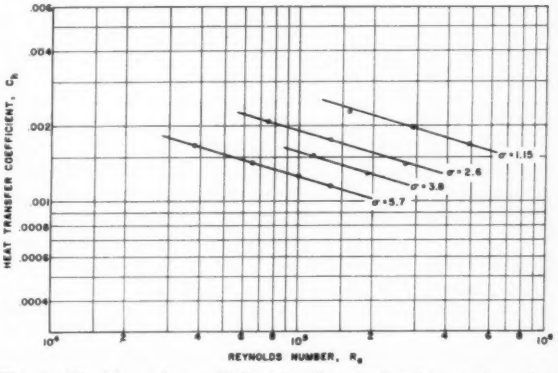

Fig. 4 Heat transfer coefficient for the rough tube as a function of Reynolds number

The largest uncertainty in determining the absolute accuracy of the measured coefficients was probably introduced by the value for the conductivity of the stainless steel tube. This quantity was needed in determining the temperature t_{wi} as shown by Equation [4]. Values ranging from $k = 0.245\ 10^{-3}$ Btu/in.-sec-°F at 100 F to $0.28\ 10^{-3}$ Btu/in.-sec-°F at 300 F were used for the present computation. Taking into account possible deviations from this value as well as other inaccuracies in the experimental results, it is estimated that the friction coefficient C_f is accurate within 2 per cent and that the heat transfer coefficient C_h is accurate within 5 per cent.

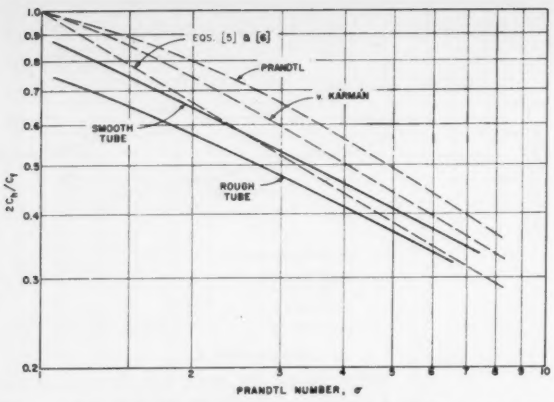

Fig. 5 The ratio $2C_h/C_f$ as a function of Prandtl number for $Re = 1.5 \times 10^5$; the results corresponding to the Prandtl analogy, to the von Kármán analogy, and to the empirical relation of Colburn are also shown for comparison

Experimental Results

The experimental results are presented in the form of several graphs. The first graph (Fig. 2) shows the variation of the friction coefficient with Reynolds number for the rough as well as for the smooth tube. The smooth tube experiments are in close agreement with published data. The curve $C_f = 0.046/Re^{0.2}$, which fits the published data for smooth tubes well, is shown in Fig. 2 for comparison. The rough tube shows a marked increase of the friction coefficient over that of the smooth tube. It is seen that the friction coefficient of the rough tube is still dependent on the Reynolds number. This shows that, at least for the range which was investigated, the tube cannot be considered "perfectly rough." For the type of roughness used here, it appears that the Reynolds number dependence extends to higher values of Reynolds numbers than for a sand-grain-surface of equal relative roughness. In Figs. 3 and 4 the heat transfer coefficient C_h is shown as a function of Reynolds number for various constant values of Prandtl number. Fig. 3 applies to the smooth tube and Fig. 4 to the rough tube. For comparison, the equation

$$C_h = \frac{0.023}{Re^{0.2}\,\sigma^{0.6}} \quad \ldots\ldots\ldots\ldots\ldots\ldots [5]$$

has also been plotted in Fig. 3. This equation is one of several similar ones frequently recommended for computing heat transfer in a smooth tube. Agreement between the empirical equation and the measured data is considered adequate to give confidence in the experimental techniques of the present series of tests. The data presented in Figs. 3 and 4 show that the roughness improves the heat transfer coefficient somewhat over that of the smooth tube. In each case, however, the increase in the friction coefficient caused by the roughness exceeds the corresponding improvement in the heat transfer coefficient.

It should be pointed out that the coefficient C_h in Figs. 3 and 4 is the isothermal value of C_h. The isothermal value was obtained experimentally as follows: At each Reynolds and Prandtl number the heat transfer coefficient was determined for several heat transfer rates q. The coefficient C_h was then plotted against q, and the curve was extrapolated to a zero heat transfer rate. The value of C_h at $q = 0$ corresponds to a zero temperature difference between the wall and the bulk fluid. This is the value of C_h which has been used in this presentation. The isothermal value was selected for this investigation because it was felt desirable not to veil the effect of roughness by the effects which are due to temperature and property variations across the boundary layer.

The effects of roughness on friction and heat transfer can perhaps be compared best by forming the ratio $2C_h/C_f$. This ratio has been plotted in Fig. 5 as a function of Prandtl number for a given Reynolds number. Two experimental curves are shown, one for the smooth tube and one for the rough tube. For comparison three theoretical relationships are also shown. The first is based on the empirical relation for C_h given by Equation [5] and on

$$\frac{C_f}{2} = \frac{0.023}{Re^{0.2}} \quad \ldots\ldots\ldots\ldots\ldots\ldots [6]$$

which very closely fits the data for the smooth tube in Fig. 2.

The other two curves are based on the analogies between heat transfer and friction as analyzed by Prandtl and von Kármán, respectively. Fig. 5 has been prepared for a particular Reynolds number. Graphs for other Reynolds numbers within the range of this investigation are quite similar.

Discussion of Results

The principal results of this set of experiments are that, for the type of roughness tested, (a) the heat transfer coefficient C_h increases with roughness and (b) the increase in the friction coefficient C_f exceeds that of the heat transfer coefficient. As a consequence, the ratio $2C_h/C_f$ decreases with roughness. These results are in agreement with the findings of previous experimenters (see for example (2 and 3)). For the rough tube tested, the ratio $2C_h/C_f$ is below that for the smooth tube for the full range of Prandtl numbers. The difference seems to be more pronounced at the lower end of the range. In the neighborhood of $\sigma = 1$ the difference in the ratios $2C_h/C_f$ for the two tubes is about 15 per cent and it decreases to about 10 per cent at $\sigma = 7$.

The results may be analyzed further in the light of Reynolds analogy. Following the usual approach, one may write for the shear near the wall of a pipe

$$\frac{\tau}{\rho} = (\nu + \epsilon_f)\,\frac{du}{dy} \quad \ldots\ldots\ldots\ldots\ldots\ldots [7]$$

The heat transfer rate per unit area may be expressed as

$$\frac{q}{\rho c} = \left(\frac{\nu}{\sigma} + \epsilon_h\right)\frac{dT}{dy} \quad \ldots\ldots\ldots\ldots\ldots\ldots [8]$$

The quantities ϵ_f and ϵ_h are the turbulent exchange coefficients for friction and heat transfer, respectively. According to Reynolds analogy ϵ_h is proportional to ϵ_f. In most analytical work the proportionality constant is set equal to unity for lack of sufficient experimental data. In that case it can be shown from the above two equations that for $\sigma = 1$ the ratio

$$2C_h/C_f = 1$$

It may be noted here that the experimental value of $2C_h/C_f$ obtained for the smooth tube does not equal 1.0 but rather 0.9 as seen from Fig. 5. The data are of course subject to the limitation in accuracy mentioned before. Nevertheless one may take this result as an indication that the proportionality constant between ϵ_h and ϵ_f differs from unity. In this connection it might also be mentioned that experiments with air in smooth tubes (see (2 and 3)) yield values of about 1.18 for the ratio of $2C_h/C_f$. The Prandtl number for air at the temperature in question is approximately 0.70. If the coefficient C_h is now assumed to be proportional to $\sigma^{-0.6}$ (see Equation [5]), the data for air may be extrapolated to a Prandtl number of unity. This extrapolation also leads to a value of $2C_h/C_f$ slightly below unity.

Let us now further examine Fig. 5 in which the ratio $2C_h/C_f$ is plotted as a function of Prandtl number for the rough as well as for the smooth tube. As is seen, both curves decrease rapidly with Prandtl number. The fact that $2C_h/C_f$ for the rough tube decreases with increasing Prandtl number

is somewhat disappointing. One might have imagined that the effect of roughness would be to increase the turbulent exchange coefficients to such an extent that $\nu \ll \epsilon_f$ and $\nu/\sigma \ll \epsilon_h$ right up to the wall. In that case it would follow from Equations [7 and 8] that

$$\frac{2C_h}{C_f} = \frac{\epsilon_h}{\epsilon_f}$$

If it is further assumed that ϵ_h/ϵ_f is independent of roughness, one would conclude that the ratio $2C_h/C_f$ for rough tubes is approximately equal to unity and independent of Prandtl number. Unfortunately, the actual experimental evidence accumulated by the present authors as well as by previous experimenters (see for example (2 and 3)) does not support the above hypotheses.

For the types of roughness tested so far, it appears that friction is more strongly affected by roughness than is heat transfer and that there is no effective increase of the turbulent exchange coefficients within the laminar boundary layer. Nunner (2) suggests the explanation that each roughness element, in addition to exerting surface drag, exerts a form drag. Vortices may be shed from these elements and flow disturbances will result. However, these disturbances are apparently too far from the surface to effectively increase the exchange coefficient ϵ_h near the surface.

As was stated in the introduction, it is hoped that the data presented in this paper will contribute to the large body of experimental information which is still needed to clarify the problem of heat transfer in a rough tube. Additional experiments will be required and several aspects of the problem may have to be studied. In view of the suggested role of form drag, an investigation of the effect of the shape of the individual roughnesses seems particularly challenging. One might even speculate on the possibility of developing roughness shapes with low form drag, which should be especially suited to heat transfer applications. If successful, the hypothesis regarding the equality between C_h and $C_f/2$ for rough tubes might still be realized in some cases. In spite of the fact that investigations involving a certain variety of roughness shapes have not so far shown any such favorable effects (2), further study of this aspect may still be justifiable.

Acknowledgment

The authors wish to take this opportunity to express their gratitude to R. Perpall who contributed greatly in planning the experiments. The authors further gratefully acknowledge the support of the Department of the Army, Ordnance Corps, under whose auspices the research was conducted.

References

1 Schlichting, H., "Boundary Layer Theory," McGraw-Hill, New York, 1953, p. 418.

2 Nunner, W., "Warmeubergang und Druckabfall in rauhen Rohren," VD1 Forschungsheft, Ausgabe B, vol. 22, 1956.

3 Sams, E. W., "Experimental Investigation of Average Heat Transfer and Friction Coefficients for Air Flowing in Circular Tubes Having Screw-Thread-Type Roughness," NACA RM E52 D17, 1952.

Generalized Trajectories for Free-Falling Bodies of High Drag[1]

R. D. TURNACLIFF[2] and J. P. HARTNETT[3]

University of Minnesota, Minneapolis, Minn.

Nomenclature

A = area of body consistent with definition of C_D, ft²
F_d = drag force, lb_f
g = acceleration due to gravity, fps²
g_0 = gravitational constant = 32.2 $lb_m ft/lb_f sec^2$
h = actual altitude, ft
h^* = reference altitude, ft
h_i = initial actual altitude, ft
m = mass of body, lb_m
s = oblique distance, ft
t = time, sec
V = velocity, fps
V_i = initial velocity, fps
x = vertical distance measured downward, ft
x_i = $h^* - h_i$, ft
α = constant, ft
ρ = local air density, lb_m/ft^3
ρ_0 = standard sea level air density, lb_m/ft^3
θ = angle of descent between vertical and direction of flight, degrees.

Dimensionless Numbers

C_D = drag coefficient
$\bar{h} = h/\alpha$
$\bar{h}_i = h_i/\alpha$
$K = 3.85 \times 10^{-2} = \frac{C_D A \rho_0 \alpha}{m \cos\theta} e^{-h^*/\alpha}$
$\bar{V} = V/\sqrt{\alpha g}$
$\bar{V}_i = V_i/\sqrt{\alpha g}$
$\bar{x} = x/\alpha$
$\bar{x}_i = x_i/\alpha$

Introduction

AT PRESENT considerable interest exists in the utilization of high drag devices such as parachutes for the recovery of missile equipment and as brakes for missiles themselves. This has led to the increased need for trajectory information on free-falling bodies over an extended range of drag-to-weight ratios. One specific application of this trajectory information involves the prediction of the temperature history of a high drag body under the influence of aerodynamic heating.

The equation of motion for a free-falling body in a gravitational field may easily be established and solved assuming an isothermal atmosphere and constant drag coefficient. The resulting solution appears in series form. For bodies of low drag-to-weight ratio, such as projectiles, this series usually converges rapidly and easily yields the approximate trajectory; however, as the drag-to-weight ratio becomes greater, the series converges too slowly for convenient use of the series solution. However, a judicious selection of the reference system for the equation of motion will allow the graphical presentation on a single coordinate diagram of the trajectories of a body of high drag for a wide range of weight-to-drag ratios, initial altitudes and initial velocities. Such a diagram eliminates the necessity for repeated evaluation of the series for each new problem. This method and its application form the content of this paper.

The Equation of Motion and Its Solution

Vertically Free-Falling Body

The equation of motion is formed by equating the time rate of change of momentum of the body to the sum of all forces acting, which for the case of a free-falling body are the gravitational force mg/g_0 and the drag force F_d.

$$\frac{d(mv)}{g_0 dt} = \frac{mg}{g_0} - F_d \quad \ldots\ldots\ldots\ldots\ldots\ldots [1]$$

Presented at the ARS 12th Annual Meeting, New York, N. Y., Dec. 2–5, 1957.

[1] Publication of the Heat Transfer Laboratory, University of Minnesota, Minneapolis, Minn.

[2] Present address: Member, Technical Staff, Space Technology Laboratory, The Ramo-Wooldridge Corp., Los Angeles, Calif. Mem. ARS.

[3] Associate Professor, Mechanical Engineering Department. Mem. ARS.

In the conventional choice of coordinates for this equation, distance is measured upward from a coordinate system fixed at the surface of the earth. The method presented in this paper deviates from common practice and fixes the coordinate system at some point in space h^* and measures the distance traveled downward, x, from this reference altitude (see Fig. 1a). The true altitude h of the body is then

$$h = h^* - x \quad [2]$$

This choice of coordinate system makes possible the generalized graphical presentation of trajectory data as will be discussed.

The drag force F_d may be expressed in terms of the dimensionless drag coefficient C_D by

$$F_d = \frac{C_D A \rho V^2}{2g_0} \quad [3]$$

Introducing Equation [3] into Equation [1] and assuming the mass m to be constant, there results

$$\frac{dV}{dt} = g - \frac{C_D A \rho V^2}{2m} \quad [4]$$

Changing the independent variable of time t to distance measured downward x by use of the relation

$$\frac{dV}{dt} = \frac{dV}{dx} \cdot \frac{dx}{dt} = V \frac{dV}{dx} = \frac{1}{2} \frac{dV^2}{dx}$$

Equation [4] now becomes

$$\frac{dV^2}{dx} = 2g - \frac{C_D A \rho V^2}{m} \quad [5]$$

This differential equation cannot as yet be solved since the density ρ is a function of the distance x. However, if an isothermal atmosphere is assumed, the density then varies with altitude h in the following way

$$\rho = \rho_0 e^{-h/\alpha} = \rho_0 e^{-(h^* - x)/\alpha} \quad [6]$$

Introducing this expression into Equation [5] gives

$$\frac{dV^2}{dx} + \frac{C_D A \rho_0}{m} e^{-h^*/\alpha} e^{x/\alpha} V^2 = 2g \quad [7]$$

This differential equation may now be expressed in dimensionless form if the following basic dimensionless numbers are defined and the quantities g and α are assumed to be constants

$$\bar{x} = x/\alpha \qquad \bar{V}^2 = V^2/\alpha g$$

Equation [7] now assumes the dimensionless form

$$\frac{d\bar{V}^2}{d\bar{x}} + \frac{C_D A \rho_0 \alpha}{m} e^{-h^*/\alpha} e^{\bar{x}} \bar{V}^2 = 2 \quad [8]$$

This equation is to be solved subject to the boundary condition

$$\bar{V} = \bar{V}_i \text{ when } \bar{x} = 0 \quad [9]$$

Inspection of Equation [8] and its boundary conditions [9] reveals that the solution will be a function of the dimensionless groups

$$\bar{V}^2 = f\left\{\bar{x},\ \bar{V}_i^2,\ \frac{C_D A \rho_0 \alpha}{m} e^{-h^*/\alpha}\right\}$$

If the coefficient of drag C_D is assumed constant, the dimensionless parameter

$$\frac{C_D A \rho_0 \alpha}{m} e^{-h^*/\alpha}$$

becomes independent of the distance x, and Equation [8] may be solved by standard methods. Its solution appears in the following infinite series form

$$\bar{V}^2 - \bar{V}_i^2 e^{\bar{K}(1-e^{\bar{x}})} = 2e^{-\bar{K}e^{\bar{x}}} \times \left\{\bar{x} + \bar{K}(e^{\bar{x}} - 1) + \frac{\bar{K}^2}{2 \cdot 2!}(e^{2\bar{x}} - 1) + \frac{\bar{K}^3}{3 \cdot 3!}(e^{3\bar{x}} - 1) + \ldots\right\} \quad [10]$$

This series solution may be easily evaluated for bodies of low drag and large mass, such as projectiles, since the series then converges rapidly. However, for bodies of high drag, such as parachutes, the infinite series converges too slowly to allow for convenient use of this equation. In such instances a graphical presentation of the general solution would be useful, since having once been prepared it could be repeatedly used. In attempting to accomplish this, one difficulty immediately arises from the fact that Equation [10] contains four variables. If this number could be reduced to three, a simple graphical presentation of the solution would become possible. Consideration of the four dimensionless numbers appearing in Equation [10] reveals that no limitation is imposed on the generalized nature of the solution if the dimensionless group

$$\frac{C_D A \rho_0 \alpha}{m} e^{-h^*/\alpha}$$

is held constant. This may appear at first to fix the drag-to-weight ratio $C_D A/m$ but such is not the case. By virtue of the choice of reference system (see Fig. 1a) the reference altitude h^* is allowed to vary and may take on any value greater than or at least equal to the true initial altitude of the body; therefore, holding the above dimensionless numbers constant simply fixes the relation that must exist between the drag-to-weight ratio and the reference altitude h^* as given by

$$\frac{C_D A \rho_0 \alpha}{m} e^{-h^*/\alpha} = \bar{K} \quad [11]$$

where the terms ρ_0 and α are constants. The number $\bar{K}$ may be somewhat arbitrarily chosen. In the present analysis a value of $\bar{K} = 3.85 \times 10^{-2}$ was selected in consideration of certain scaling needs. With the afore-mentioned dimensionless group held fixed, the solution to the equation of motion now contains only three variables

$$\bar{V}^2 = f\{\bar{x},\ \bar{V}_i^2\}$$

This makes possible a graphical presentation of the solutions as a family of curves on a single coordinate diagram as shown in Fig. 2. These curves are actually the trajectories of a free-falling body for a wide range of initial altitudes, initial velocities and weight-to-drag ratios.

(a) (b)

Fig. 1 Reference systems for equation of motion. (a) Vertically free-falling body. (b) Obliquely free-falling body

Obliquely Free-Falling Body

The equation of motion and solution developed for the special case of a vertically falling body may easily be extended to the more general case of an obliquely falling body (see Fig. 1b). For such a condition the equation of motion may be written as

$$\frac{d(mV)}{g_0 dt} = \frac{mg \cos \theta}{g_0} - F_d \quad [12]$$

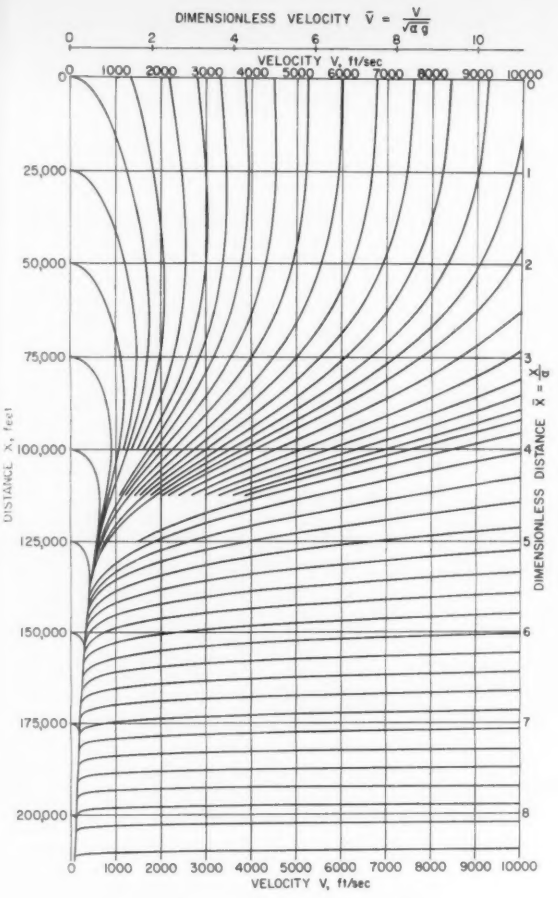

Fig. 2 Generalized trajectory diagram

In terms of the drag coefficient, and assuming constant mass, Equation [12] becomes

$$\frac{dV}{dt} = g \cos \theta - \frac{C_D A \rho V^2}{2m} \quad \ldots\ldots\ldots\ldots [13]$$

Changing the independent variable of time t to distance measured vertically downward (x) by use of the relations

$$\frac{dV}{dt} = \frac{dV}{ds} \cdot \frac{ds}{dt} = \frac{dV}{dx} \cdot \frac{dx}{ds} \cdot \frac{ds}{dt} = V \cos \theta \frac{dV}{dx} = \frac{\cos \theta}{2} \frac{dV^2}{dx}$$

Equation [12] now becomes

$$\frac{dV^2}{dx} = 2g - \frac{C_D A \rho V^2}{m \cos \theta} \quad \ldots\ldots\ldots\ldots [14]$$

By assuming the same variation of air density with altitude as previously given by Equation [6] and by using the same dimensionless numbers as before, Equation [14] becomes

$$\frac{d\bar{V}^2}{d\bar{x}} + \frac{C_D A \rho_0 \alpha}{m \cos \theta} e^{-h^*/\alpha} e^{\bar{x}} \bar{V}^2 = 2 \quad \ldots\ldots\ldots [15]$$

This equation and its solution are identical to those previously given for the vertically free-falling body with the exception of the presence of the cos θ term in the coefficient. The graphical solutions given in Fig. 2 are still applicable. However, the relation between the drag-to-weight ratio C_D and the reference altitude h^* is now given by

$$\frac{C_D A \rho_0 \alpha}{m \cos \theta} e^{-h^*/\alpha} = \bar{K}$$

This represents the more general situation of which the vertically falling body is a special case for cos $\theta = 1$. Graphical presentation of this equation appears in Fig. 3, which presents $C_D A \alpha / m$ as a function of h^*/α for various angles of descent.

The next section discusses in more detail the characteristics of the generalized trajectory plot given in Fig. 2 and its application in solving for trajectories.

Generalized Trajectory Diagram for Bodies of High Drag

The graphical presentation of the solution to the trajectory equation is given in Fig. 2 and applies over an approximate range in drag-to-weight ratio $C_D A/m$ from 4 to 4×10^{-5} ft^2/lb_m, in initial altitude from sea level to 250,000 ft, and in initial velocity from zero to 10,000 fps. This figure presents the dimensionless velocity $\bar{V}$ vs. the dimensionless distance $\bar{x}$ for various dimensionless initial velocities with the dimensionless number $\bar{K}$ held constant at a value of 3.85×10^{-2}. The resulting curves represent the solution to the equation of motion given in Equation [10].

To simplify use of these curves, the basic dimensionless numbers on the coordinates have been evaluated for the usual case of $g = 32.2$ fps^2 and $\alpha = 25{,}000$ ft with this scale also presented in addition to the dimensionless coordinates. It should be noted that the resulting dimensionless scales are slightly restricted by the choice of $\alpha = 25{,}000$ ft. However, if the altitude range of interest is more limited, the best possible approximation may be a slightly different value of α.

In Fig. 2 the ordinate scale begins at the top with $\bar{x} = 0$ and all distances $\bar{x}$ are measured downward from this point. In order to apply significance to such a measurement it is necessary to fix the origin $\bar{x} = 0$ with respect to the surface of the earth. This is accomplished through use of the reference al-

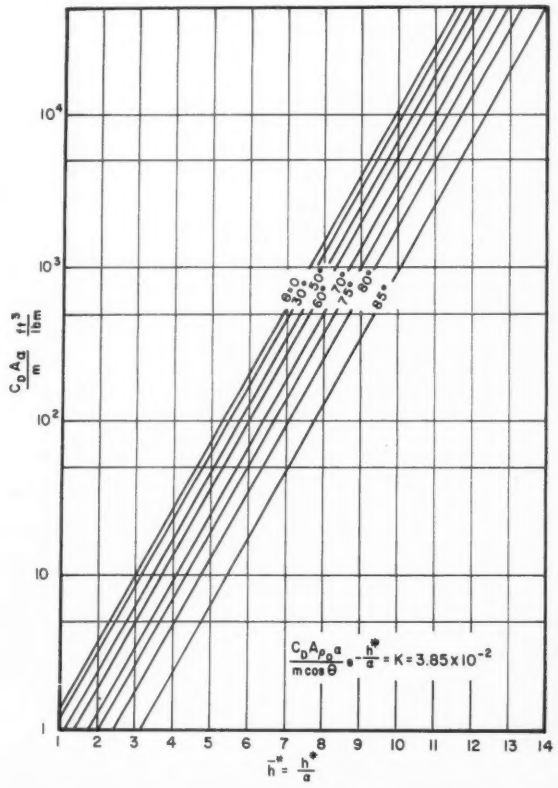

Fig. 3 Reference altitude vs. drag-to-weight ratio

titude h^* which appears in the dimensionless number $\bar{K}$

$$\bar{K} = \frac{C_D A \rho_0 \alpha}{m \cos \theta} e^{-h^*/\alpha} = 3.85 \times 10^{-2} \quad \ldots\ldots [16]$$

For convenience in calculation, Equation [16] has been interpreted graphically in Fig. 3 and $\bar{h}^*$ may be read directly from this figure once the drag-to-weight ratio and angle of descent are specified. The reference altitude in this way established the origin of the ordinate scale with respect to the surface of the earth. In general, the reference altitude will not be equal to the initial altitude of the body, the only requirement being that h^* must not be less than the initial altitude. Once this ordinate scale has been fixed in the above manner for a body of specified drag-to-weight ratio, the problem of applying these curves to situations involving various initial altitudes and velocities has to be considered. In this regard it should be noted that a characteristic of the trajectory of a free-falling body makes it possible to enter the curve representing the trajectory once it has started, provided one enters with a body of the same drag-to-weight ratio at an initial velocity corresponding to the local velocity for that altitude. Consideration of the equation of motion shows this to be true since the forces acting on the body in both cases will be the same. With this in mind it is now possible to enter Fig. 2 at any initial altitude less than the reference altitude and at any initial velocity up to 10,000 fps, provided the ordinate scale has been fixed by the weight-to-drag ratio as previously mentioned.

In the following section several sample problems will be worked to illustrate the use of the trajectory diagram.

Sample Problems

1 *Vertically Free-Falling Body of High Drag*

Given:

Drag-to-weight ratio $C_D A/m = 1$ ft²/lb$_m$
Initial velocity $V_i = 5000$ fps
Initial altitude $h_i = 200{,}000$ ft
Angle of descent $\theta = 0$ deg

Find: Velocity vs. altitude of the body.

Step 1: Assuming a value of $\alpha = 25{,}000$ ft enter Fig. 3 at $C_D A\alpha/m = 25{,}000$ for $\theta = 0$ and read off $\bar{h}^* = 10.84$. The point $\bar{x} = 0$ on the trajectory diagram now corresponds to an actual altitude of

$$h = h^* = \alpha \bar{h}^* = 271{,}000 \text{ ft}$$

Step 2: Establish the relationship between the true altitude h and the distance traveled downward x through use of the general equation

$$h = h^* - x \quad \text{or} \quad \bar{h} = \bar{h}^* - \bar{x}$$

which for this special problem becomes

$$\bar{h} = \frac{271{,}000}{\alpha} - \bar{x} \quad \text{or} \quad x = 271{,}000 - \text{h}$$

Step 3: Enter the trajectory diagram on Fig. 2 by locating the points

$$\text{Abscissa: } \bar{V}_i = \frac{5000}{\sqrt{25{,}000 \times 32.2}} = 5.56$$

$$\text{Ordinate: } \bar{X}_i = 10.84 - \frac{200{,}000}{25{,}000} = 2.84$$

or

$$\text{Abscissa: } V_i = 5000 \text{ fps}$$
$$\text{Ordinate: } X_i = 271{,}000 - 200{,}000 = 71{,}000 \text{ ft}$$

Step 4: Select the trajectory curve passing through the point as located in Step 3. In most instances it will be necessary to interpolate between existing curves. Read off the value for the dimensionless velocity $\bar{V}$ for selected values of $\bar{x}$ which are then made dimensional through multiplying by $\sqrt{\alpha g}$ and α, respectively. The distance x is converted to true altitude h, as before, through the equation

$$h = h^* - x \qquad h = 271{,}000 - x$$

Results: See Table 1.

Table 1 Velocity vs. altitude data for parachute in sample problem 1

h, ft	x,[1] ft	$\bar{X}$	$\bar{V}$	V,[1] fps
200,000	71,000	2.84	5.56	5000
175,000	96,000	3.84	3.36	3000
150,000	121,000	4.84	1.01	900
125,000	146,000	5.84	0.38	345
100,000	171,000	6.84	0.25	220
75,000	196,000	7.84	0.14	125
50,000	221,000	8.84	...	...
25,000	246,000	9.84	...	...
Sea level	271,000	10.84	...	...

[1] For $\alpha = 25{,}000$ ft and g = 32.2 fps².

2 *Obliquely Free-Falling Body of High Drag*

Given:

Drag-to-weight ratio $C_D A/m = 1$ ft²/lb$_m$
Initial altitude $h_i = 200{,}000$ ft
Initial velocity $V_i = 5000$ fps
Angle of descent $\theta = 30$ deg

Find: Velocity vs. altitude of the body.

Step 1: Assuming a value of $\alpha = 25{,}000$ ft, enter Fig. 3 at $C_D A\alpha/m = 25{,}000$ for $\theta = 30$ deg, and read off $\bar{h}^* = 11.00$. The point $\bar{x} = 0$ on the trajectory diagram now corresponds to an actual altitude of

$$h = h^* = h^*\alpha = 275{,}000 \text{ ft}$$

Step 2: As in the case of a vertically falling body establish the relationship between the true altitude h and the distance traveled downward x through use of the general equaton

$$h = h^* - x \quad \text{or} \quad \bar{h} = \bar{h}^* - \bar{x}$$

which for this problem becomes

$$\bar{h} = \frac{275{,}000}{\alpha} - \bar{x} \quad \text{or} \quad \bar{x} = 275{,}000 - x$$

Step 3: Enter the trajectory diagram on Fig. 2 by locating the point

$$\bar{V} = \bar{V}_i = 5.56$$

$$\bar{x} = \bar{x}_i = 3.00$$

or

$$V = V_i = 5000 \text{ fps}$$

$$x = x_i = 275{,}000 - 200{,}000 = 75{,}000 \text{ ft}$$

Step 4: Select the trajectory curve passing through the point as located in Step 3. In most instances it will be necessary to interpolate between existing curves. Read off the value for the dimensionless velocity $\bar{V}$ for selected values of $\bar{x}$ which are then made dimensional through multiplying by $\sqrt{\alpha g}$ and α, respectively. The distance x is converted to true altitude h as before through the equation

$$h = h^* - x \quad \text{or} \quad h = 275{,}000 - h$$

Acknowledgments

The authors wish to acknowledge the support of the Equipment Laboratory, Parachute Division, Wright Air Development Center, Wright-Patterson Air Force Base, Ohio, and the aid of D. J. Kruskopf, Mechanical Engineering Department, in preparing the trajectory diagram.

Kodak reports on:

running up the flag of arsenic-cross-linked selenium . . . a use for Biphenyl in aerodynamics research . . . big deal over 0.009 roentgen

Out to 25μ

We find that mechanically and optically decent inorganic polymers can be made out of sulfur's lesser known sister, who was named after the moon. Acquaintance with arsenic-cross-linked selenium has ripened into intimacy. The issue is a kind of glass with refractive index 2.45 or higher. Black as pitch by reflected visible light, it has a transmittance that is optically useful out to a prodigious 25μ, practically long enough to modulate with your favorite TV situation comedy.

This 92% Se - 8% As glass is quite a different animal from arsenic trisulfide, which begins falling off at 9μ. Except for an absorption band at about 12.6μ, most of its transmission loss arises from Fresnel reflection due to the high refractive index, and there are said to be ways of fixing that. The high index, on the other hand, is a blessing when infrared detectors are embedded in the glass in order to boost their geometrical radiation-collecting effectiveness.

Kodak Selenium Glass retains its rigidity to about 70 C and does not crystallize after long exposure to this temperature.

Though the production scale is still modest, we would like to try supplying it in molded shapes to manufacturers determined to outdo us on optical systems employing it.

Potential competitors and other friends are most cordially invited to submit inquiries about Kodak Selenium Glass *to Eastman Kodak Company, Apparatus and Optical Division, Rochester 4, N. Y.*

Wind writing

"Photography" means "light writing." To get light to write meaningful records of air movement, the wind tunnels of the world are festooned with complex and delicate optical arrangements.

Why not use the wind itself to write with? the men of the Ames Aeronautical Laboratory of the National Advisory Committee for Aeronautics asked themselves. Like the wind patterns in snow around a fence. It worked fine.

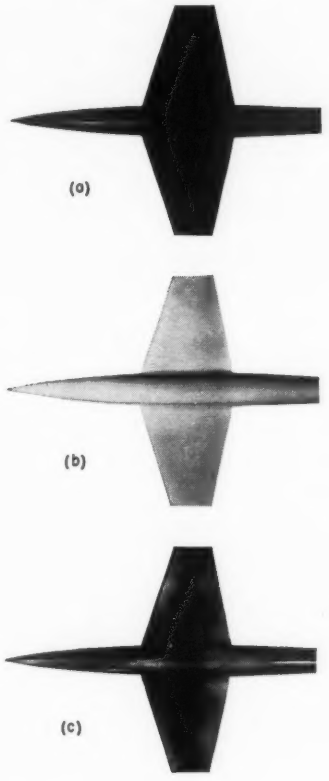

At (a) is a wind-tunnel model before and at (b) after spraying with a thin coating of *Biphenyl;* at (c), after the wind has etched into the subliming stuff a pattern that tells of laminar, turbulent, and separated flows and locates the shock waves.

Our connection with this is that we supplied the Biphenyl. *Not that* Biphenyl *is big business for us. (Color and black-and-white film for schlieren and interferometric studies in aerodynamics is much bigger business!) The point we make is that somebody had an idea requiring a certain organic compound, looked into our catalog of some 3600 of them, and found it there. You, too, can get a copy by asking Eastman Organic Chemicals Department, Distillation Products Industries, Rochester 3, N. Y. (Division of Eastman Kodak Company).*

A modest contribution

Man comes home from work and his wife asks him what kind of a day he's had. "Same old yackety yak," he reports. "Heap-big all-afternoon powwow over the fact that whereas it used to take 0.019 roentgens of radium gamma radiation to produce a density of .05, they have now made x-ray film that takes 0.010 roentgens of gamma radiation to produce a density of .05. Cauliflower tonight again?"

•

Eastman Kodak Company is pleased to announce that significant progress has been made in its continuing program of improving the sensitivity of film to ionizing radiation. One result of this program is that physicians are enabled to obtain required diagnostic information from *Kodak No-Screen Medical X-ray Film* with fully 50% less exposure of the patient to x-rays.

Another result, of interest to those engaged in industrial radiography and in the atomic energy field, is that the film badges worn to check on their body exposure to radiation can now be made capable of at least 50% more sensitivity than previously.

While it is realized that the end of the effort to reduce human exposure to radiation is nowhere in sight, it is felt that even modest technological advances in this direction serve the interests of general welfare.

For cumulative monitoring of occupational exposure to x-rays and gamma rays, the enhanced sensitivity is now available in *Kodak Personal Monitoring Film, Type 1.* Maximum sensitivity is attained for radiation quality of approximately 50 kvcp. Approximately 30 times the same roentgen value is required to produce equivalent densities with radium gamma rays.

In *Kodak Personal Monitoring Film, Type 2,* with a low-sensitivity emulsion on one side of the film and a high-sensitivity emulsion on the other side, the range of assessment is extended to emergency levels of exposure. Other modifications are available for the measurement of neutron exposure.

Full information about these monitoring films is obtainable from Eastman Kodak Company, Special Sensitized Products Division, Rochester 4, N. Y.

This is another advertisement where Eastman Kodak Company probes at random for mutual interests and occasionally a little revenue from those whose work has something to do with science

Kodak
TRADE MARK

New Patents

George F. McLaughlin, *Contributor*

Inwardly opening breech closure for rocket launcher (2,820,398). W. E. Good, Riverton, N. J., assignor to the U. S. Army.

Launcher tube with a breech housing secured to a flanged rear end. The breech block has a conical surface to engage the inner part of a conical seat with a tight fit, providing a gas-tight seal.

Rocket propellent support (2,820,410). D. T. Tarr, Sierra Madre, Calif., assignor to the War Dept.

A member is molded around a reinforcing base and sealed against the walls of the tube. A propellant grain fits within the tube and is bonded to the sealing member.

Axial flow compressors (2,820,588). A. J. Penn and L. A. Nevard, Liverpool, England, assignors to D. Napier & Son, Ltd.

Disengageable coupling means between first and second rotors. When the second stage rotor attains a predetermined speed, windmilling of the first compression part is stopped and becomes driven with the later stages.

Dual unit jet propulsion plant (2,820,599). J. Ackeret and C. Keller, Kusnachi, Switzerland, assignors to Aktiengesellschaft fuer Technische Studien.

Combination of a turbojet power unit in which the exhaust is directed as a propulsion jet. A further jet propulsion unit comprises a turbine and compressor whereby the compressed air is directed as a propulsion jet.

Automatic jettisoning system for aircraft seats (2,820,602). E. V. Foster, Manhattan Beach, Calif., assignor to Northrop Aircraft, Inc.

Personnel survival system consisting of ejectable seats catapulted upon release of a pressurized fluid initiated by a gas generator.

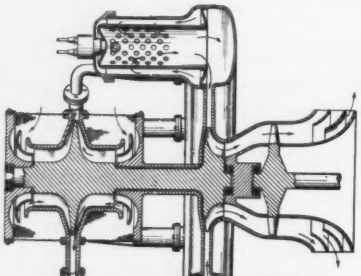

Combustion chamber construction in a gas turbine engine (2,821,067). H. C. Hill, Seattle, Wash., assignor to Boeing Airplane Co.

Each combustion chamber comprises an outer wall opening at one end to the collector chamber. An inner shell within the wall opens at one end to the nozzle box. A burner is admitted to each inner shell at the end away from the box.

Compound power plant (2,819,765). E. E. Chatterton, London, England, assignor to D. Napier & Son, Ltd.

Master control connected with an adjustable governor to regulate the speed of a reciprocating engine. The control also regulates the transmission ratio between the engine crankshaft and the compressor and turbine rotors.

Exhaust temperature regulator for gas turbine power plant (2,821,065). N. E. Starkey, Schenectady, N. Y., assignor to General Electric Co.

Means of controlling the rate of fuel consumption in the hot gas generating area as a function of load output desired from the turbine rotor.

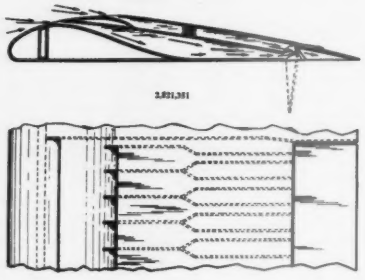

Airplane wing structure embodying jet engine (2,821,351). V. V. Utgoff, Alexandria, Va.

Pulsejet units side-by-side inside the wing. The top surface skin provides an intake. An exhaust communicates from the jets to the wing exterior spanwise of the trailing edge. The major portion of exhaust flow is deflected below a trailing edge flap.

Firing system for jet type perforating gun (2,821,136). J. H. Castel, Houston, Tex., assignor to P. G. A. C. Development Co.

Shaped charges and a cable for lowering a perforating gun into a borehole. Explosive charges are sequentially fired by transmitting direct and alternating currents to the gun.

Military rocket structure (2,821,137). G. A. Lyon, Detroit, Mich.

Bowed spring strips with helically angled edges movable laterally relative to the projectile body. Edges of the strips cooperate with rifling in the projectile barrel.

Dive control system for pilotless aircraft (2,821,349). H. Sohn, Essex, Md., assignor to The Martin Co.

Torque producing means for precessing a gyroscope at a predetermined variable rate. Torque is modified by accelerations due to wind lift. Aerodynamic means responsive to the gyroscope position control the attack angle of the aircraft.

Jet airplane construction (2,821,350). J. Smurik, Fort Lee, N. J.

Fins on each side of the body longitudinally dividing the space into a central channel with a channel on either side. Combustion products from the central burner are conducted to the side burners, raising their temperature to facilitate starting.

Fin stabilized projectile (2,821,924). L. J. Hansen and P. Rosenberg, Chicago, Ill., assignors to the U. S. Army.

Shell comprising a boat-tail fixed to the rear and carrying nested extensible fins imbedded in the propelling charge. Fins extend outward upon movement of pistons actuated in response to differential pressure between the chamber and the atmosphere.

Improvements in a device for starting gas turbine plants (2,822,665). C. R. Nicolin, Finspond, Sweden.

Separate compressor in front of the air intake of a turbine for delivering compressed air. A slidably mounted surrounding cover is placed into engagement to form a closed air passage between the compressors during the starting period.

Propellant feed system (2,822,667). C. F. Drexel, Los Angeles, Calif., assignor to the Garrett Corp.

Container with a movable wall dividing it into propellant and gas chambers. A combustion chamber in the gas chamber permits direct transfer of heat energy to cause thermal expansion of the gas.

Aircraft with jet propulsion engine and gun firing means (2,822,732). T. L. Metcalfe, Ashbourne, England, assignor to Rolls-Royce Ltd.

Gun firing means which opens a valve to bleed off from the delivery of the compressor air compressed when the gun is actuated.

Thermal arrangement for rocket missiles (2,822,756). N. G. Kuller and K. T. Thorildsson, Bofors, Sweden, assignors to Aktiebolaget Bofors Corp.

Electric terminals defining a groove for connecting the detonating device with a distant power supply. Terminals have outwardly tapering bushings with portions protruding into the groove.

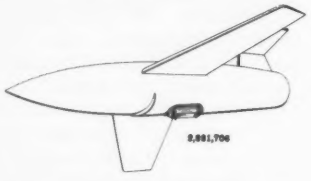

Antenna mounting for a guided missile (2,821,706). H. J. Rels and W. V. Foley, Middle River, Md., assignor to The Martin Co.

Stub pattern antennas for transmitting radiant energy. A disk-shaped fairing forms a ground plane whereby radiation extends above a horizontal plane passing through the antennas.

Cursor generator with a height finding adaptation (2,823,374). L. S. Michels, Inglewood, Calif., assignor to Gilfillon Bros., Inc.

Production of pulses representing a cursor line for use as a height finder. Each pulse corresponds to the intersection in time between a first signal representing the cursor angle and a second variable angle signal representing a scan angle position.

Target seeker head for guided missiles (2,823,612). A. Cox and C. Ledda, New York, N. Y., assignors to the U. S. Air Force.

Pyramidal-shaped body with flat glass plate side windows separated by narrow stringers at the base. Light rays focus on a plane through the central opening of an annular concave mirror for the use of the control mechanism.

EDITORS NOTE: Patents listed above were selected from the Official Gazette of the U.S. Patent Office. Printed copies of patents may be obtained from the Commissioner of Patents, Washington 25, D. C., at a cost of 25 cents each; design patents, 10 cents.

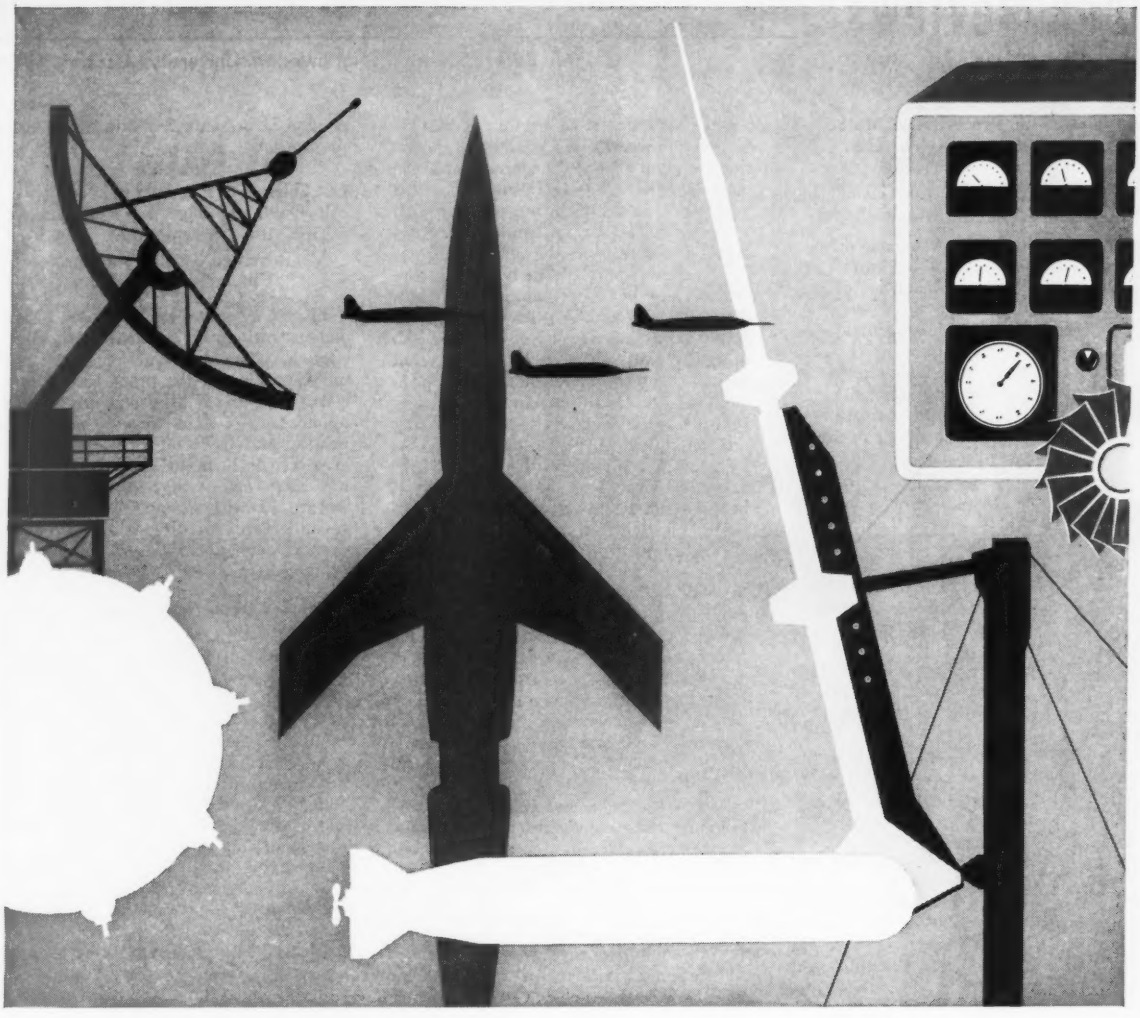

Throughout the Pattern of Modern Defense...

AMF has experience you can use

• Most defense problems fit into AMF's "big picture"... a picture drawn from AMF's tremendous backlog of experience in defense work. Wherever you are, there's probably an AMF defense component or integrated system... a product of AMF experience... operating near you. • Guided missiles ride on AMF equipment to AMF launching sites ... to be loaded, fueled and fired by AMF-built equipment. Under the sea, AMF-built weapons wait for unfriendly submarines on the prowl. Along our borders, AMF radarscopes search the sky for "stranger" aircraft. • There is little room for failure where the job is the nation's defense. And the nation looks to companies like AMF to design, test and produce a variety of defense products. With a wide range of experience in the most sensitive fields of defense work, AMF may well be the answer to your problems... in defense or industry.

- *Armament*
- *Ballistics*
- *Radar Antennas*
- *Guided Missile Support Equipment*
- *Auxiliary Power Supplies*
- *Control Systems*

AMF DEFENSE PRODUCTS

Defense Products Group
AMERICAN MACHINE & FOUNDRY COMPANY
1101 North Royal Street, Alexandria, Va.

Asbury Park • Atlanta • Boston • Brooklyn • Dallas • Dayton • Los Angeles • Seattle • Tucson • Washington, D. C.

Book Reviews

Ali Bulent Cambel, Northwestern University, *Associate Editor*

Principles of the Properties of Materials, by J. P. Frankel, McGraw-Hill, New York, 1957, 228 + xiv pp. $6.

Reviewed by DONALD S. CLARK
California Institute of Technology

This is an interesting book based upon a philosophy to which all educators will not subscribe. Some teachers of engineering materials will agree with the author that one should concentrate on principles rather than practice or techniques. This is the more modern way of looking at engineering training. Such an approach becomes necessary because of the more scientific character and stringent requirements of engineering. While much of the practice of engineering is empirical, more of it can be approached from an analytical point of view. The student should have a good grounding in principles which will permit him to understand present practices and by which he may be able to obtain better solutions to complex problems. This is the basis on which this book has been written. In some two hundred pages, Professor Frankel has attempted to present the principles of knowledge concerning the properties of materials.

The entire approach to the subject is one of apparent sophistication. This is an attitude that should not be laid on so thick. The author has probably overemphasized the basic concepts without sufficient illustration to clarify the significance of the approach. While the material presented is interesting, it has its deadly aspect as far as the student is concenred. Much of the material could be expanded, particularly as to application, and yet an instructor would be necessary to assist in interpretation.

The author states in the preface that the book is a text, not a treatise. Certainly he is correct that it is not a treatise. However, one may also question if it is a text. A text is a complete story for the purpose of educating the reader in a particular subject. It may or may not be a treatise. This reviewer is of the opinion that the book is too much of a survey text to be of real value for the education of sophomores in engineering.

The book lacks clarity in many instances, particularly in definition. For example, reference is made to phases, but there is not an adequate definition of a phase. Some reference is made to age hardening, but the student is not made familiar with the mechanics of age hardening in preparation for the discussion of such a property. There seems to be an atmosphere of fear of mentioning specifics in spite of the existence of some excellent examples of practical applications. The sophisticated approach seems to be of more importance than a clear understanding of application of principles of physics to materials.

The subject is covered in two parts, the first on physicochemical foundations and the second on properties. The first part is a good discussion of fundamental concepts starting with certain phases of atomic physics, thermodynamic considerations, crystal structure, cohesion and the metallic state. These subjects are covered very nicely as a survey, but possibly with a "holier than thou" attitude, and without sufficient depth.

The second part of the book on properties is fine, but it does not show the student the real significance of these properties in engineering. For example, an understanding of phase relations is not easy to grasp by the beginner. The principles laid by the author are not sufficient to permit the student to secure a basic understanding of phase diagrams, etc., by merely reading another book. The subjects covered include conductivity, heating, diffusion, electrochemistry, elasticity, plasticity, fracture, viscosity and general subjects.

The author is to be complimented on bringing this type of material to the sophomore level. The criticism given in this review is not intended to discourage the use of the author's approach, but to point out certain basic deficiencies. Possibly in the next edition, the material can be expanded so as to clarify many of the points. This review recommends that every teacher of the subject of engineering materials not only read this book, but make use of much of the basic material in his course. Such use will mean decreasing the amount of material given on specific reduction practices and composition of specific alloys and their properties. A reduction of this type of material is possible without seriously interfering with a proper education of our future engineers. The following statement at the close of the book can well be a closure for this review, because many teachers are not sufficiently cognizant of its importance: "Not only will the student be called on soon to solve problems his teachers could not solve, but also he must be able to solve problems his teachers could not even imagine."

Exploring the Atmosphere's First Mile. Vol. I: Instrumentation and Data Evaluation; Vol. II: Site Description and Data Tabulation, by Heinz H. Lettau and Ben Davidson, Pergamon Press, New York, 1957, 376 pp. (Vol. I), 578 pp. (Vol. II).

Reviewed by S. F. SINGER
University of Maryland

The volumes report the proceedings of the Great Plains Turbulence Field Program carried out in Nebraska. These were elaborate meteorological experiments performed in open prairie country with the primary objective to study the profiles of wind, temperature and other meteorological quantitities in the lowest part of the atmosphere. The subject matter properly falls into the fields of micrometeorology. Volume I contains an introductory article, giving history, summary and general conclusions, and 65 scientific papers which describe in detail the multitude of instrument types used in the field program. Volume II presents the data of the seven observational periods.

The Science of Engineering, edited by J. E. Goldman, John Wiley & Sons, New York, 1957, 528 pp., $12.

Reviewed by J. P. FRANKEL
University of California

This book contains a series of lectures demonstrating the application of knowledge in chemistry and physics to the understanding of the properties of materials. The first four lectures deal with the applications of solid state science in engineering and basic information as to the structure of the material. Lectures 5 to 10 are concerned with metals and alloys; lecture 11 with surfaces; the remaining seven lectures are divided almost entirely among magnetic properties, properties of semiconductors and dialectrics, and noncrystalline materials.

The treatment is that of a review of basic results in the field. Few or no derivations are enclosed. Generally, the results are stated in the "it can be shown" style. For complete understanding of the subject material, the reader must bring to the book an understanding of the basic concepts of quantum mechanics and statistical thermodynamics. The treatment in lecture 2 of the foundations of quantum mechanics is inadequate for the reader with no background and superficial to those who have already studied quantum mechanics. There is no review of statistical thermodynamics corresponding to the review of quantum mechanics.

Not withstanding these defects (which may perhaps be a result of the different authorship of different chapters), the book is an excellent summary of the methods used to investigate and rationalize the behavior of the materials. With respect to the mechanical properties of solids, the treatment is more complete than that usually found in text books on solid state physics.

In summary, the book is an excellent reference for people in other fields who would like a quick view of the basic procedures of solid state physics, and therefore can be considered a "must" for teachers of courses in the properties of materials in engineering colleges.

Solar Eclipses and the Ionosphere, by W. J. G. Beynon and G. M. Brown, Pergamon Press, New York, 330 pp. $21.

Reviewed by S. F. SINGER
University of Maryland

This volume forms No. 6 of a series of supplemental volumes to the *Journal of Atmospheric and Terrestrial Physics.* The first one was "Rocket Exploration of the Upper Atmosphere"; another in the series has been "Vistas in Astronomy," a two-volume edition.

The present work is the result of a symposium held in London in August 1955 to discuss in the fullest possible way the effects of solar eclipses on the ionosphere.

Such observations are of great value in the interpretation of many geophysical phenomena. This book gives a full account of the various influences of solar eclipses on the earth's atmosphere.

The effects, of course, relate mainly to the sudden removal of solar ultraviolet and x-rays which normally cause the ionosphere. There are therefore some theoretical considerations on these points followed by a large section giving results of ionospheric radio observations during the eclipses. Then follows a series of theoretical papers which discuss the radiation from the sun and its production of the ionosphere. Next, there are four papers dealing with the recombination process in the ionosphere which removes ions and electrons.

Because of the fact that the ionosphere carries electric currents and contributes to the earth's magnetic field, eclipses also give geomagnetic effects. These are discussed in a series of four papers. An interesting set of papers deals with solar radio noise during the eclipse.

An extensive bibliography which goes back as far as 1912 lists the literature of solar eclipses and the ionosphere.

Books Received

Dynamics of Machinery, by A. R. Holowenko, Wiley, New York, 1955, 461 pp. $7.50.

Glass Reinforced Plastics, by Phillip Morgan, Philosophical Library, New York, 1957, 276 pp. $15.

Basic Mathematics for Radio and Electronics, by F. M. Colebrook and J. S. Head, Philosophical Library, New York, 1957, 359 pp. $6.

Radio Aids To Air Navigation, by J. H. H. Grover, Philosophical Library, New York, 1957, 138 pp. $6.

The Expanding Case for the UFO, by M. K. Jessup, Citadel Press, New York, 1957, 253 pp. $3.50.

Arizona's Meteorite Crater, by H. H. Nininger, World Press, Denver, 1956, 232 pp. $3.75.

Industrial Electronics Circuits, by R. Kretzmann, Philosophical Library, New York, 1957, 194 pp. $10.

Case Problems in Transportation Management, by George P. Baker and Gayton E. Germane, McGraw-Hill, New York, 1957, 685 pp. $8.50.

Radio Telemetry, by M. H. Nichols and L. L. Rauch, 1956, 461 pp. $12.

Control-system Dynamics, by Walter R. Evans, McGraw-Hill, New York, 1954, 282 pp.

The Chemistry of Organometallic Compounds, by Rochow, Hurd and Lewis, John Wiley & Sons, New York, 1957, 344 pp. $8.50.

Advances in Geophysics, Vol. II, by H. E. Landsberg, Academic Press, New York, 1957, 378 pp. $8.80.

Digital Differential Analyzers, by George F. Forbes, published by G. F. Forbes, Pacoima, Calif., 1957, 154 pp.

Modern Chemistry for the Engineer and Scientist, by G. R. Robertson, McGraw-Hill, New York, 1957, 442 pp. $9.50. This volume is a compilation of the lectures given at U.C.L.A. by the following outstanding scientists: Kenneth S. Pitzer, Paul H. Emmett, W. Albert Noyes, Jr., Norman Davidson, Clifford S. Garner, Laszlo Zechmeister, Saul Winstein, Herman F. Mark, Nelson W. Taylor, Eugene G. Rochow, Theodore W. Evans, George C. Kennedy, John E. Dorn, Joseph A. Pask, Donald K. Tressler, Robert L. Metcalf, Gordon A. Alles, Theodore A. Geisman, Linus Pauling.

Elements of Heat Transfer, by Max Jakob and George A. Hawkins, John Wiley & Sons, New York, 1957, 317 pp. $6.75. This constitutes the third edition of the well-known elementary textbook. It includes new data, and places more emphasis on analysis of heat transfer problems.

Advances in Geophysics, by H. E. Landsberg, Academic Press, New York, 1956, 378 pp. $8.80. This book should be of interest to all geophysicists, particularly those involved in the IGY. It contains the following contributions:

A. P. Crary—Arctic Ice Island Research
Zdenek Sekera—Recent Developments in the Study of the Polarization of Sky Light
Perry Byerly—Subcontinental Structure in the Light of Seismological Evidence
E. C. Bullard, A. E. Maxwell and R. Revelle—Heat Flow through the Deep Sea Floor
J. A. Jacobs—The Interior of the Earth
P. H. Jones, H. E. Skibitzke—Subsurface Geophysical Methods in Ground-Water Hydrology
S. F. Singer—Geophysical Research with Artificial Earth Satellites

Internationale Tagung Uber Staustrahlen und Raketen, edited by Eugen Sänger, Irene Sänger-Bredt, Ernst von Olnhausen, Germany, 1956, 358 pp. This volume constitutes the proceedings of the International Conference on Jets and Rockets held in Freudenstadt, Feb. 6–8, 1956. It includes the addresses and technical contributions of the following: Franz Ludwig Neher, B. Eckert, H. C. Seebohm, A. Seifriz, H. Veit, E. Sänger, Maurice Roy, J. Dupin, I. Sänger-Bredt, R. W. Porter, J. Corbeau, W. Michely, E. Sharer, A. Gerber, W. Pilz, L. J. Sedov, G. G. Czerny, H. Maecker, Th. Peters, H. J. Kaeppeler, F. Winterberg.

This compilation is a contribution of the Forschungsinstitut für Physik der Strahlantriebe.

Higher Oxo Alcohols, by L. F. Hatch, John Wiley & Sons, New York, 1957, 120 pp. $4.50.

Principles of Electrical Measurements, by H. Buckingham and E. M. Price, Philosophical Library, New York, 1957, 600 pp. $15.

Automation: Its Purpose & Future, by Magnus Pyke, Philosophical Library, New York, 1957, 191 pp. $10.

Practical Astronomy, by W. Schroeder, Philosophical Library, New York, 1957, 206 pp. $6.

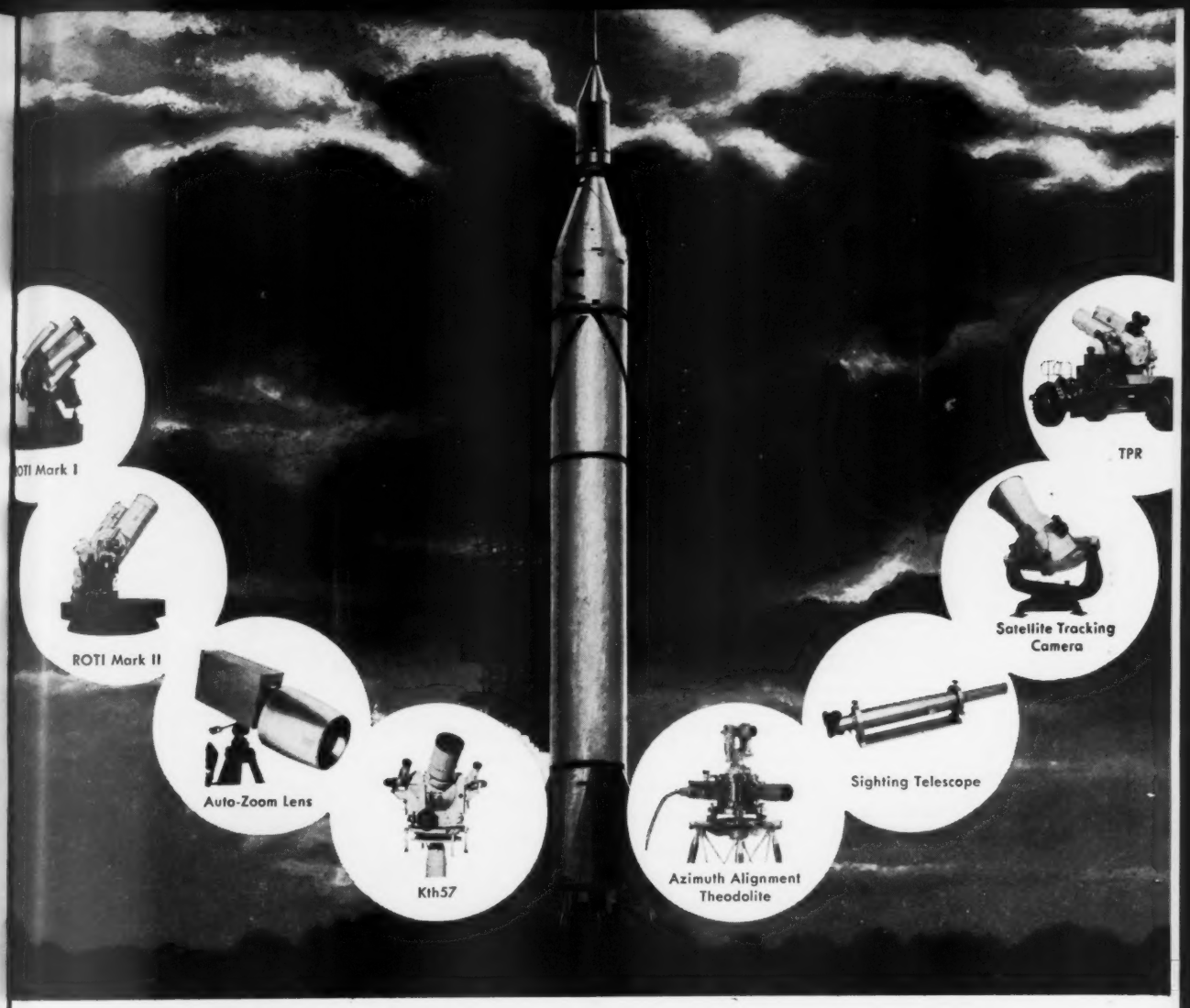

P-E optical range instrumentation provides vital missile data

checks behavior from production through flight

Engineers must *see* what is happening to a missile at every stage of its life. And Perkin-Elmer optical range instruments help them see . . . on the production line where stable platforms are aligned by P-E theodolites . . . at the launching site where P-E instruments first lay the missile for flight and then record vital data about its ascent . . . downrange where P-E tracking instruments let observers watch – and learn from – its meteoric journey across the skies.

Data grows more complex as the state of the art advances and the demands upon optical range instrumentation multiply. That calls for a high order of creative engineering. The number of P-E instruments in the missile program today demonstrates the emphasis that Perkin-Elmer places on this singular talent.

ROTI (Recording Optical Tracking Instrument) Mark I — Twin telescopes equipped with cameras track and record flight data on missiles and airborne objects.

ROTI Mark II — Single telescope and camera with velocity memory circuits for tracking objects that pass behind clouds or other obstructions.

TPR (Telescopic Photographic Recorder) — A mobile unit similar in function to ROTI, but designed for easy mobility to any site accessible to prime mover.

Kth57 Cine-Theodolite—Intermediate range instrument for evaluation of AA fire, monitoring bombing runs, etc.

Azimuth Alignment Auto-Theodolite — Short, intermediate and long range models align inertial guidance systems at assembly and at the missile launching site.

Sighting Telescope — Combines wide field of view and high magnification for quick target acquisition.

SATRACK (Satellite Tracking Camera) — Employs P-E aspheric optical systems. High light-gathering power, wide field of view will enable camera to photograph IGY satellites.

Auto-Zoom* Lens— Extends versatility and range of standard closed circuit TV cameras. Permits remotely controlled wide-angle or closeup observation of action, target or instruments.

An interesting booklet, "Optical Tracking Instruments," describes these and other P-E instruments for the Space Age more fully. Write for it. *T.M.

ENGINEERING AND OPTICAL DIVISION

Perkin-Elmer *Corporation*

NORWALK, CONNECTICUT

#2 This picture shows slightly less than one minute of a record perhaps 10 minutes long. It is a good interferometer record, though not quite as "pretty as #1. It has a very good record of WWV timing signals.

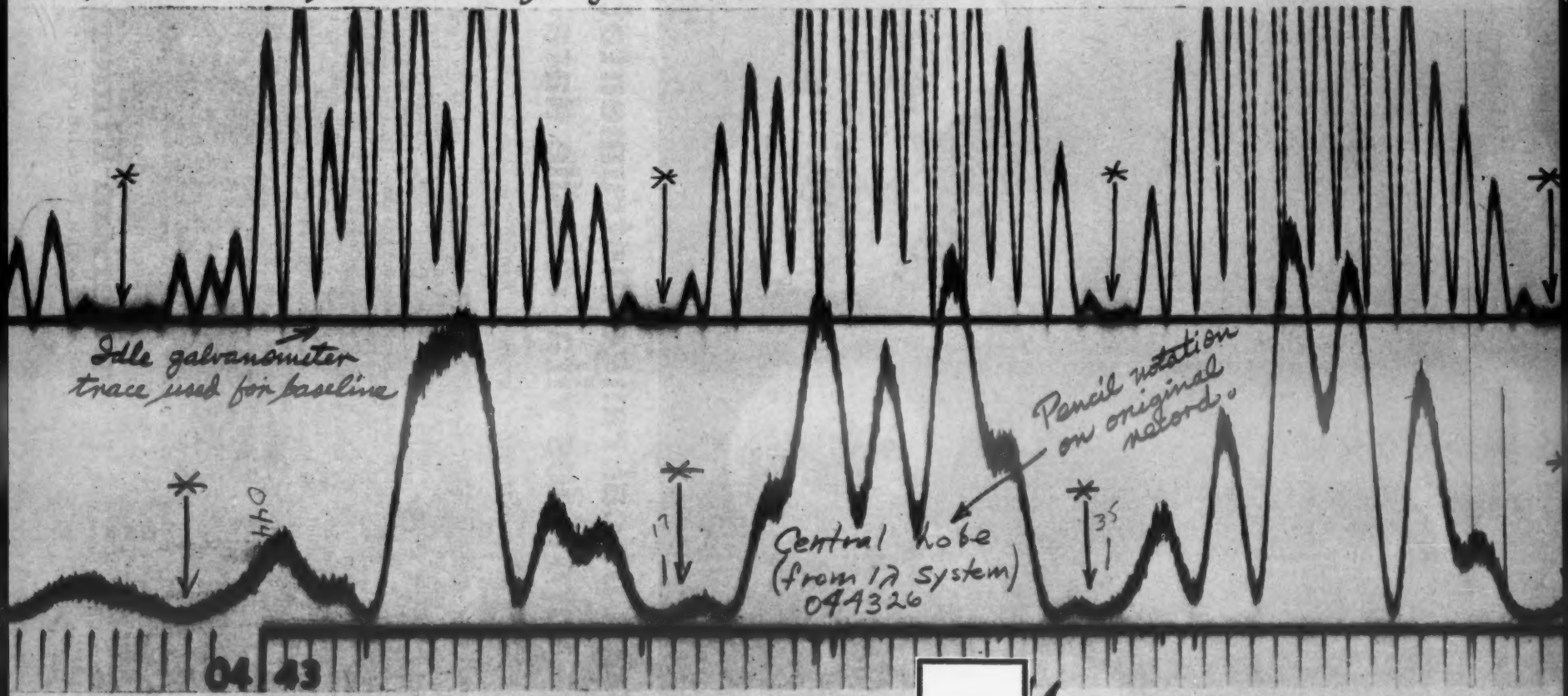

Timing "ticks" (seconds) from WW[illegible] this

*- Nulls in pattern of interferometer antenna[illegible]. The other lobes & nulls (fine structure) are signal fading.

The Visicorder has charted the orbit of Sputnik I

A Model 906 Honeywell Visicorder Oscillograph wrote this record of the signals from Sputnik I for the Department of Electrical Engineering at the University of Illinois at Urbana. The marginal notes are those of Edgar Hayden, the research associate who took the record.

Interferometer-type antenna systems (2 dipole elements ⅛ wave length above ground spaced several wavelengths along a north-south baseline) received the two signals for communications-type radio receivers. The beat oscillators generated audio output signals, a semi-conductor bridge curcuit rectified them, and the d-c output, filtered by an R-C network with a time constant of about .003 seconds, was used to drive the Visicorder galvanometers directly.

The Visicorder, teamed with the interferometer antenna, quickly established a record of the orbit of Sputnik I.

s is a record of Sputnik I

The HONEYWELL VISICORDER is the first high-frequency, high-sensitivity direct recording oscillograph. In laboratories and in the field everywhere, instantly-readable Visicorder records are pointing the way to new advances in product design, rocketry, computing, control, nucleonics . . . in any field where high speed variables are under study.

To record high frequency variables—and monitor them as they are recorded—use the Visicorder Oscillograph. Call your nearest Minneapolis Honeywell Industrial Sales Office for a demonstration.

Reference Data: Write for Visicorder Bulletin

Minneapolis Honeywell Regulator Co.,
Industrial Products Group, Heiland Division
5200 E. Evans Ave., Denver 22, Colo.

MINNEAPOLIS
Honeywell

Heiland Division

Technical Literature Digest

M. H. Smith, *Associate Editor,* **and M. H. Fisher,** *Contributor*
The James Forrestal Research Center, Princeton University

Jet and Rocket Propulsion Engines

The Design and Testing of an Axial Compressor Having a Mean Stage Temperature Rise of 30 deg. C, by A. D. S. Carter, S. J. Andrews and E. A. Fielder, *Gt. Brit., Aeron. Res. Council, Rep. & Mem.* 3985 (formerly *A.R.C. Tech. Rep.* 16775; *Nat. Gas Turbine Estab., Rep.* R148), 1957, 14 pp.

A Survey of the Alternating Pressures Exciting High Frequency Vibrations in Gas Turbines, by J. R. Forshaw, *Gt. Brit., Aeron. Res. Council, Rep. & Mem.* 2989 (formerly *A.R.C. Tech. Rep.* 17133; *Nat. Gas Turbine Estab., Rep.* R148), 1957, 20 pp.

Design and Performance of an Experimental Axial Discharge Mixed Flow Compressor, III: Over All Performance of Impeller and Supersonic Diffuser Combination, by Ward W. Wilcox and William H. Robbins, *NACA RM* E51A02, April 1951, 26 pp. (Declassified from Confidential by authority of *NACA Res. Abs.* 119, p. 16, 8/16/57.)

Performance Investigation of Can Type Combustor from British Turbojet Engine and Comparison of This Combustor with Can Type Combustor from U. S. Turbojet Engine, by William P. Cook and Richard G. Koch, *NACA RM* E9H29, Feb. 1950, 25pp. (Declassified from Confidential by authority of *NACA Res. Abs.* 119, p. 16, 8/16/57.)

Approximation for the Effect of Twist on the Vibration of a Turbine Blade, by A. I. Martin, *Aeron. Quart.*, vol. 8, Aug. 1957, pp. 291–308.

Aero-engine Survey, *Aeroplane,* vol. 93, Sept. 6, 1957, pp. 376–380.

Ignition Systems Must Keep up with Engine Performance, by Kurt R. Stehling, *Aviation Age,* vol. 28, Sept. 1957, pp. 56–61.

Liquid-Rocket Engine Control, by Rudolph H. Reichel, *Missiles and Rockets,* vol. 2, Sept. 1957, pp. 101–102, 104, 106.

Propulsion Systems Evaluation, by George P. Sutton, *Missiles and Rockets,* vol. 2, Sept. 1957, pp. 123–124, 126.

Aerodynamics of Jet Propelled Vehicles

Aspects of High Energy Ballistics, by Louis Gold, *J. Franklin Inst.*, vol. 264, Oct. 1957, pp. 301–311.

Criteria for the Generalized Dynamic Stability of a Rolling Symmetric Missile, by Charles H. Murphy Jr., *J. Aeron. Sci.*, vol. 24, Oct. 1957, pp. 773–774.

A Comparative Analysis of the Performance of Long-range Hyper-velocity Vehicles, by Alfred J. Eggers Jr., H. Julian Allen and Stanford E. Neice, *NACA TN* 4046, Oct. 1957, 66 pp.

A Study of the Motion and Aerodynamic Heating of Missiles Entering the Earth's Atmosphere at High Supersonic Speeds, by H. Julian Allen and A. J. Eggers Jr., *NACA TN* 4047, Oct. 1957, 61 pp. (supersedes RM A53D28).

Motion of a Ballistic Missile Angularly Misalined wih the Flight Path Upon Entering the Atmosphere and Its Effect Upon Aerodynamic Heating, Aerodynamic Loads, and Miss Distance, by H. Julian Allen, *NACA TN* 4048, Oct. 1957, 66 pp. (supersedes RM A56F15).

On the Nature of the Sonic Line for Supersonic and Hypersonic Flow over Blunt Bodies, by Ronald F. Probstein, *Wright Air Dev. Center, TN* 57-349 (*ASTIA-AD* 142037), Sept. 1957, 17 pp.

Heat Transfer and Fluid Flow

Simplified Method for Calculating the Heating Surfaces at Low Combustion Product Temperatures, by Jiri Possner, *Strojirenstvi,* vol. 7, Feb. 1957, pp. 107–111 (in Czechoslovakian).

Effect of Agitation on the Critical Temperature Difference for a Boiling Liquid, by F. S. Pramuk and J. W. Westwater, *Chem. Engng. Progr., Symposium Series,* vol. 52, no. 18, 1956, pp. 79–83.

Ebullition from Solid Surfaces in the Absence of a Pre-existing Gaseous Phase, *Trans. ASME,* vol. 79, May 1957, pp. 735–740.

Heat Transfer to Flowing Gas-solids Mixtures in a Circular Tube, by Leonard Farbar and M. J. Morley, *Ind. Engng. Chem.*, vol. 49, July 1957, pp. 1143–1150.

Exchange Processes in Steam Containing Air, by F. von Bosnjakovic, *Kylteknisk Tidskrift,* no. 3, 1957, pp. 142–146 (in Swedish).

Calculating Three-phase Flow in Horizontal Pipe Lines, by D. P. Sobocinski and R. L. Huntington, *Pipe Line Ind.*, vol. 6, no. 1, Jan. 1957, pp. 43–45.

Plane Couette Flow at Low Mach Number According to the Kinetic Theory of Gases, by Hsun-Tias Yang and Lester Lees, *GALCIT Hydrodynamics Lab., Rep.* M-36, Feb. 1, 1957, 37 pp.

Heat Transfer in Pipe Flow at High Speeds, by J. E. Bialokoz and O. A. Saunders, *Proc. Inst. Mech. Engng.*, vol. 170, no. 12, 1956, pp. 389–406.

Study of Heat Transfer in a Spiral Canal, by V. G. Fastovskii and A. E. Rovinskii, *Teploenergetika,* vol. 4, Jan. 1957, pp. 39–41 (in Russian).

On the Pressure Losses for Turbulent Flow in Smooth Pipe Bends, by H. Ito, *Tohoku University, Inst. High Speed Mech., Rep.*, vol. 7, 1956, pp. 149–174.

Capillary Two-phase Flow, by H. A. Whitesel, *Refriger. Engng.*, vol. 65, April 1957, pp. 42–44, 98–99.

One-dimensional Transient Flow in Pipe with Two Gases, by R. S. Benson, *Engng.*, vol. 202, Nov. 16, 1956, pp. 687–691.

Pipe Friction Loss at High Pressures, by J. G. Slater, J. R. Villemonte, and H. J. Day, *Proc. Am. Soc. Civil Engrs.*, vol. 83 (*J. Hydraulics Div.*), Feb. 1957 (*Paper* 1163), 21 pp.

Some Plane Problems in the Theory of

EDITOR'S NOTE: Contributions from E. R. G. Eckert, J. P. Hartnett, T. F. Irvine Jr. and P J. Schneider of the Heat Transfer Laboratory, University of Minnesota, are gratefully acknowledged.

NOW YOU CAN PROCESS THIS

FASTER

WITHOUT ODOR!

The new Du Pont Lino-Writ Rapid Processing Chemicals Kit enables you to process Lino-Writ 4 faster at temperatures up to 135 degrees. And we've done away with the disagreeable odor previously associated with high-temperature processing. Now you can develop up to 20 feet per minute, and still get the same sharp, clear results that Lino-Writ is famous for. That means that on some runs you can now process your paper *twice as fast* as you previously could.

Two big extras from Du Pont: quicker processing than ever before . . . without the disadvantage of offensive odor. Ask your dealer about the new Du Pont Lino-Writ Rapid Processing Chemicals Kit. He's stocking it now.

E. I. du Pont de Nemours & Co. (Inc.), Photo Products Department, Wilmington 98, Delaware. In Canada: Du Pont Company of Canada (1956) Limited, Toronto.

DU PONT
REG. U. S. PAT. OFF.

Better Things for Better Living . . . *through Chemistry*

This advertisement was prepared exclusively by Phototypography.

Thermal Waves, by B. G. Korenev, *Doklady Akademii Nauk SSSR*, vol. 112, Jan.-Feb. 1957, pp. 29–32 (in Russian).

Thermodynamical Theory of Thermal Conduction of Dielectrics under Electric Fields, by S. Mascarenhas, *Nuovo Cimento*, vol. 5, no. 4, May 1957, pp. 1118–1121.

Analog Computers Calculate Heat Transfer, by Robert S. Schechter, *Petroleum Refiner*, vol. 36, Feb. 1957, pp. 112–114.

Difference Methods for the Calculation of Temperature Processes in One-dimensional Heat Flow in Bodies, by Herbert Schuh, *VDI Forschungsheft*, no. 459, 1957, 43 pp.

The Solutions of Boundary Value Problems on a REAC Analog Computer, by M. Yanowitch, *Computers and Automation*, vol. 6, Feb. 1957, pp. 26–29.

Half Values as Units of Measurement in Steady State Exchange, by F. von Bosnjakovic, *Chemic-Ingenieur-Technik*, vol. 29, no. 3, 1957, pp. 187–197.

Experimental Study of the Velocity and Temperature Distribution in a High-velocity Vortex-type Flow, by J. P. Hartnett and E. R. G. Eckert, *Trans. ASME*, vol. 79, May 1957, pp. 751–758.

On the Formulation and Analysis of Numerical Methods for Time-Dependent Transport Equations, by Herbert B. Keller and Burton Wendroff, *New York Univ., Inst. Math. Sci.*, (U. S. Atomic Energy Comm.), NYO-7694, Dec. 1956, 38 pp.

Turbulent Mixing of Plane Hot Air Flows, by W. Szablewski, *Ing. Arch.*, No. 1, 1957, pp. 10–25 (in German).

Aerothermal Seminar of the Faculty of Sciences of Paris, *France, Ministere de l'Air, Note Tech.* 63, 1957, 110 pp. (in French).

Thermal Transpiration: Application of Liang's Equation, by M. J. Bennett and F. C. Tompkins, *Trans. Faraday Soc.*, vol. 53, Feb. 1957, pp. 185–192.

Determination of Thermal Conductivities of Metals by Measuring Transient Temperatures in Semi-infinite Solids, by S. T. Hsu, *Trans. ASME*, vol. 79, July 1957, pp. 1197–1202.

Analysis of Heat-driven Oscillations of Gas Flows, by H. J. Merk, *Appl. Sci. Res.*, Sec. A., vol. 6, no. 4, 1957, pp. 317–336.

What Are Heat Transfer Characteristics of Wire and Tube Condensers? by O. W. Witzell and W. E. Fontaine, *Refrig. Engng.*, vol. 65, March 1957, pp. 33–37, 127.

Heat Transfer Characteristics of Liquid Metal in Closed Thermosyphon, by F. J. Bayley and N. Bell, *Engng.* vol. 183, March 8, 1957, pp. 300–302.

The Use of Sodium and of Sodium-Potassium Alloy as a Heat-transfer Medium, by W. B. Hall and T. I. M. Crofts, *Proc., Inst. Mech. Engrs.*, vol. 170, no. 10, 1956, pp. 281–305.

Temperature and Velocity Distribution and Transfer of Heat in a Liquid Metal, by H. E. Brown, B. H. Amstead, and B. E. Short, *Trans., ASME*, vol. 79, Feb. 1957, pp. 279–285.

Utilization of Solar Furnaces in High-temperature Research, by Pol Duwez, *Trans. ASME*, vol. 79, July 1957, pp. 1014–1018.

Research on Application of Cooling to Gas Turbines, by J. B. Esgar, J. N. B. Livingood, and R. O. Hickel, *Trans. ASME*, vol. 79, April 1957, pp. 645–651.

Analysis of Large Aperture Parabolic Mirrors for Solar Furnaces, by Joseph Farber and Burton I. Davis, *J. Optical Soc. America*, vol. 47, March 1957, pp. 216–220.

The Cooling Process in Periodic Equipment. Heat Exchangers, Economic Size of the System. Operating Costs, by Ugo Fasoli, *Chimica e l'Industria*, vol. 39, Feb. 1957, pp. 83–92 (in Italian).

Heat Transfer to Vibrating Air Columns, by W. B. Harrison, W. C. Boteler, T. W. Jackson, A. Lowi, Jr., and F. A. Thomas, Jr., *NACA* (unpublished), (N-94857), 1955, 38 pp.

Measurements on the Velocity of Sound in Nitrogen under High Pressure, by A. van Itterbeek, W. de Rop and G. Forrez, *Applied Sci. Res.*, vol. 6, Sect. A, no. 5–6, 1957, pp. 421–432.

On the Use of Matrices for Solving Periodic Heat Flow Problems, by G. W. T. White, *Applied Sci. Res.*, vol. 6, Sect. A, no. 5–6, 1957, pp. 433–444.

On the Existence of Periodic Waves Near Critical Speed, by Walter Littman, *Comm. Pure Appl. Math.*, vol. 10, May 1957, pp. 241–269.

Deposition of Suspended Particles from Turbulent Gas Streams, by S. K. Friedlander and H. F. Johnstone, *Ind. Engng. Chem.*, vol. 49, July 1957, pp. 1151–1156.

Electrical Conductivity of Thermally Ionized Air Produced in a Shock Tube, by Lawrence Lamb and Shao-Chi Lin, *J. Appl. Phys.*, vol. 28, July 1957, pp. 754–759.

Shock Hugoniot of Air, by W. E. Deal, *J. Appl. Phys.*, vol. 28, July 1957, pp. 782–784.

Quantum-mechanical Effects in Gas Dynamics, by E. V. Laitone, *J. Chem. Phys.*, vol. 26, June 1957, pp. 1560–1566.

Thermal Conductivity of Gas Mixtures in Chemical Equilibrium, by James N. Butler and Richard S. Brokaw, *J. Chem. Phys.*, vol. 26, June 1957, pp. 1636–1642.

An Electronic Analogue for Supersonic Flow, by Leslie S. G. Kovasznay, *J. Fluid Mech.*, vol. 2, June 1957, pp. 383–396.

On the Stability of Plane Shock Waves, by N. C. Freeman, *J. Fluid Mech.*, vol. 2, June 1957, pp. 397–411.

Simplified Equations for Calculating Local and Total Heat Flux to Nonisothermal Surfaces, by E. R. G. Eckert, J. P. Hartnett, and Roland Birkebak, *J. Aeron. Sci.*, vol. 24, July 1957, pp. 549–551.

The Relation between the Flow of Non-Newtonian Fluids and Turbulent Newtonian Fluids, by R. S. Rivlin, *Quarterly Appl. Math.*, vol. 15, July 1957, pp. 212–215.

Intermolecular Free Length in Liquids in Relation to Sound Velocity, by Otohilo Nomoto, *J. Physical Soc. Japan*, vol. 12, June 1957, p. 739.

The Direct Measurement of Local Skin Friction on Aerobee Hi Rockets in Free Flight, by Felix W. Fenter and W. C. Lyons, Jr., *Texas Univ., Defense Res. Lab. CM-877* (*DRL* 391), May 1957, 47 pp., 27 fig.

The Evaporation of Fuel Sprays, I. Theorectical Treatment, by G. W. Benson, *Canada, Nat. Aeron. Estab., Lab. Rep.* LR-181, (*ASTIA AD* 121803), Nov. 1956, 38 pp.

States of Partial Equilibrium behind Shock Waves in O_2, N_2, CO, CO_2, and N_2O, by Wayland C. Griffith and Anne Kenny, *Princeton Univ., Dept. Phys., Tech. Rep.* II-23, March 1957, 16 pp., 6 tab., 6 fig.

Measurements of the Thrust Produced by Convergent-Divergent Nozzles at Pres-

sure Ratios up to 20, by P. F. Ashwood, G. W. Crosse and Jean E. Goddard, *Gt. Brit., Aeron. Res. Council, Current Paper* 326, 1957, 15 pp., 10 fig. (formerly *ARC Tech. Rep.* 18,771; *Gt. Brit., Natl. Gas Turbine Estab.* Mem., M.288).

Heat Transfer Research Holds Key to Better Rocket Cooling, by Kurt R. Stehling, *Aviation Age,* vol. 28, Aug. 1957, pp. 36–43.

Mechanical Design Analysis of Several Noncritical Air-Cooled Turbine Disks and a Corrugated-Insert Air-Cooled Turbine Rotor Blade, by Merland L. Moseson, Morton H. Krasner and Robert R. Ziemer, *NACA RM* E53E21, July 1953, 49 pp. (Declassified from Confidential by authority of *NACA Res. Abs.* 119, p. 19, 8/16/57.)

Investigation of Water-spray Cooling of Turbine Blades in a Turbo-jet engine, by John C. Freche and William J. Stelpflug, *NACA RM* E53A23, March 1953, 45 pp. (Declassified from Confidential by authority of *NACA Res. Abs.* 119, p. 19, 8/16/57.)

Analytical Comparison of Turbine-blade Cooling Systems Designed for a Turbojet Engine Operating at Supersonic Speed and High Altitude, I: Liquid-cooling Systems, by Wilson B. Schramm, Alfred J. Nachtigall and Vernon L. Arne, *NACA RM* E52J29, Jan. 1953, 52 pp. (Declassified from Confidential by authority of *NACA Res. Abs.* 119, p. 18, 8/16/57.)

Analytical Comparison of Turbine-blade Cooling Systems Designed for a Turbojet Engine Operating at Supersonic Speed and High Altitude, II: Air-cooling Systems, by Wilson B. Schramm, Vernon L. Arne and Alfred J. Nachtigall, *NACA RM* E52J30, Jan. 1953, 50 pp. (Declassified from Confidential by authority of *NACA Res. Abs.* 119, p. 18, 8/16/57.)

An Analytical Method for Evaluating Factors Affecting Application of Transpiration Cooling to Gas Turbine Blades, by Jack B. Esgar, *NACA RM* E52G01, Sept. 1952, 68 pp. (Declassified from Confidential by authority of *NACA Res. Abs.* 119, p. 17, 8/16/57.)

An Experimental Cascade Study of the Effects of a Solidity Reduction on the Two-Dimensional Aerodynamic Characteristics of a Turbine-rotor Blade Suitable for Air Cooling, by Henry W. Plohr and William J. Nusbaum, *NACA RM* E52B27, May 1952, 17 pp. (Declassified from Confidential by authority of *NACA Res. Abs.* 119, p. 17, 8/16/57.)

Cold-air Investigation of a Turbine with Nontwisted Rotor Blades Suitable for Air Cooling, by Thomas R. Heaton, William R. Slivka and Leonard F. Westra, *NACA RM* E52A25, March 1952, 34 pp. (Declassified from Confidential by authority of *NACA Res. Abs.* 119, p. 17, 8/16/57.)

Aerodynamic Studies in the Shock Tube, by Josef Rabinowicz, *Calif. Inst. Tech., Hypersonic Res. Project, Mem.* 38, June 10, 1957, 111 pp., 38 ref.

Pressure Recovery, Drag, and Subcritical Stability Characteristics of Three Conical Supersonic Diffusers at Stream Mach Numbers from 1.7 to 2.0, by Theodore J. Nussdorfer, Leonard J. Obery and Gerald W. Englert, *NACA RM* E51H27, Feb. 1952, 31 pp. (Declassified from Confidential by authority of *NACA Res. Abs.* 119, p. 17, 8/16/57.)

Pressure Recovery, Drag, and Subcritical Stability Characteristics of Conical Supersonic Diffusers with Boundary-layer Removal, by Leonard J. Oberey, Gerald W. Englert and Theodore J. Nussdorfer, *NACA RM* E51H29, Feb. 1952, 25 pp. (Declassified from Confidential by authority of *NACA Res. Abs.* 119, p. 17, 8/16/57.)

Development and Application of a Technique for Steady State Aerodynamic Heat Transfer Measurements, by Frederic W. Hartwig, *Calif. Inst. Tech., Hypersonic Res. Project, Mem.* 37, June 1, 1957, 48 pp., 13 ref.

Formulas for Thermal Conductivity of Ternary Gas Mixtures, by B. N. Srivastava and S. C. Saxena, *J. Chem. Phys.,* vol. 27, Aug. 1957, pp. 583–584.

The Laminar and Turbulent Mixing of Jets of Compressible Fluid, Part I. Flow Far from the Orifice, by L. J. Crane and D. C. Pack, *J. Fluid Mech.,* vol. 2, July 1957, pp. 449–455.

The Secondary Flow in a Cascade of Turbine Blades, by W. D. Armstrong, *Gt. Brit., Aeron. Res. Council, Rep. & Mem.* 2979 (formerly *A.R.C. Tech. Rep.* 17442), 1957, 14 pp.

Radiant Heat Exchange in a Gas Filled Enclosure, by H. C. Hottel and E. S. Cohen, *Project Squid Tech. Rep.,* MIT-14-P (*ASTIA AD* 138820), 1957 (available only on microcards).

Results of Systematic Investigations on Secondary Flow Losses in Cascades, Part I: Secondary Flow Losses in Compressor Cascades of Profile NACA 8410, by K. Gersten, *Braunschweig, Tech. Hochschule, Inst. für Stromungsmechanik, Rep.* 54/29a, June 1955, 32 pp.

Equations, Tables, and Figures for Use in the Analysis for Helium Flow at Supersonic and Hypersonic Speeds, by James N. Mueller, *NACA TN* 4063, Sept. 1957, 178 pp.

Mollier Chart for Air in Dissociated Equilibrium at Temperatures of 2000°K to 15000°K, by I. Korobkin and S. M. Hastings, *NAVORD Rep.* 4446 (*Aeroballistics Res. Rep.* 368), May 1957, 7 pp.

Analysis of Shock Motion in Ducts during Disturbances in Downstream Pressure, by Herbert G. Hurrell, *NACA TN* 4090, Sept. 1957, 11 pp.

An Analysis of the Interaction of Shock Waves with Unseparated Turbulent Boundary Layers, by Andrew G. Hammitt, *Princeton Univ., Dept. Aeron. Engng., Rep.* 371 (*AFOSR-TN-57-108; ASTIA AD* 120460), Feb. 1957, 14 pp.

A Basic Approach to Shock Front Analysis, by Ph. J. Theodorides, *Univ. Maryland, Inst. Fluid Dynamics Appl. Math., TN* BN-93 (*AFOSR-TN-57-59; ASTIA-AD* 115099), Jan. 1957, 31 pp.

The Structure of a Shock Wave in a Gas Having a Long Relaxation Time, by L. Talbot, *Univ. Calif., Inst. Engng. Res., Tech. Rep.* HE-150-145, March 1957, 23 pp.

Some Notes on Shock Wave Boundary Layer Interactions and on the Effect of Suction on the Separation of Laminar Boundary Layers, by K. N. C. Bray, *Gt. Brit., Aeron. Res. Council, Current Paper* 332 (formerly *A.R.C. Tech. Rep.* 18631; *Handley Page Ltd., Aero. Res. Rep.* 24), 1957, 7 pp.

A Phenomenal Theory of the Free Turbulent Flow of a Non-Reacting Binary Gas Mixture, by Luigi G. Napolitano, *Brooklyn Polytech. Inst., Dept. Aeron. Engng. Appl. Mech., Rep.* 317 (*AFOSR-TN-57-39; ASTIA AD* 115077), Dec. 1956, 46 pp.

Turbulent Mixing of Two Non-Reacting Gases, by Luigi G. Napolitano, *Brooklyn Polytech. Inst., Dept. Aeron. Engng. Appl. Mech., Rep.* 323 (*AFOSR-TN-57-41; ASTIA AD* 115079), Jan. 1957, 29 pp.

Pneumatic controls

AiResearch is the largest designer and manufacturer of pneumatic controls for the aircraft and associated industries. During the past 10 years more than 300,000 units have been produced and are in service.

Temperatures of the fluids (including gas and liquids) range from −400°F to +2000°F at pressures to +6000 psig. The units operate at any ambient pressure at ambient temperatures from −300°F to over +1000°F. Line diameters range from ⅛ inch to 15 inches.

This equipment is developed and tested in the finest pneumatic facilities in the world. Your inquiries are invited.

ENGINEERING REPRESENTATIVES: AIRSUPPLY AND AERO ENGINEERING, OFFICES IN MAJOR CITIES

THE GARRETT CORPORATION

AiResearch Manufacturing Divisions

Los Angeles 45, California • Phoenix, Arizona

Systems, Packages and Components for: AIRCRAFT, MISSILE, ELECTRONIC, NUCLEAR AND INDUSTRIAL APPLICATIONS

Approximation Methods in Compressible Fluid Dynamics, Part I, Chapters I–IV; Part II, Chapters V–VII, by Isao Imai, *Univ. Maryland, Inst. Fluid Dynamics Appl. Math., TN* BN-95 (*ASTIA AD* 128411), March 1957, 184 pp.

Further Investigations of the Laminar Turbulent Transition in a Free Jet (Annular Nozzle), *AFOSR-TN*-57-31 (*ASTIA AD* 126494), Dec. 1956, 22 pp.

Statistical Studies on the Turbulent State of Motion, Part I: Kinematics, by Hans Gebelein and Erik Svenson, *AFOSR-TN*-57-278 (*ASTIA AD* 126539), 1957, 42 pp.

A Hydrodynamic Study of Small Diameter Orifices in Thin Plates, by Henry L. Herman and Milton V. Ashley, *Picatinny Arsenal, Samuel Feltman Ammunition Labs., Tech. Rep.* 2450, Aug. 1957, 19 pp.

Combustion, Fuels and Propellants

Combustion Performance Evaluation of Magnesium Hydrocarbon Slurry Blends in a Simulated Tail Pipe Burner, by Leonard K. Tower and J. Robert Branstetter, *NACA RM* E51C26, May 1951, 53 pp. (Declassified from Confidential by authority of *NACA Res. Abs.* 116, p. 14, 7/5/57.)

Effect of Particle Size and Stabilizing Additives on the Combustion Properties of Magnesium Slurry, by Albert M. Lord and Vernida E. Evans, *NACA RM* E52K12, Jan. 1953, 28 pp. (Declassified from Confidential by authority of *NACA Res. Abs.* 116, p. 15, 7/5/57.)

An Experimental Investigation of the Combustion Properties of a Hydrocarbon Fuel and Several Magnesium and Boron Slurries, by Albert M. Lord, *NACA RM* E52B01, April 1952, 30 pp. (Declassified from Confidential by authority of *NACA Res. Abs.* 116, p. 14, 7/5/57.)

Experimental Investigation of Physical and Combustion Properties of Several Residual Fuel Oils and Magnesium-fuel-oil Slurries in a Ram-jet-type Combustor, by Preston N. Cook, Jr., Vernida E. Evans and Erwin A. Lezberg, *NACA RM* E53D30, June 1953, 23 pp. (Declassified from Confidential by authority of *NACA Res. Abs.* 116, p. 15, 7/5/57.)

Magnesium-Slurry Combustion Performance in 6/5-inch-diameter Ram-jet Engine Mounted in Connected-pipe Facility, by J. Robert Branstetter, James B. Gibbs and Warner B. Kaufman, *NACA RM* E53E27, Aug. 1953, 63 pp. (Declassified from Confidential by authority of *NACA Res. Abs.* 116, p. 15, 7/5/57.)

The Internal Ballistics of a Recoilless High-Low Pressure Gun, by J. N. Kapur, *Appl. Sci. Res.*, vol. 6, Sect. A, no. 5–6, 1957, pp. 445–466.

Boron Fuel Production to Start, by J. S. Butz, Jr., *Aviation Week*, vol. 67, July 15, 1957, p. 27.

Decomposition of Alcohols over a Fischer-Tropsch Iron Catalyst, by S. R. Srinivasan and N. G. Basak, *Fuel*, vol. 36, July 1957, pp. 277–285.

Supersaturation in Hydrocarbon Systems, n-Pentane in the Liquid Phase, by W. B. Nichols, L. T. Carmichael, and B. H. Sage, *Ind. Engng. Chem.*, vol. 49, July 1957, pp. 1165–1172.

Decomposition of Hydrogen Peroxide Vapor on Relatively Inert Surfaces, by C. N. Satterfield and T. W. Stein, *Ind. Engng. Chem.*, vol. 49, July 1957, pp. 1173–1180.

GIANT CAPACITOR SYSTEM POWERS ADVANCED EXPERIMENTS ON ELECTRICAL PROPULSION

A report to Engineers and Scientists from Lockheed Missile Systems—where expanding missile programs insure more promising careers

■

Lockheed experiments on electrical power sources for space craft are using electrical energy stored in a giant capacitor system, one of the largest in the aircraft industry. This propulsion research—based on electrohydrodynamics—is an example of the advanced work being conducted in Division laboratories near Stanford University in the electrical, chemical and nuclear fields.

The giant capacitor bank is capable of a 5 million kilowatt jolt of electricity, used to fire Lockheed's new "hotshot" wind tunnel to 18,000 degrees Fahrenheit with speeds up to 15,000 miles an hour.

Research in such sophisticated areas by Division scientists has earned Lockheed leadership in missiles. Nose cone reentry studies, for example, have helped speed delivery dates on Polaris, Lockheed's submarine fleet ballistic missile.

With expansion on our IRBM and other advanced programs, new positions have opened for engineers and scientists... positions that call for the utmost in creative ability.

These areas include: **Propulsion, Aerodynamics-Thermodynamics, Guidance, Electronics, Flight Controls, Structures, Design.**

If you are qualified, you are invited to write M. W. Peterson, Research and Development Staff, Sunnyvale 20, California for further information.

Lockheed

MISSILE SYSTEMS

A DIVISION OF LOCKHEED AIRCRAFT CORPORATION

SUNNYVALE • PALO ALTO • VAN NUYS
SANTA CRUZ • CALIFORNIA
CAPE CANAVERAL, FLORIDA
ALAMOGORDO, NEW MEXICO

Discussing characteristics of the capacitor system are research scientist Dr. Edward Fisher of the Propulsion Staff, right, and Dr. Terry E. Turner, Hot Shot Tunnel Group Leader. The two groups are engaged in a joint effort on advanced propulsion experiments.

Flame Propagation Rates, Chemical Nature of Attachment Surface, by Leon Lapidus, J. B. Rosen and R. H. Wilhelm, *Ind. Engng. Chem.*, vol. 49, July 1957, pp. 1181–1186.

Derivation and Precision of a New Vapor Pressure Correlation for Petroleum Hydrocarbons, by J. B. Maxwell and L. S. Bonnell, *Ind. Engng. Chem.*, vol. 49, July 1957, pp. 1187–1196.

Theory of Multi-component Fluid Mixtures, I: Statistical Order-Disorder Analysis in Multi-component Fluid Mixtures, by Zevi W. Salsburg, Peter J. Wojtowicz, and John G. Kirkwood, *J. Chem. Phys.*, vol. 26, June 1957, pp. 1533–1541.

Entropy of Chemisorbed Hydrogen, by Tetsuo Takaishi and Akio Kobayashi, *J. Chem. Phys.*, vol. 26, June 1957, pp. 1542–1543.

Infrared Spectra and Force Constants of Cyanoacetylene, by George C. Turrell, Walter D. Jones and Arthur Maki, *J. Chem. Phys.*, vol. 26, June 1957, pp. 1544–1548.

Electronic Spectrum and Dissociation Energy of Fluorine, by A. L. G. Rees, *J. Chem. Phys.*, vol. 26, June 1957, pp. 1567–1571.

Mechanism of the Gas Phase, Thermal Decomposition of Ozone, by Sidney W. Benson and Arthur E. Axworthy, Jr., *J. Chem. Phys.*, vol. 26, June 1957, pp. 1718–1719.

Reaction of Carbon Monoxide and Ozone, by P. Harteck and S. Dondes, *J. Chem. Phys.*, vol. 26, June 1957, pp. 1734–1735.

Preliminary Investigation of Propane Combustion in a 3-inch-diameter Duct at Inlet-air Temperatures of 1400° to 1600°F, by Erwin A. Lezberg, *NACA TN* 4028, July 1957, 19 pp.

Reaction of Fluorine with Carbon as a Means of Fluorine Disposal, by Harold W. Schmidt, *NACA RM* E57E02, July 1957, 17 pp.

Propellant Vaporization as a Criterion for Rocket Engine Design; Calculations of Chamber Length to Vaporize a Single n-heptane drop, by Richard J. Priem, *NACA TN* 3985, July 1957, 41 pp.

Combustion Instability in Liquid Rocket Propellant Motors, 20th Quarterly Progress Report, Feb. 1-April 30, 1957, by Jerry Grey, *Princeton Univ., Dept. Aeron. Engng., Rep.* 216-t, June 1, 1957, 25 pp.

Investigation of Jet Flame-holders, II, by A. W. Noon, *Wright Air Dev. Center, TN* 56-316, Part II, April 1957, 30 pp.

Drop Burning Rates of Hydrocarbon and Nonhydrocarbon Fuels, by Arthur L. Smith and Charles C. Graves, *NACA RM* E57F11, Aug. 1957, 22 pp.

Streamlined Method for Determining the Available Diphenylamine Content of Propellants, by W. Dewey Tullis and Milton Roth, *Picatinny Arsenal Rep.* 2432, July 1957, 9 pp.

Effect of Fuel Volatility on Altitude Starting Limits of a Turbo-jet Engine, by H. D. Wilstead and J. C. Armstrong, *NACA RM* E50G10, Sept. 11, 1950, 27 pp. (Declassified from Confidential by authority of *NACA Res. Abs.* 118, p. 7, 8/16/57.)

Energy Limitations of Liquid Rocket Propellants, by J. F. Tormey, *Aircraft Engng.*, vol. 29, Aug. 1957, pp. 248–251.

Hydrogen Cyanide-Fluorine-Oxygen Flame, by Charles S. Stokes and A. V. Crosse, Jr., *Ind. Engng. Chem.*, vol. 49, Aug. 1957, pp. 1311–1314.

Solid Fuel Industry Roundup, *Missiles and Rockets*, vol. 2, Aug. 1957, pp. 67–73.

Swing to Solid Propellants, by John Wilson, *Missiles and Rockets*, vol. 2, Aug. 1957, pp. 92–94.

Machining for Solid Propellant Rockets, by Joachim H. Kauffmann, *Missiles and Rockets*, vol. 2, Aug. 1957, pp. 105–111.

Processing for Solids at Thiokol, *Missiles and Rockets*, vol. 2, Aug. 1957, pp. 112–113.

The Hunt is on for New Sources of Propulsion Energy, by Hugh Harvey, *SAE J.*, vol. 65, Aug. 1957, pp. 17–20.

An Unclassified Literature Survey on Combustion Pressure Oscillations in Liquid Propellant Rocket Motors, by J. R. Osborn and M. J. Zucrow, *Purdue Univ., Rocket Lab., Tech. Mem.* 57-1, June 1957, 134 pp., 64 ref. (Contract N7-onr 39418).

Experimental and Calculated Histories of Vaporizing Fuel Drops, by R. J. Priem, G. L. Borman, M. M. El Wakil, O. A. Uyehara and P. S. Myers, *NACA TN* 3988, Aug. 1957, 66 pp.

Stability Limits and Burning Velocities for Some Laminar and Turbulent Propane and Hydrogen Flames at Reduced Pressure, by Burton Fine, *NACA TN* 4031, Aug. 1957, 49 pp.

Simulated High Altitude Combustion Research, *MIT, Fuels Res. Lab., Quarterly Progress Rep.* 6 (Contract AF33(6163037), Sept. 1-Nov. 31, 1956, Jan. 11, 1957, 19 pp. (*ASITA AD*-122,931), (DSR-7361).

Investigation of Ionization in Flames, I. A Method for the Extraction of the Ions from a Flame, by A. Van Tiggelen, L. Vanreusal, and J. Deckers. **II. Meas-**

urement of Ionization in Flames by a Conductivity Method, by J. Poncelet, *Louvain Univ.*, Nov. 1956, 25 pp. (Contract AF 61(514)-922).

Spark Ignition of Flowing Gases, by Clyde C. Swett, Jr. *NACA Rep.* 1287, 1956, 18 pp.

Method for Combustion of Metals, by A. V. Grosse, *U. S. Patent.* No. 2,764,109, Sept. 25, 1956, 9 pp.

Starting Characteristics and Combustion Performance of Magnesium Slurry in 6/5-inch-diameter Ram-jet Engine Mounted in Connected-pipe Facility, by James B. Gibbs, *NACA RM* E53K05, Jan. 1954, 25 pp. (Declassified from Confidential by authority of *NACA Res. Abs.* 116, p. 16, 7/5/57.)

Performance of Slurries of 50 per cent Boron in JP-4 Fuel in 5-inch Ram-jet Burner, by Thaine W. Reynolds and Donald P. Haas, *NACA RM* E54D07, June 1954, 31 pp. (Declassified from Confidential by authority of *NACA Res. Abs.* 116, p. 17, 7/5/57.)

Combustion of Elemental Boron, Quarterly Summary Report for March-May 1957, *Experiment Inc., TM*-952, June 1957, 11 pp.

Blow-out Velocities of Various Petroleum Slurry and Hydride Fuels in a 1 7/8 Inch Diameter Combustor, by Preston N. Cook, Jr., Albert M. Lord, and Samuel Kaye, *NACA RM* E54A28, April 1954, 20 pp. (Declassified from Confidential by authority of *NACA Res. Abs.* 116, p. 17, 7/5/57.)

Stabilization of 50-percent Magnesium-JP-4 Slurries with Some Aluminum Soaps of C_8 Acids, by Robert M. Caves, *NACA RM* E54C10, May 1954, 48 pp. (Declassified from Confidential by authority of *NACA Res. Abs.* 116, p. 17, 7/5/57.)

Preparation and Properties of Concentrated Boron-Hydrocarbon Slurry Fuels, by Irving A. Goodman and Virginia O. Fenn, *NACA RM* E54F18a, Aug. 1954, 35 pp. (Declassified from Confidential by authority of *NACA Res. Abs.* 116, p. 18, 7/5/57.)

Effect of Surface-Active Additives on Physical Behavior of 50-Percent Slurries of 1.5-Micron Magnesium in n-Decane, by Murray L. Pinns, *NACA RM* E54K22a, Feb. 1955, 54 pp. (Declassified from Confidential by authority of *NACA Res. Abs.* 116, p. 18, 7/5/57.)

Blow-Out Velocities of Several Slurry and Liquid Fuels in a 1 7/8 Inch Diameter Combustor, by James F. Morris, Robert M. Caves, and Albert M. Lord, *NACA RM* E54L27a, Feb. 1955, 12 pp. (Declassified from Confidential by authority of *NACA Res. Abs.* 116, p. 18, 7/5/57.)

Performance of Pure Fuels in Single J33 Combustors. II. Hydrocarbon and Nonhydrocarbon Fuels, by Arthur L. Smith and Jerrold D. Wear, *NACA RM* E55B02, 63 pp. (Declassified from Confidential by authority of *NACA Res. Abs.* 116, p. 19, 7/5/57.)

NACA Research on Slurry Fuels Through 1954, by Walter T. Olson and Roland Breitweiser, *NACA RM* E55B14, April 1955, 30 pp. (Declassified from Confidential by authority of *NACA Res. Abs.* 116, p. 19, 7/5/57.)

Preparation and Handling of Magnesium-Hydrocarbon Slurries for Jet-Engine Applications, by Henry C. Barnett, A. M. Lord, and P. H. Wise, *NACA RM* E55D01, June 1955, 60 pp. (Declassified from Confidential by authority of *NACA Res. Abs.* 116, p. 19, 7/5/57.)

Preparation of 50 Percent Boron-Hydrocarbon Slurries Using Combinations of Glycerol Sorbitan Laurate With Var-

Seventy-five Years ◇◇◇

TEN MILES an hour was "speed" in 1883 when Wyman-Gordon started to make forgings for the high-wheel bicycle. Through the 75 intervening years forgings have made important contributions to the phenomenal advances in propulsion. Progress from the first "horseless carriages"... from the early "flying machines"... to the supersonic speeds of today ...would not have been possible without forgings produced by the most advanced techniques of the day.

Wyman-Gordon is proud of its achievements in these fields and, as the largest producer of automotive and aircraft forgings, is prepared to accept the challenge of the future. Today, as for 75 years, there is no substitute for Wyman-Gordon quality and experience.

WYMAN-GORDON COMPANY

Established 1883

FORGINGS OF ALUMINUM • MAGNESIUM • STEEL • TITANIUM

WORCESTER 1, MASSACHUSETTS
HARVEY, ILLINOIS • DETROIT, MICHIGAN

ious Thickeners, by Irving A. Goodman and Virginia O. Fenn, *NACA RM* E55E17, July 1955, 30 pp. (Declassified from Confidential by authority of *NACA Res. Abs.* 116, p. 19, 7/5/57.)

Effect of Temperature on Viscosity of Slurries of Boron and Magnesium in JP-5 Fuel, by Harold F. Hipsher, *NACA RM* E55E19, July 1955, 20 pp. (Declassified from Confidential by authority of *NACA Res. Abs.* 116, p. 19, 7/5/57.)

Some Dielectric Properties of Suspensions of Boron Powders in Mineral Oil, by Aubrey P. Altshuller, *NACA RM* E55F02, Aug. 1955, 21 pp. (Declassified from Confidential by authority of *NACA Res. Abs.* 116, p. 19, 7/5/57.)

Materials of Construction

The Physical Properties of Several Materials for Use in Photo-Thermelastic Investigations, by Herbert Tramposch and George Gerard, *N.Y. Univ., Coll. Engng., Res. Div., Tech. Rep.* SM 57-5 (*AFOSR-TN-57-282*), May 1957, 27 pp.

Internal Friction and Shear Modulus of Thorium at High Temperatures, by C. L. Dixon and H. Hori, *Atomic Energy Comm.*, NAA-SR-1846, Apr. 1957, 12 pp.

The Anode Oxidation of Some Dilute Binary Zirconium Alloys, by George B. Adams Jr., Curtis E. Borchers and Pierre Van Rysselberghe, *Atomic Energy Comm.*, AECU-3388, Jan. 1957, 26 pp.

Properties of Titanium Compounds and Related Substances, by Frederick D. Rossini, Phyllis A. Cowie, Frank O. Ellison, Clarence C. Browne and William C. Arsen, *Office Naval Res., Rep.* ACR-17, Oct. 1956, 448 pp.

Creep Behavior of Circular Plates, by B. Venkatraman and P. G. Hodge Jr., *Brooklyn Polytech. Inst., Dept. Aeron. Engng. Appl. Mech., Rep.* 369 (*AFOSR-TN-57-135; ASTIA AD* 120491), Apr. 1957, 24 pp.

Calculated and Measured Stresses in Simple Panels Subject to Intense Random Acoustic Loading Including the Near Noise Field of a Turbojet Engine, by Leslie W. Lassiter and Robert W. Hess, *NACA TN* 4076, Sept. 1957, 33 pp.

Practical Solution of Plastic Deformation Problems in Elastic-Plastic Range, by A. Mendelson and S. S. Manson, *NACA TN* 4088, Sept. 1957, 52 pp.

Special Welding Techniques; Final Summary Report for 1954, Glenn L. Martin Co., *Atomic Energy Comm.*, AECU-3174, Jan. 1955, 41 pp.

Corrosion Properties of Various Materials in High Temperature Waters, by C. J. Lancaster and W. L. Williams, *Naval Engng. Expt. Sta., Rep.* 4A(23)966870 (*Office Tech. Services,* PB 111963), Jan. 1953, 13 pp.

Report on Performance of Materials Tested in Water at High Temperature, by C. J. Lancaster, *Naval Engng. Expt. Sta., Rep.* 4A(16)966870 (*Office Tech. Services,* PB 111962), March 1952, 6 pp.

Anodized Aluminum Wire Takes 1000 Deg F, *Aviation Age,* vol. 28, Sept. 1957, pp. 64–67.

Re-usable Hermetic Seal Takes High Temperatures, *Aviation Age,* vol. 28, Sept. 1957, pp. 88–91.

"Exotic" Metals Look Good for Tomorrow's High Temperature Structures, by Irwin Stambler, *Aviation Age,* vol. 28, Sept. 1957, pp. 42–47.

Aluminum Alloys, by R. L. Horst,

Indust. Engng. Chem., vol. 49, Sept. 1957, Pt. 2, pp. 1578–1583.

Carbon and Graphite, by W. M. Gaylord, *Indust. Engng. Chem.*, vol. 49, Sept. 1957, Pt. 2, pp. 1584–1587.

Ceramics, by John W. Lennon, *Indust. Engng. Chem.*, vol. 49, Sept. 1957, Pt. 2, pp. 1588–1592.

Less Common Metals, by E. M. Sherwood, *Indust. Engng. Chem.*, vol. 49, Sept. 1957, Pt. 2, pp. 1612–1617.

Nickel Including High-Nickel Alloys, by R. M. Fuller, *Indust. Engng. Chem.*, vol. 49, Sept. 1957, Pt. 2, pp. 1618–1628.

Protective Coatings, by Francis Scofield, *Indust. Engng. Chem.*, vol. 49, Sept. 1957, Pt. 2, pp. 1639–1642.

Stainless Steels Including Other Ferrous Alloys, by Walter A. Luce, *Indust. Engng. Chem.*, vol. 49, Sept. 1957, Pt. 2, pp. 1643–1652.

Titanium, by H. B. Bomberger, *Indust. Engng. Chem.*, vol. 49, Sept. 1957, Pt. 2, pp. 1658–1662.

Non-metallics for Missiles, by John H. Lux and Robert L. Noland, *Missiles and Rockets*, vol. 2, Sept. 1957, pp. 137–138, 141–142, 144.

Cooperative Investigation of Relationship between Static and Fatigue Properties of Wrought N-155 Alloy at Elevated Temperatures, NACA Subcommittee on Power Plant Materials, *NACA Rep.* 1288, 1956, 35 pp. (supersedes *NACA TN* 3216).

Generalized Master Curves for Creep and Rupture, by George J. Heimerl and Arthur J. McEvily Jr., *NACA TN* 4112, Oct. 1957, 31 pp.

High-Temperature Oxidation and Ignition of Metals, by Paul R. Hill, David Adamson, Douglas H. Foland and Walter E. Bressette, *NACA RM* L55L23b, March 1956, 12 pp. (Declassified from Confidential by authority of *NACA Res. Abstracts* 120, p. 8, 10/3/57.)

Investigation of a Cermet Gas-turbine-blade Material of Titanium Carbide Infiltrated with Hastalloy C, by Charles A. Hoffman, *NACA RM* E55H12, Jan. 1956, 23pp. (Declassified from Confidential by authority of *NACA Res. Abstracts* 120, p. 8, 10/3/57.)

Investigation of Some Mechanical Properties of Thermenol Compressor Blades, by Donald F. Johnson, *NACA TN* 4097, Oct. 1957, 14 pp.

Experimental Investigation of Cermet Turbine Blades in an Axial-Flow Turbojet Engine, by William C. Morgan and George C. Deutsch, *NACA TN* 4030, Oct. 1957, 20 pp.

Theoretical Study of Decomposable Varnishes for Combustion Chamber Wall Protection, by H. Gelly, *Fusées et Recherche Aeron.*, vol. 2, no. 13, July 1957, pp. 219–228 (in French).

Thermal Behavior of Titanium and Its Alloys, by R. Syre, *Fusées et Recherche Aeron.*, vol. 2, no. 3, July 1957, pp. 229–235 (in French).

Uses of Glass Cloth Reinforced Plastics in Aviation, Missiles and Rockets, by J. Duflos, *Fusées et Recherche Aeron.*, vol. 2, no. 3, July 1957, pp. 237–240 (in French).

Instrumentation, Data Recording, Telemetering

Time Constants and Frequency Response of Coated Hot Wires as Turbulence Sensing Elements, by Avis Borden, *David Taylor Model Basin, Rep.* 952, June 1957, 48 pp.

Project Vanguard Report 18. Minitrack. Report No. 1-Phase Measurement, by C. A. Schroeder, C. H. Looney Jr. and H. E. Carpenter Jr., *Naval Res. Lab. Rep.* 4995, July 1957, 28pp.

Programming and Coding for ORDVAC, by Tadeusz Leser and Michael Romanelli, *Aberdeen Proving Ground, Ballistic Res. Labs., Rep.* 997, Oct. 1956, 278 pp.

What You Should Know for Reliable Missile Circuitry, by D. D. Zimmerman, *Aviation Age*, vol. 28, Sept. 1957, pp. 50–55.

A Digital System for Collecting and Processing Flight Test Data, by H. W. Royce, *SAE Preprint* 192, Oct. 1957, 3 pp.

How Badly Are High Temperature Electronic Systems Really Needed? by Robert R. Janssen, *SAE Preprint* 230, Oct. 1957, 6 pp.

North Atlantic Treaty Organization, Advisory Group for Aeronautical Research and Development, Flight Test Manual, vol. 4: Instrumentation Systems, 1957.

Hot Wire Apparatus for Measurement of Transpiration Effects on Heat Transfer Coefficients, by John M. Lenoir, *Calif. Inst. Tech., Jet Propulsion Lab., Progress Rep.* 20–300, Nov. 1956, 30 pp.

Guidance Systems and Components

Systems Analysis Approach to Firebee Flight Control Systems Development, by C.D. Corden and H. J. Hansen Jr., *SAE Prepr.* 230, Oct. 1957, 8 pp.

Aids to Inertial Navigation, by Frederick Stevens and Frank W. Lynch, *Aeron. Engng. Rev.*, vol. 16, no. 11, Nov. 1957, pp. 43–47.

Missile-Tracking Camera, by George L. Christian, *Aviation Week*, vol. 67, no. 17, Oct. 28, 1957, pp. 110–111, 114.

Radius of Action of a Guided Missile; Its Dependence Upon Certain Arbitrary Parameters, by H. R. Voellmy, *Fusees et Recherche Aeron.*, vol. 2, no. 3, July 1957, pp. 213–218 (in French).

Servomechanisms and Controls

Requirements, Parameters and Design Considerations for Pneumatic Inlet Control Systems, by R.W. Matzdorff and C.F. Newberry, *SAE Preprint.* 236, Oct. 1957, 21pp.

Packaged Hydraulic Systems for Missiles, by A. L. Stone and J. W. Woodward, *SAE Prepr.* 214, Oct. 1957, 6 pp.

Why Hate High Pressure Pneumatics? by H. E. Wright, *SAE Prepr.* 237, Oct. 1957, 7 pp.

Hydraulic Pumps and Motors for High Velocities, by C. R. Himmler, *Fusées et Recherche Aeron.*, vol. 2, no. 3, July 1957, pp. 248–250 (in French).

Flight Vehicle Design and Testing

Proceedings, Symposium on Environmental Testing of Aircraft and Missiles, *SAE, Special Publication* SP141, Dec. 5–7, 1955.

Guided Missile Sensation at Farnborough, by Miles, *Interavia*, vol. 12, no. 10, Oct. 1957, p. 1004.

Helium Comes into Its Own in Missile Technology, by Kurt R. Stehling, *Aviation Age*, vol. 28, Oct. 1957, pp. 86–92.

Jupiter-Thupiter-Thorpiter-Thor? *Missiles and Rockets*, vol. 11, no. 10, Oct. 1957, p. 45.

Missiles and Rockets Around the Globe, *Missiles and Rockets*, vol. 11, no. 10, Oct. 1957, pp. 71–106.

Missiles for NATO, by Normal L. Baker, *Missiles and Rockets*, vol. 11, no. 10, Oct. 1957, pp. 107.

French Missile Production, by Jean-Marie Riche, *Missiles and Rockets*, vol. 11, no. 10, Oct. 1957, p. 112.

Air-to-Air Rockets, by F. I. Ordway III and R. C. Wakeford, *Ordnance*, vol. 38, no. 224, Sept.-Oct. 1957, p. 239.

Guided Missiles of the U. S. Armed Forces, *Ordnance*, vol. 38, no. 224, Sept.-Oct. 1957, p. 264.

British Guided Missiles, by James Hay Stevens, *Aeronautics*, vol. 37, Sept. 1957, pp. 60–64.

Maximum Ranges of Intercontinental Missiles, by Derek F. Lawden, *Aeron. Quarterly*, vol. 8, Aug. 1957, pp. 269–278.

Guided Weapon Engineering, by Brigadier J. Clemow, *Aircraft Engng.*, vol. 29, Sept. 1957, pp. 258–267.

French Test Ramjet-Powered Missiles, by Robert Roux, *Aviation Age*, vol. 28, Sept. 1957, pp. 62–65.

Space Flight

The Simulation of Gravity, by Derek F. Lawden, *J. Brit. Interplanet. Soc.*, vol. 16, no. 3, July-Sept. 1957, pp. 134–140.

On the Equation of Rocket Motion, by G. Leitmann, *J. Brit. Interplanet, Soc.*, vol. 16, no. 3, July-Sept. 1957, pp. 141–147.

The Use of Probe Rockets, by C. A. Cross, *J. Brit. Interplanet. Soc.*, vol. 16, no. 3, July-Sept. 1957, pp. 148–162.

Moon Cities Planned by Red Civil Defense Chief, *Missiles and Rockets*, vol. 11, no. 10, Oct. 1957, p. 45.

Project Far Side, *Missiles and Rockets*, vol. 11, no. 10, Oct. 1957, pp. 120–128.

Sectional Satellites, by George W. Hoover, *Missiles and Rockets*, vol. 11, no. 10, Oct. 1957, pp. 135–137.

Summing Up the Satellite, *The Aeroplane*, vol. 93, no. 2407, Oct. 18, 1957, pp. 581–582.

Bridgehead in Space, by O. C. Winzen, *Interavia*, vol. 12, no. 10, Oct. 1957, pp. 1040–1041.

Orbital Behavior of Earth Satellites, by Robert E. Roberson, *J. Franklin Inst.*, vol. 264, no. 3, Sept. 1957, pp. 181–202.

Orbital Behavior of Earth Satellites, II, by Robert E. Roberson, *J. Franklin Inst.*, vol. 264, Oct. 1957, pp. 269–285.

Spiral and Elliptical Orbits, by E. F. Relf, *J. Royal Aeron. Soc.*, vol. 61, Sept. 1957, pp. 635–641.

Air Force Research and Development in Space Technology, by Thomas A. Power, *Aeron. Engng. Rev.*, vol. 16, Sept. 1957, pp. 36–39.

Spectroscopic Evidence for Vegetation on Mars, by William M. Sinton, *Astrophys. J.*, vol. 126, Sept. 1957, pp. 231–239.

Astrophysics, Aerophysics

Gas-Dust Interaction in the Accretion of Interstellar Dust by the Sun, by Charles B. Stephenson, *Astrophys. J.*, vol. 126, July 1957, pp. 195–201.

Cosmic Ray Nuclear Interactions in Nitrogen Gas, by Saburo Miyake, Kensaku Hinotani, Itsuo Katsumata and Tatsunosuke Kaneko, *J. Physical Soc. Japan*, vol. 12, Aug. 1957, pp. 845–854.

Nuclear Propulsion

An Experiment on the Structure of the Electron, I, by G. K. O'Neill and J. A. Ball, *Atomic Energy Comm.*, NYO 8015, July 1957, 15pp.

A Series of Thermal, Epithermal and Fast Neutron Measurements in the MTR, by J. B. Trice, *Atomic Energy Comm.*, CF-55-10-140, Oct. 1955, 88pp.

A Review of the Reaction Kinetics of Deuterium and Tritium Compounds, VII: Oxidation Reduction Reactions, by Lawrence M. Brown, *Atomic Energy Comm.*, NBS-4877, Nov. 1956, 25pp.

Unclassified U. S. Atomic Energy Commission Reports on Controlled Thermonuclear Processes; A Literature Search, by Sidney F. Lanier, *Atomic Energy Comm.*, TID 3506, Jan. 1957, 7pp.

Preliminary Results on the Kinetic Behavior of Water Boiler Reactors, by D. L. Hetrick, J. W. Flora, E. L. Gardner, B. R. Moskowitz, D. R. Muller, M. E. Remley, and R. K. Stitt, *Atomic Energy Comm.*, NAA-SR-1896, Apr. 1957, 20pp.

A General Method for Comparing Thermal Performance of Fuel Element Geometries and Coolants for Non-boiling Reactors, by G. A. Freernd and A. L. London, *Atomic Energy Comm.*, ANL-5589, Jan. 1957, 30 pp.

Unclassified U. S. Atomic Energy Commission Reports on Reactor Safety, A Literature Search, by Hugh E. Voress, *Atomic Energy Comm.*, TID-3503, Nov. 1956, 9 pp.

Symposium on Reactor Instrumentation, Part I, *Atomic Energy Comm.*, WAPD 20, June 1950, 46pp.

Coulomb Effects in Inner Bremsstrahlen, by R. R. Lewis, Jr., and G. W. Ford, *Physical Rev.*, vol. 107, Aug. 1, 1957, pp. 756–765.

Nuclear-powered Seaplane, by A. D. Struble, Jr., *SAE J.*, vol. 65, Sept. 1957, pp. 64–66.

Thermal Conductivity of Insulating Materials for Use in Nuclear Reactors, by W. R. Morgan and W. G. Baxter, *ASME Paper* 57-F-9, Sept. 1957, 5 pp.

Direct Interaction Theory of Inelastic Scattering, III: Numerical Calculations, by Carl A. Levinson and Manoj K. Banerjee, *Atomic Energy Comm.*, NYO-8012, Sept. 1957, 22 pp.

Solid State Physics; Semiannual Progress Rep. July-Dec. 1956, North American Aviation, Inc., Atomic International, *Atomic Energy Comm.*, NAA-SR-1885, June 1957, 40 pp.

New Concepts and Materials Needed for Nuclear Accessory Systems, by John P. Wittry, *Aviation Age*, vol. 28, Oct. 1957, pp. 32–35.

Chemical Effects of Hot Atoms, by Louis Monchick, Koichi Funabashi and John L. Magee, *J. Chem. Phys.*, vol. 27, Sept. 1957, pp. 734–739.

The Application of Nuclear Power to Logistic Aircraft Systems, by Robert W. Middlewood and Robert B. Ormsby, Jr., *SAE Preprint* 206, Oct. 1957, 11 pp.

Economics of the Reactor Fuel Cycle, by Harlan W. Nelson, *Battelle Tech. Rev.*, vol. 6, Oct. 1957, pp. 9–16.

Nuclear Planes Break Range Barrier, by R. W. Middlewood and R. B. Ormsby Jr., *SAE J.*, vol. 65, no. 11, Oct. 1957, pp. 32–34.

Power from Fusion Reactions, by Clayton R. Lewis, *SAE J.*, vol. 65, no. 11, Oct. 1957, pp. 48–49.

Index to Advertisers

AEROJET-GENERAL CORPORATION ..... Back Cover
D'Arcy Advertising Co., Los Angles, Calif.

AMERICAN MACHINE & FOUNDRY CO. 269
Fletcher D. Richards, Inc., New York, N. Y.

AMERICAN POTASH & CHEMICAL CORPORATION 285
The McCarty Company, Los Angles, Calif.

APPLIED PHYSICS LABORATORY, THE JOHNS HOPKINS UNIVERSITY 278
M. Belmont ver Standig, Inc., Washington, D. C.

ARNOUX CORPORATION 288
Kay-Christopher Advertising, Hollywood, Calif.

AVCO MANUFACTURING CORPORATION, RESEARCH AND ADVANCED DEVELOPMENT DIVISION 218
Benton & Bowles, Inc., New York, N. Y.

BECCO CHEMICAL DIVISION, FOOD MACHINERY & CHEMICAL CORPORATION .. 215
John Mather Lupton Company, New York, N. Y.

THE BRISTOL COMPANY 282
James Thomas Chirurg Co., New York, N. Y.

CONVAIR, A DIVISION OF GENERAL DYNAMICS CORPORATION ..... Third Cover
Buchanan & Company, Inc., Los Angeles, Calif.

DIVERSEY ENGINEERING COMPANY 222
Roark & Colby Advertising, Chicago, Ill.

DOUGLAS AIRCRAFT COMPANY, INC. 216, 217
J. Walter Thompson Company, Los Angeles, Calif.

DU PONT DE NEMOURS, E. I., AND COMPANY
EXPLOSIVES DEPARTMENT 291
Charles L. Rumrill & Co., Inc., Rochester, N. Y.

PHOTO PRODUCTS 277
N. W. Ayer & Son, Inc., Philadelphia, Pa.

EASTMAN KODAK COMPANY 267
The Rumrill Company, Inc., Rochester, N. Y.

EXCELCO DEVELOPMENTS, INC. 220
Melvin F. Hall Advertising, Inc., Buffalo, N. Y.

THE GARRETT CORPORATION, AIRESEARCH MANUFACTURING COMPANY ... 280, 281
J. Walter Thompson Co., Los Angeles, Calif.

GENERAL ELECTRIC COMPANY, FLIGHT PROPULSION LABORATORY 286
Deutsch & Shea, Inc., New York, N. Y.

GRIEVE-HENDRY COMPANY, INC. 284
Jacobson and Tonne Advertising, Chicago, Ill.

HEILAND DIVISION, MINNEAPOLIS-HONEYWELL 274, 275
Tool & Armstrong Advertising, Denver, Colo.

HOFMAN LABORATORIES 286
Paul M. Healy, Montclair, N. J.

LAVEZZI MACHINE WORKS 288
R. W. Sayer Co., Chicago, Ill.

LOCKHEED AIRCRAFT COMPANY, MISSILE SYSTEMS DIVISION 283
Hal Stebbins, Inc., Los Angles, Calif.

LUKENS STEEL COMPANY 221
J. M. Mathes, Inc., New York, N. Y.

MORRIS BEAN & COMPANY 272
Odiorne Industrial Adv., Inc., Yellow Springs, Ohio

PERKIN-ELMER CORPORATION 273
G. M. Basford Co., New York, N. Y.

RADIO CORPORATION OF AMERICA 271
Al Paul Lefton Co., Philadelphia, Pa.

THE RAMO-WOOLDRIDGE CORPORATION, SPACE TECHNOLOGY LABORATORIES 292
The McCarty Company, Los Angeles, Calif.

RHEEM MANUFACTURING COMPANY 290
Getz & Sandborg, Inc., Beverly Hills, Calif.

ROCKETDYNE, A DIVISION OF NORTH AMERICAN AVIATION, INC. 276, 289
Batten, Barton, Durstine & Osborn, Inc., Los Angeles, Calif.

SERVOMECHANISMS, INC. 219
Sanger-Funnell, Inc., New York, N. Y.

SOUTHWEST PRODUCTS COMPANY 284
O. K. Fagan Adv. Agency, Los Angeles, Calif.

THIOKOL CHEMICAL CORPORATION ..... Second Cover
Dancer-Fitzgerald-Sample, Inc., New York, N. Y.

THE THOMPSON-RAMO-WOOLDRIDGE PRODUCTS COMPANY 213
The McCarty Company, Los Angeles, Calif.

WESTVACO CHLOR-ALKALI DIVISION, ALLIED CHEMICAL & DYE CORPORATION 279
James J. McMahon, New York, N. Y.

WYMAN-GORDON COMPANY 287
John W. Odlin Co., Inc., Worcester, Mass.